University of Kentucky

UKnowledge

2011

ACHIEVING ULTRAFINE GRAINS IN Mg AZ31B-O ALLOY BY CRYOGENIC FRICTION STIR PROCESSING AND MACHINING

Anwaruddin Mohammed
University of Kentucky, reach2anwar@gmail.com

Right click to open a feedback form in a new tab to let us know how this document benefits you.

ACHIEVING ULTRAFINE GRAINS IN *Mg AZ31B-O* ALLOY BY CRYOGENIC
FRICTION STIR PROCESSING AND MACHINING

_____

THESIS

_____

A thesis submitted in partial fulfillment of the
requirements for the degree of Master of Science in
Manufacturing Systems Engineering in the College of Engineering
at the University of Kentucky

By

Anwaruddin Mohammed

Lexington, Kentucky

Director: Dr. I.S. Jawahir, Professor of University of Kentucky

Lexington, Kentucky

2011

ABSTRACT OF THESIS

ACHIEVING ULTRAFINE GRAINS IN *Mg AZ31B-O* ALLOY BY CRYOGENIC
FRICTION STIR PROCESSING AND MACHINING

This thesis presents results from the application of cryogenic cooling on multiple-pass friction stir processing and the subsequent orthogonal machining on friction stir processed and as-received *Mg AZ31B-O* disks, and shows their combined effects on microstructure and microhardness values. A simple friction stir tool, a specially designed fixture and liquid nitrogen are used to perform multiple-pass friction stir processing experiments on *Mg AZ31B-O* alloy. The friction stir processed and as-received sheets are then made into disks for the orthogonal machining experiments. This study analyzes the microhardness, microstructure changes by cryogenic friction stir processing and the effect of machining conditions such as dry, MQL and cryogenic and cutting parameters on the *Mg AZ31B-O* alloy. Four different speeds and three different feed rates are used for the orthogonal machining experiments. The effects of stirring parameters such as the translational feed, rotational speed, cooling conditions and the machining parameters are studied. The resulting microstructure and microhardness from these processes hold a key to the mechanical properties of the alloy. This analysis would help to understand and evaluate the specific aspects of grain size and microhardness that influence the fatigue life of a component.

Keywords: Friction Stir Processing, Cryogenic Cooling, Orthogonal Machining, Microstructure, Microhardness

Anwaruddin Mohammed

7th December 2011

ACHIEVING ULTRAFINE GRAINS IN *Mg AZ31B-O* ALLOY BY CRYOGENIC
FRICTION STIR PROCESSING AND MACHINING

By

Anwaruddin Mohammed

Dr. I.S. Jawahir

(Director of Thesis)

Dr. D.P. Sekulic

(Director of Graduate Studies)

Date: 12/07/2011

To:

My Parents, Family and Friends

ACKNOWLEDGEMENT

TABLE OF CONTENTS

CHAPTER 3: FRICTION STIR PROCESSING (FSP) EXPERIMENTS

LIST OF TABLES

CHAPTER 1

INTRODUCTION

1.1 Introduction

The focus of this research is on friction stir processing of *Mg AZ31B-O* alloy using cryogenic cooling followed by orthogonal machining at different cooling conditions and with various cutting parameters.

1.2 Objective

Light-weight alloys are being used extensively in aerospace and automotive industries. For issues concerning sustainability, these alloys have high strength-to-weight ratio properties and hence are ideal for use in those industries. The mechanical properties of these alloys can be improved by refining and homogenizing the microstructure. Smaller grain size and a more homogenous grain structure improve the mechanical properties of the light-weight alloys such as strength-to-weight ratio, corrosion resistance, tensile strength [1] and Superplastic Formability [1].

The widespread utilization of light-weight alloys is however hindered due to the difficulty in producing uniform ultrafine grain-structured bulk material by the industry. Conventional grain refinement techniques such as hot rolling which involves thermo-mechanical processing are costly, time-consuming, and negatively affect the environment due to high energy consumption [1]. Hence, there is a need to look for alternative processing techniques. There are several advanced processing techniques which effectively refine the grain structure, such as: the equal channel angular extrusion (ECAE) and torsional strain induced severe plastic deformation (TSPD). However, they have major drawbacks such as limited size capabilities, high load and long processing time. This limits the wide industrial applications of such techniques [1].

Friction Stir Processing (FSP) is an innovative technique that can be used to produce fine and homogeneous grain structure in thin plates. This technique is based on the older Friction Stir Welding (FSW) technique and will be described later in the thesis. It is a simple, affordable and productive technique for modifying the grain structure of sheet metals. It is a solid-state process in which a specially designed tool is plunged into the sheet rotated and moved thereby causing intense plastic deformation through a complex stirring action. This yields a dynamically recrystallized material having a fine-grain microstructure. Some of the main advantages of FSP over other refinement techniques are:

- Simplicity of the process
- Simple tooling
- Readily available machine
- Easy automation of the process
- Energy efficiency (dry FSP)

The formability of light weight alloys at room temperature is critical for aerospace and automotive applications. The objective of this thesis work is to investigate how to improve the formability of *Mg AZ31B-O* alloy by refining and homogenizing its microstructure using FSP as well as further improvements of other properties by a following machining process.

Processing the sheets completely and then cutting disks from the sheet for machining experiments is a new method for experimental analysis, which apparently has never been tried before. Many researchers have studied superplasticity, tensile strength, microstructure and microhardness results of different FSP light-weight alloys. However, they did not use a machining process on the specimens which were already worked as FSP sheet which is sometimes required for giving final properties and shape to the product.

This research work consists of two stages - first one deals with the FSP and the second stage involves the orthogonal machining of the Friction stir processed sheet. *Mg AZ31B-O* sheet is fully processed by multiple overlapping passes and by using different cooling techniques such as flood cooling, cryogenic cooling at tool and sheet interface as well as underneath the fixture. In addition, the process parameters, i.e., translational speed and rotational speed are also varied in order to generate smaller grains with a homogenous grain structure throughout the sheet thickness. This improves the superplastic formability, corrosion resistance, the overall surface integrity, and induces high hardness values in some of the light-weight alloys. The process parameters are fixed to reduce the number of experiments. Thirty six FSP sheets are produced at these fixed conditions and subsequently machined at varied cutting conditions. Another thirty six as-received disks are also machined at the same conditions as FSP disks for comparing the results.

1.3 Statement of problem to be studied

Super Plastic Forming (SPF) is a process in which metals undergo extraordinary tensile ductility, in excess of 200%. This ductility feature attracted the investigators for its potential benefits in the area of metal forming. The wide use of SPF has not yet become popular for a number of factors such as the cost of initial processing equipment to prepare superplastic materials and slow forming process due to low forming strain-rates. Grain size has a significant effect on the superplastic properties. Light-weight alloys such as aluminum alloys, magnesium alloys, other composites and ceramics are some examples of superplastic materials.

There are many challenges involved in making the FSP process commercially viable. The mechanical properties for different light-weight alloys can be enriched by the utilization of FSP. One of the significant points which is critical for the commercial acceptance of this technique is to fully process the sheet and then study the microstructure and microhardness results. The practical applications of this technique in aerospace and automotive industries demand such a study.

An additional novel area in this project is the comparison of the microstructure and microhardness results on the FSP samples processed using different cooling conditions such as flood, dry and cryogenic cooling during machining.

1.4 Overview of thesis

This dissertation consists of six chapters.

Chapter two presents an introduction on friction stir welding, friction stir processing, multiple-pass friction stir processing, different cooling methods for friction stir processing, machining magnesium alloys and different cooling conditions in machining. Also presented is a review of and some of the previous work that had been in done in the field.

Chapter three explains in detail about the multiple-pass friction stir processing experimental setup and the experiments performed. The microstructure and microhardness results are also discussed in detail. It also gives a detailed description of sample preparations used for the metallographic analysis.

Chapter four presents the experimental setup for machining and the machining experiments performed under different cooling conditions: dry, MQL and cryogenic. Cutting and feed force values produced under each machining condition at different cutting parameters of cutting speed and feed rate are discussed. Chips obtained under different cutting speed and feed rate are briefly discussed.

Chapter five discusses the microstructure and microhardness results of the machined samples. The microstructure parameters such as surface layer grain size, surface layer thickness, microhardness values near surface layer are studied for all specimens.

Chapter six concludes this work with a summary, conclusions and the recommendations for future work.

CHAPTER 2

LITERATURE REVIEW

2.1 Background

The researchers at The Welding Institute (England) found their motivation from the welding of aluminum, which has always been a great challenge, and they invented a new advanced welding technique called the Friction Stir Welding, FSW, process [2].

2.2 Friction Stir Welding (FSW)

FSW is a process which involves the joining of metals without using any filler materials. It plasticizes the material using a non-consumable tool which rotates and penetrates into the materials to be welded. The central pin, followed by the shoulder, is brought into contact with the two parts to be joined as shown in Figure 2.1. The material is plasticized by the rotation of the tool which heats the material as the tool moves along the joint line. The material from the front of the tool is swept around this plasticized annulus to the rear, eliminating the interface. Hence, the welds are created by the combined action of frictional heating and mechanical deformation due to the rotation of the tool. High temperature is generated to the order of 0.8 of the melting temperature. The tool consists of a circular section, and at the end, there is a threaded probe or more complicated flute. This portion of the tool excluding the probe is known as the shoulder. The probe, or the pin, penetrates the workpiece completely and the shoulder comes into contact with the surface, generating a force and rubbing the top surface. The friction between the rotating-translating tool and the workpiece generates heat. Also, there is adiabatic heating due to the large plastic deformation near the pin.
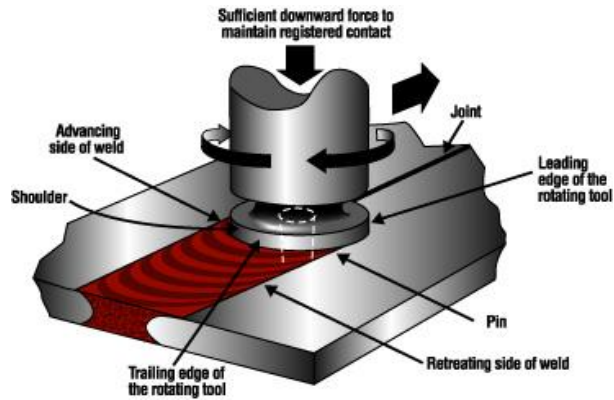
Figure 2.1: Friction stir welding process [3]

Many friction stir techniques exist: rotary friction welding, linear friction welding, radial friction welding, friction plunge welding. The FSW methods are based upon this principle [4].

FSW has many significant advantages over other joining processes:

- A solid state joining process
- No creation of a molten pool which shrinks significantly on resolidification
- Low distortion after welding
- Equiaxed fine grain structure in the weld zone
- High weld quality
- Capable of joining dissimilar metals of different melting temperatures and physical properties
- Quick process
- High reproducibility – necessary for mass production industry
- No consumables are required (filler wire, flux or gas)
- No fume production
- Negligible material loss

2.3 Friction Stir Processing (FSP)

Considering the advantages of FSW, the process was extended to a new advanced microstructural modification process in the late 1990's and called Friction Stir Processing (FSP). Since then, many researchers have worked on this new technique. FSP is reported to have enhanced the superplasticity of light-weight materials by producing an equiaxed ultrafine grain structure; thereby enhancing some mechanical properties of the light-weight alloys [5-8].

In FSP process, a specially-designed simple tool, which consists of a pin and a shoulder, is used. The tool is held into the spindle of the milling machine and is made to rotate. The rotating pin is plunged into the sheet, and it is then made to traverse in the desired direction. Simultaneously the shoulder rubs against the surface of the sheet, thus generating enough heat to soften the material under the tool. The mechanical stirring is caused by the plunged rotating pin which forces the softened material to undergo intense plastic deformation. Under the correct set of speeds, this yields a processed zone characterized by dynamically recrystallized fine grain structure. The schematic views for FSP are shown in Figure 2.2 and Figure 2.3 which show a step by step view of this process.
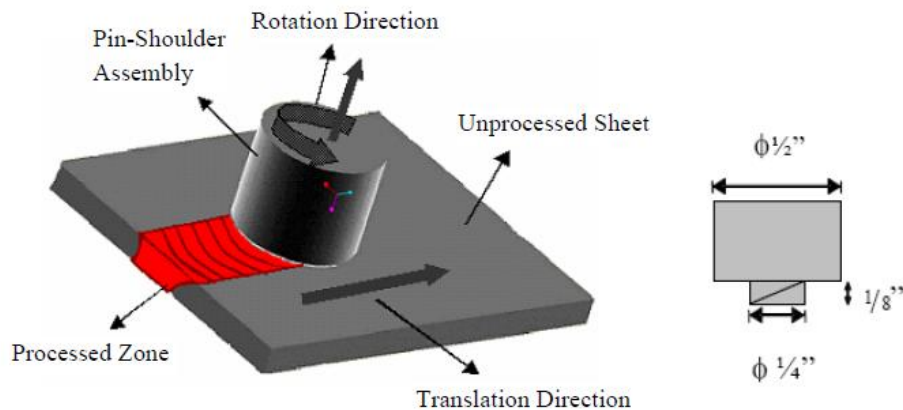
Figure 2.2: Schematic for friction stir processing (FSP) [3]
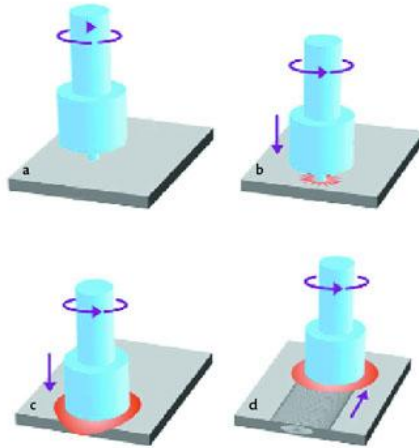
Figure 2.3: Schematic for friction stir processing (FSP) in steps [3]

FSP has many advantages over conventional and other newer material processing techniques.

- ➢ Simple process
- ➢ Simple and inexpensive tool
- ➢ Utilizes a readily available machine such as a milling machine to conduct the process
- ➢ Easily automated
- ➢ Reduced time for operation
- ➢ Energy-efficiency
- ➢ Cost-effectiveness

However, there are some limitations that need to be addressed through research.

- ➢ The high heat generated during this process especially in multiple pass FSP causes grain growth during additional thermal cycles. Therefore, there is a need for an aggressive cooling system for the dissipation of heat.
- ➢ Non-uniform distribution of material (grain size) from the top to the bottom surface of the processed sheet occurs.

2.4 Previous work

FSP produces fine grain structure which makes this technique a significant area of focus for researchers. The effects of FSP on superplastic behavior, microstructure and microhardness have been investigated for different materials using different process parameters. [5-8]

Single pass FSP process has only a limited benefit such as the basic understanding and estimating of the effects of process parameters on the microstructure, surface roughness, microhardness and residual stresses of the processed materials. Multiple overlapping passes FSP are required for fully processing the sheet for use in large-scale applications. Several researchers have attempted to study the effects of multiple pass FSP, but apparently only few of them considered fully processing the sheet and evaluating the obtained results. They focused on one particular region, called the nugget region, which according to them, has the most refined grains due to the high stirring action in that region. But, for practical applications, we need a sheet which has very uniform grain structure throughout the thickness of the material and also along in the longitudinal and transverse directions of the sheet. In this chapter, the work investigated by different researchers in single and multiple pass FSP is reviewed.

Results from Mahony et al. [9] on FSP of aluminum sheet suggested that it enhanced the superplasticity behavior by obtaining higher strain-rate sensitivity value at lower temperatures and higher strain-rate than that of the unprocessed material. Johannes and Mishra [10] were able to create superplastic sheets by multiple pass FSP on *7075 Al* alloy. They studied the effect of four multiple pass FSP in this alloy on tensile strength of the sample. The elongation of the initial *Al* alloy was less than 200%, and hence it was not superplastic. With multiple pass FSP, they were able to achieve elongation values in the range of 1000-1440 % in the nugget region. Grain sizes obtained were different for different passes (1-4), and were in the range of 3.6-5.4 μm, whereas in single pass it was small and consistent at 3.6 μm. They found better final material elongations when using just the single processing pass. Cavaliere and Marco [11] performed FSP on *AZ91*

9

magnesium alloy. Their results showed a decrease in the elongation and strain-rate sensitivity value of the material. Ma et al. [12] investigated FSP of commercial *7075 Al* rolled plates with different processing parameters and demonstrated that a decrease in grain size resulted in significantly enhanced superplasticity. Johannes et al. [13] studied the effects of FSP on the superplastic behavior of aluminum alloy *AA5083*. Their results showed that the FSP samples exhibited 2-3 times the elongation of the as-cast samples.

Mishra et al. [14] studied the effects of multiple overlapping FSP passes on the superplastic behavior of *7075 Al* alloy sheets. Samples were taken from various areas of the FSP sheet for the tensile tests. They compared the results with the as-received (AR) samples and found that the AR samples did not show any superplastic behavior whereas the FSP sample did. Ma et al. [7] conducted single pass FSP at different temperatures and strain-rates on cast *A356 Al* alloy. Mini tensile samples were selected for the tests and they concluded that FSP converted a non-superplastic cast *A356* sample into a superplastic alloy. Charit et al. [15] achieved superplasticity in *2024 Al* alloy at a high strain-rate and low temperature by FSP. They found that FSP produced microstructure suitable for superplasticity at high strain-rates, low temperatures and low flow stresses.

Different mechanical tests have been conducted such as hardness tests, tensile tests, fatigue tests, etc., on the FSP samples. Most researchers focused on light-weight materials such as aluminum alloys while a few have done some work on steel, titanium, copper and magnesium [16-27]. Itharaju and Khraisheh [3] studied the effects of process parameters on *5052 Al* alloys. Mishra et al [5, 14] examined the effects of FSP on several aluminum alloys: *7075*, *2024* and cast *A356* producing fine grain structures.

XingHao and Baolin [28] have used two pass friction stir process on *MgAZ61* alloy and obtained nano grains in the nugget region having high hardness values, which are almost three times that of the substrate. By application of cryogenic fluids under the copper mould using an efficient cooling system, they were able to generate nano grains as small as 100 nm and hardness values as large as 155 HV in the nugget region. The material for their project study was commercial *AZ61 Mg* alloy with the chemical composition *Mg-*

6Al-1.01Zn (in mass %) with an original grain size of 75 µm. Liquid nitrogen was applied on the copper mould under the fixture for quick dissipation of heat from the sample. The first-pass FSP was performed without liquid nitrogen cooling; however, the liquid nitrogen cooling was employed during the second FSP pass. A 500 nm grain size was obtained after the first pass, and a more refined 100 nm grain size was obtained by a second overlapping pass with the use of the liquid nitrogen. The observation was focused on the bottom of nugget zone in the study, which experienced the highest cooling rate. They found that the temperature gradients exist from top to bottom in the processed zone. However, the temperature difference depends upon the high thermal conductivity of the alloy. This results in a decrease in average grain size from top to bottom in the processed zone.

Su et al. [6] studied the microstructure results of FSP on the commercial *7075 Al* alloy with rapid cooling. They used a mixture of water, methanol, and dry ice to quench the plate immediately behind the FSP tool. Four multiple overlapping passes were used to refine the grain size in commercial *7075 Al* alloy to a sub-micron scale (250 nm), with a relatively uniform microstructure. However, the processed zone exhibits a non-uniform microstructural distribution with the average grain size decreasing from 300 nm in the top to 250 nm in the center and the bottom regions. The coolant used was a mixture of water, methanol, and dry ice, to quench the plate immediately behind the FSP tool to create an ultrafine-grained structure. They found a large disorientation between the individual grains. The microstructure observation suggested that non-uniform plastic deformations were introduced in the recrystallized grains during FSP. They concluded that multiple overlapping passes could be used to produce any desired sheet size of an ultrafine grained microstructure and high hardness values. However, they found it difficult to actually refine grain size to the nano-scale using this technique.

2.4.1 Microstructure and dynamic recrystallization

Ma et al. [29] investigated the effect of multiple pass FSP on the microstructure and the tensile properties of the processed sheet by using five-pass FSP with 50% overlap on cast

A356 aluminum alloy. The microstructure results show that the overlapping FSP did not improve it. They found that in the multiple pass process, the strength of the processed zones kept decreasing with subsequent passes because of over-aging due to the FSP thermal cycles.

Johannes and Mishra [10] studied the effect of multiple pass FSP on the microstructure and superplasticity of *7075 Al* alloy. They used four passes of FSP under identical conditions. They studied the effect of multiple passes by adding one pass at a time to a total of four passes as shown in Figure 2.4. They did so in order to compare single pass FSP with multiple pass FSP for up to four passes. Tensile tests were performed in the temperature range of 673 to 763 K with initial strain-rates ranging from 1×10^{-3} to 1×10^{-1} s^{-1}. The results showed the effect of multiple pass FSP in creating large areas of superplastic material. They also found that the multiple passes can coarsen the grain in the additional thermal cycles on the plate. They found that the largest elongations were observed for the single pass material.
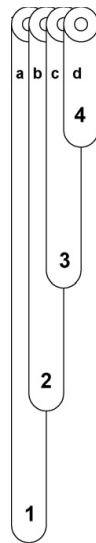
Figure 2.4: Configuration used to create one through four pass samples under identical conditions [10]

Chang et al. [30] conducted experiments to achieve ultrafine-grains (UFG) in solution-hardened *AZ31 Mg–Al–Zn* alloy. They combined FSP with a rapid heat sink to prepare

UFG *AZ31 Mg* alloys with only one single FSP pass. The highly effective cooling system that they used is shown in Figure 2.5. The mean grain size of the specimens was refined from an initial 75 µm to an ultrafine scale (100–300 nm). The mean value of the Vickers microhardness of the UFG region reached 120 HV, which is more than twice as high as that of the *AZ31* initial matrix. The grain refinement kinetics is analyzed and the results are self-consistent. They used the measured average grain size, and the calculated strain-rate to calculate the working temperature using the relationship given in Equation (1.1) which has been found to be 200 °C.

$$Z = \dot{\varepsilon}\exp(\frac{Q}{RT}) \tag{1.1}$$

where Z is the Zener-Holloman parameter, Q is the activation energy of lattice diffusion of the sheet's material, R is the gas constant, and $\dot{\varepsilon}$ is the effective strain-rate. They concluded that with proper control of the working temperature history, an ultrafine and uniform grained structure can be achieved. The grain boundaries are well defined and the mean grain size can be refined to 100–300 nm from the initial 75 µm by a single FSP pass.
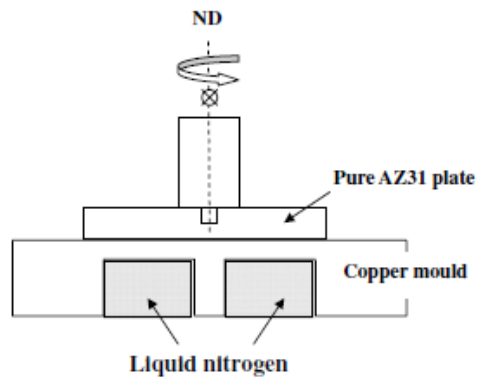
Figure 2.5: Schematic drawing of the newly designed cooling system [30]

Itharaju and Khraisheh [3] studied the effect of process parameters such as rotational and translational speeds on the microstructure and the generated forces in FSP aluminum alloy *AA5052* sheets. They were able to refine the grain from an average of 37.5 µm of the as-received material to a 1.5 µm and 3.5 µm. They found that rotational speed

increases the plunging force and it is almost independent of the translational speed. Bensavides et al. [31] performed friction stir welds on *Al 2024* alloy and compared the grain size of FSW processed zone at room temperature and at low temperature (-30°C). They found an increase in the weld zone equiaxed grain size from bottom to top at room temperature, whereas the difference is small at low temperatures.

At present, there are only a few models, which can predict the grain size that can be achieved by using multiple pass FSP. However, many models do exist for single pass FSP.

Fratini et al. [32] developed a numerical model for the determination of the average grain size due to continuous dynamic recrystallization phenomena in FSW of *AA6082 T6* aluminum alloy. The model took into account the local effects of strain, strain-rate and temperature on the average grain size. The recrystallized grain was influenced by the local value of the field variables, such as the strain, the strain-rate, temperature levels and the material.

Aljoaba et al. [33] developed a three dimensional Computational Fluid Dynamics (CFD) model that can predict the strain-rate distribution and the deformation zone in the friction stir processed zone as a function of process parameters. His model also included the thermal effects of FSP and he applied it to *Mg AZ31B-O* sheet. FSP simulation was done using the STAR CCM+ CFD commercial software package. The effects of process parameters on temperature, strain-rate, flow stress and material velocity fields in and around the nugget zone were investigated. The Zener-Holloman parameter was used to predict the grain size distribution in the processed zone based on the process parameter values. He calculated the grain size after recrystallization, using an empirical relationship (Equation 1.2) that relates it to the Zener-Holloman parameter, via (Eq 1.1).

$$Z = \dot{\varepsilon}\exp(\frac{Q}{RT})$$

$$\ln d = 8.65 - 0.21 \ln Z \tag{1.2}$$

Rearranging Equation (1.2) which was obtained by Darras [1], Equation (1.3) is obtained. Dividing Equation 1.3 by the original average grain size of the as-received sheet (d_0), which is about 10 μm, the new expression for the average grain size is given in Equation 1.4.

$$d = e^{8.656}/(Z^{0.21}) \tag{1.3}$$

$$d/d_0 = 568.74/Z^{0.21} \tag{1.4}$$

Aljoaba [36] used the constraint value, temperature higher than 500° K (temperature range for recrystallization of the magnesium alloy is 523-753° K [1]).

Aljoaba [36] incorporated different stirring conditions into his model and their affects on material flow and microstructural modification were investigated. The average grain size values that were predicted from his CFD simulations were close to the experimental results obtained by Darras [1].

Darras [1] calculated the Zener-Holloman parameter and obtained the constants of the linear relationship shown in Figure 2.6.
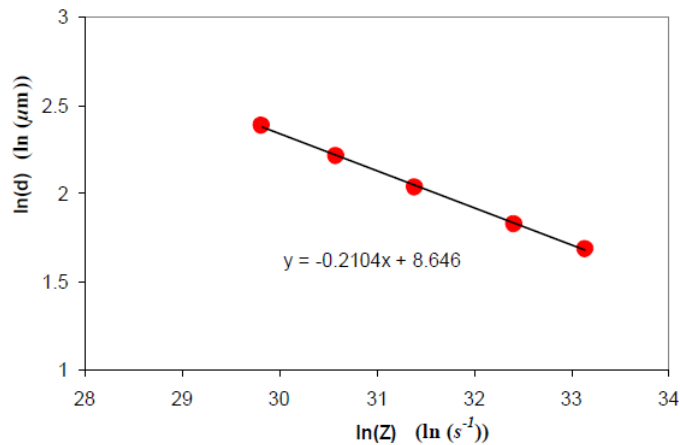
Figure 2.6: Grain size-Zener-Holloman relationship of *Mg AZ31B-O* [1]

It is difficult to measure the strain-rate experimentally. Aljoaba [36] used STAR CCM+ software to calculate the strain-rate during FSP. He predicted the strain-rate values and their distributions under different conditions for all tool-pin geometries. He observed that the strain-rate is influenced by the rotational speed and increases with an increase in it. He found the zone in contact with the outer edge of the tool's shoulder to have highest values, where the temperature and the material speed are the highest. He found the best strain-rate distribution and the maximum strain-rate value of 4750 s^{-1} in the case of trimmed tool-pin due to the superior interface between the tool and the sheet. Figure 2.7 shows the predicted strain-rate values for flat-tool pin and the maximum strain-rate value of 1200 s^{-1} is found in the case of rotational speed of 1750 rpm.
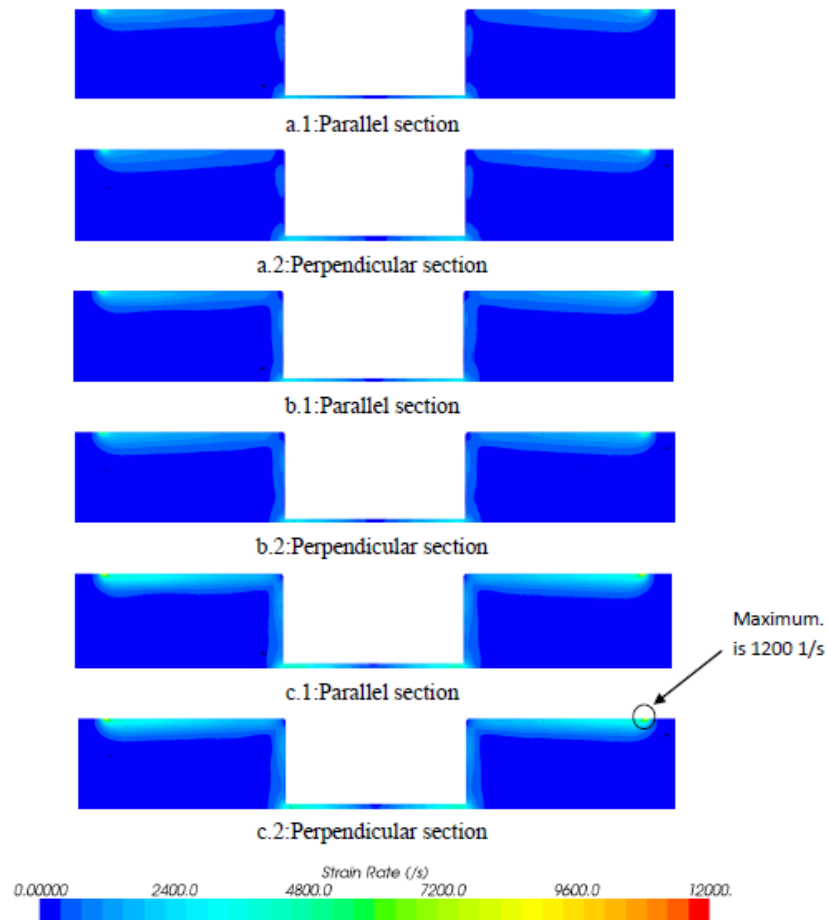
Figure 2.7: Strain-rate values in the sheet for FSP with flat-tool pin at rotational speeds of (a) 1000 rpm, (b) 1200 rpm, and (c) 1750 rpm [36]

16

He also predicted the temperature distributions on the FSP sheet at the coolant rates of 0.5 Kg/s, and 1 Kg/s. He found the maximum temperature at the tool's shoulder with and without cooling application. The temperature values obtained in zones close to the bottom of the sheet are smaller for the case of coolant application than for the case of without coolant application due to the heat removed by the coolant. The temperature distribution is shown in Figure 2.8. He also observed that the temperature in the zones close to the bottom of the sheet is lower when the coolant's mass flow rate is increased from 0.5 Kg/s to 1 Kg/s. Comparing the difference of the green color intensity in Figure 2.8 and Figure 2.9 indicates the crucial role of the coolant.
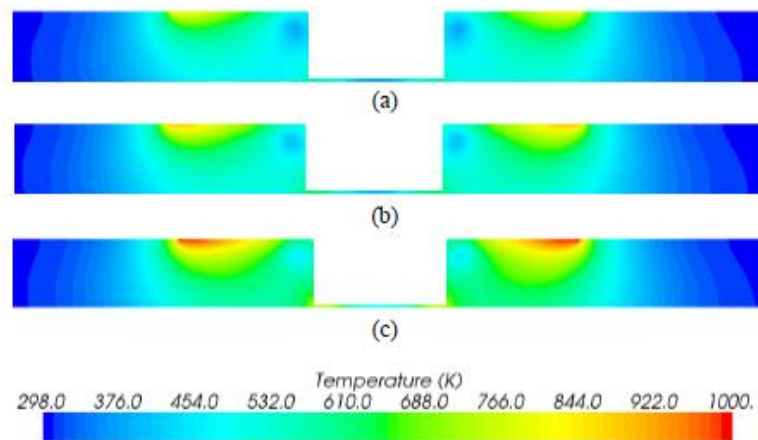
Figure 2.8: Simulated temperature distribution at 0.5 Kg/s of coolant mass flow rate and at rotational speeds of: (a) 1000 rpm, (b) 1200 rpm, (c) 1750 rpm [36]
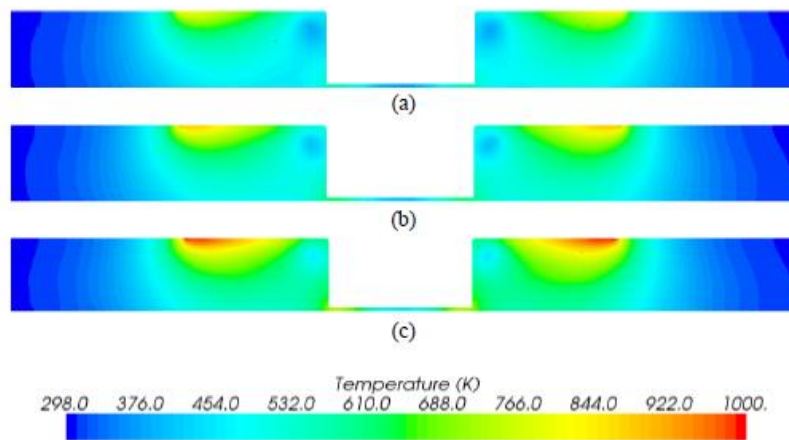
Figure 2.9: Simulated temperature distribution at 1 Kg/s of coolant mass flow rate and at rotational speeds of: (a) 1000 rpm, (b) 1200 rpm, (c) 1750 rpm [36]

Buffa et al. [34] studied the effects of the thermal and mechanical actions occurring in FSP operations of *AA7075-T6* aluminum alloy. They concluded that the strain-rates caused by the mechanical action of the tool pin, together with the generated heat flux is responsible for the dynamic recrystallization phenomena observed in the nugget region.

XingHao and BaoLin [28] used rotational speed of 1000 rpm, and translational speed of 37 mm/min with 1.5º tilt to process two passes of 10 cm long. They applied the coolant in the second pass while nothing was applied in the first pass. They proposed a two-type recrystallization mechanism which is responsible for the formation of nano-scale microstructure. They assumed that in the first pass a continuous dynamic recrystallization (DRX) was occuring, while a discontinuous DRX taking place in the second pass. Their resulting microstructure had equiaxed grains ranging from 40 to 200 nm with an average grain size of less than 100 nm with maximum microhardness reaching 155 HV.

Chang et al. [35] suggested a relation between the grain size of friction stir processed *AZ31 Mg* alloys and the Zener-Holloman parameter. Their results have shown that the strain-rate and the working temperature have a great influence on the resulting grain size. Hence, they used the Zener-Holloman parameter to predict the final grain size as a function of strain-rate, temperature and material constants. Then, they calculated the deformation during FSP along with the temperatures and obtained the grain sizes using optical microscopy and scanning electron microscopy (SEM). They made a simple linear assumption that the average material flow to be half the pin rotational speed. The material flow during FSP is related to the pin rotational speed which may be equal or less than the pin rotational speed. They related the grain diameter to the Zener-Holloman parameter during FSP of *AZ31 Mg* alloy by using the experimental results. The empirical relationship between the resulting grain diameter, Zener-Holloman parameter and initial grain diameter was obtained by Darras [1] as given by equations 1.2 and 1.3.

From the above study it is clear that high temperatures and strain-rates are involved in the FSP. Controlling the temperatures during the process in order to refine grains and prevent the grain growth due to thermal cycles demands an aggressive cooling system.

Application of overlapping multiple pass FSP in order to process the sheet fully is itself an innovative idea. But, due to multiple passes, additional thermal cycles are added to the sheet's temperature which affects the grain size. Hence, the effect of different process parameters such as rotational speed, translation feed and the effect of cooling methods have to be investigated to establish this effect on magnesium alloy's mechanical properties.

Most researchers focused on investigating the microstructure and mechanical properties of FSP aluminum alloys. Other important light-weight alloys such as magnesium alloys need to be studied to investigate the effect of various process parameters on the resulting microstructure and mechanical properties.

2.5 Cooling methods for FSP

The multiple pass FSP process results in the generation of high temperature due to multiple thermal cycles created by eight FSP passes. The grains are recystallized after the process of dynamic recrystallization in FSP and the grain size can increase by a process of recovery due to these high temperatures. Hence, to retain ultrafine refined grain, we need cooling of the sheet during the process.

The cooling methods that can be applied in FSP are as follows:

1. Conventional flood cooling underneath the fixture

   In this type, the coolant can be made to pass through the channel of the fixture holding the sheet. A uniform 'S' channel could be used for uniform dissipation of heat. No direct cooling is applied on the work sheet. Swiss Lube-30 is used as the coolant. The coolant is applied during all eight multiple passes on the sheet. An outlet is provided on the fixture to release the coolant.

2. Conventional flood cooling on top and underneath the fixture

This type of cooling could help in proper dissipation of heat from the sheet undergoing high thermal cycles with each FSP pass. Cooling is applied on top of the work sheet in addition to underneath the fixture. Swiss Lube-30 is used as the coolant. The coolant is applied at high rate on the top of the sheet at the tool and sheet interface as well as underneath the fixture as described above. This type of cooling is applied for all eight multiple passes on the sheet.

3. Cryogenic cooling

The high temperature involved in multiple pass overlapping FSP demands an aggressive cooling process such as cryogenic application. It uses liquid nitrogen for cooling the workpiece. Liquid nitrogen can be applied at different positions of the FSP tool and the sheet, as well as, underneath the fixture. The fixture used to hold the plate for processing can be frozen by precooling for sufficient time before running the experiment in order to prevent the growth of small recrystallized grains achieved in this process.

The effects of cooling methods on surface quality of FSP, microstructure and microhardness are studied in detail in this thesis work. After achieving a refined and homogeneous grain structure throughout the sheet thickness, the process parameters and cooling method will be fixed. The next step is to cut disks from these FSP samples and perform orthogonal machining on them under dry, MQL and cryogenic conditions.

2.6 Selection of work material

Due to the shortage of resources and the increase in environmental pollution causing ecological imbalance, there is a dire need to look for alternative materials for some applications. Automotive and aerospace industries reduce the equipment weight by replacing heavy materials by light-weight ones such as glass by plastics and steel by light

metals or plastics. Light-weight materials such as aluminum and magnesium alloys are easier to machine and much stronger than plastics. They can also be easily recycled. Hence, their sustainability performance is more appealing than many other materials from the point of view of the life cycle of a product [37].

Aluminum alloys are extensively used in chassis, motor and the gear system, as well as in the body, in the form of rolled and pressed semi-finished goods and as forged and cast parts. Magnesium alloys, however, have only recently been used to replace aluminum in the automotive industry.

Magnesium has a hexagonal crystal lattice due to which it has poor plasticity at low temperatures, and can only be formed at elevated temperatures (>200°C) [38]. But, these alloys have certain disadvantages such as easy ignition, poor formability, etc [39].

2.7 Cutting tool for machining

Magnesium alloy is an easy to cut material. Hence, many different tool materials could be used for machining magnesium. Therefore, an uncoated carbide tool insert is used [40].

2.8 Machinability of magnesium alloys

Magnesium alloys are relatively easier to machine with respect to tool-wear, cutting force, and power consumption. The cutting forces are very low due to the hexagonal close-packed structure. Cutting temperatures in this alloy are found to be low compared to steels and other high temperature alloys such as titanium, inconel etc., because of its low melting temperature of 600°C. Arai et al. [41] have shown that magnesium alloys provide high quality surface finish even without grinding. High cutting speeds can be used for magnesium ranging from 500 to 1700 m/min. Simple carbide tools can be used for machining these magnesium alloys. Not much machining research has been done on this alloy due to an ignition effect, low strength when compared to other heavy alloys, and also due to the difficulty in the metal forming process. Hence, the current work will

attempt to refine the grain size in order to improve the mechanical properties of magnesium alloys and then to examine its resulting properties from machining.

2.9 Cooling methods for machining

Mg AZ31B-O alloy can be machined by using different cooling techniques. The following are the common cooling methods that have been used in machining different alloys. Cooling is required to retain the refined grain on the machined layer.

a) Water-based flood coolant

Water and a small percent (<5%) of soluble oil is used in the commonly known as water-based cooling. Even though the coolant helps to flush away the chips, the major disadvantages with this cooling method are that it can cause chronic health problems to operators, including cancer, and it is not environmentally friendly due to the problem of its waste disposal in the landfills, rivers etc., and hence, polluting the environment. This is the major reason why this type of cooling is not recommended for machining magnesium alloys [42, 43].

b) Oil-based coolant

Oil-based coolants are used in finishing and fine feed rate operations, and are much safer than the water-based flood coolant. But, the oil mist with the high temperature magnesium chip can still cause ignition. Chip has to be washed after the process for recycling, and hence, it is not sustainable [42, 43].

c) Dry machining

Dry machining is a sustainable process as there is no need for any coolant. But, the cutting speed and feed have to be within prescribed limits in order to avoid ignition and prevent undesirable microstructural changes. It is an environmentally friendly process

due to the absence of any coolant. Chips can also be easily recycled. Hence, it is a sustainable process [42, 43].

d) Minimum Quantity Lubrication (MQL)

A fine mist or spray of oil-based fluid is used for the lubrication of the tool-work piece interface which facilitates smooth cutting of the workpiece. This is eco-friendly and sustainable process as the cooling is in the form of spray, and hence, the pollution caused by flood coolant is avoided. Spray helps to avoid the ignition at high cutting speeds.

e) Cryogenic coolant

Liquid nitrogen helps in reducing the work temperature, and thereby suppresses the grain growth of the recrsytallized grain structure. The coolant is generally applied at the flank side of the cutting tool insert. The process is highly sustainable as nitrogen is environment friendly with a ventilation outlet provided for nitrogen gas outlet as high amounts can cause breathing problems. Application of low temperature jet of nitrogen helps in generating good surface finish, micro structure, microhardness and residual stress values. But, excess of liquid nitrogen can cause suffocation in breathing. The equipment is turned off during the loading and unloading time of the workpiece to avoid suffocation and the waste of liquid nitrogen. It is an environmentally friendly method as no flood coolant is used for disposal as waste. *ICEFLY®* cryogen delivery system from Air Products Inc. was used for the liquid nitrogen application in machining reported in this thesis. The *ICEFLY®* cryogen delivery *system* enables intense cooling through the delivery of a cryogen via a "tube-in-tube" configuration.

2.10 Cutting speed and cutting temperature

Fang et al. [39] used magnesium alloy *AZ91* as work material for machining with micro-grain tungsten carbide tools. They studied the mean temperature on the flank face by conducting high speed dry milling of magnesium alloy to evaluate the safe cutting speed

so that the temperature does not exceed the melting point to cause ignition. The temperature was detected by using a thermocouple. They observed the chips using the SEM and found no burn marks at the cutting speed of 816 m/min and undeformed chip thickness of 9 µm. The measured mean flank temperature was 302 ℃. They concluded that it is easy to predict fire occurrence by flank temperature. Hence, it is necessary to use medium range of cutting speeds in order to avoid the ignition problem. The cutting forces generated are extremely small, *Mg* alloy being a light-weight alloy, when compared to steels, etc. Magnesium has a low melting temperature of 600 °C and when the temperature (400 – 600 ℃) is exceeded there is a danger of fire ignition [41, 45].

Tönshoff and J. Winkler [38] observed the interactions between workpiece material and tool coating material, respectively by performing the turning experiments on *AZ91 HP* alloy. They found that dry machining of magnesium at cutting speeds over 900 m/min, flank build-up due to adhesion between the cutting tool and the workpiece occurs.

Hence a medium range of cutting speed values, i.e. 50 – 350 m/min were used for machining the workpiece in the current work. Friction stir processed, and as-received disks were machined under the same conditions to allow the comparison of the obtained data.

CHAPTER 3

FRICTION STIR PROCESSING (FSP) EXPERIMENTS

3.1 Introduction

The FSP experiments are carried out on the 115 mm X 115 mm X 3 mm *Mg AZ31B-O* sheet. The research plan, experimental set-up, experiments and the microstructure results are discussed in the following sections.

3.2 Research plan

Figure 3.1 shows the research plan for this thesis project which consists of machining FSP disks as well as as-received, AR disks in order to have a good comparison between the results of machining experiments carried out using the same cutting parameters. A commercial magnesium alloy *AZ31B-O* in the form of 3.22 mm (0.25 in) thick, cut from an O-temper heat treated sheets, which is fully annealed sheet have been used in this study. The nominal composition of the *Mg AZ31B-O* alloy (weight percentage) is shown in Table 3.1 [46].

Table 3.1: Composition of *Mg AZ31B-O* alloy

Component % by Weight		
Mg - 97	*Fe* – Max 0.005	*Ni* – Max 0.005
Ca – Max 0.04	*Al* – 2.5 - 3.5	*Si* – Max 0.1
Cu – Max 0.05	*Mn* – 0.2	*Zn* – 0.6-1.4

This research plan consists of two stages. The first stage deals with the friction stir processing and the second stage involves the orthogonal machining of the FSP disk. *Mg AZ31B-O* alloy sheet is fully processed by multiple overlapping FSP processing passes while using different cooling techniques such as flood cooling, cryogenic cooling at tool and sheet interface, as well as, underneath the fixture. The other process parameters that

are varied are the translational and the rotational speeds of the tool to attempt to generate small grains with a homogenous grain structure throughout the sheet thickness. Both of these characteristics improve the superplastic formability, corrosion resistance, surface integrity and induce high hardness values in this alloy. The stirring conditions of speed and feed and machining conditions are later fixed while attempting to obtain better experimental results which give more refined and uniform grain size throughout the sheet thickness. Thirty six FSP sheets are obtained at these fixed conditions. There was more variation of the grain size than we would like to have obtained.

The second stage of the research work is to cut circular disc specimens from the FSP sheets, as well from the AR material, in order to conduct the orthogonal machining experiments using different cooling/lubrication conditions, i.e., cryogenic machining, minimum quantity lubrication, and dry machining. The cutting parameters, i.e., feed and cutting speed used are varied so as to attempt to produce ultra fine grains which in turn impart high hardness and high residual stress values to the surface of the machined disk. These mechanical properties are critical to increase the fatigue life of the disk that may influence the functional performance of a final product. Cutting forces are measured during the machining experiments. Microstructure and microhardness results are measured after the FSP of the sheet and after the machining tests.
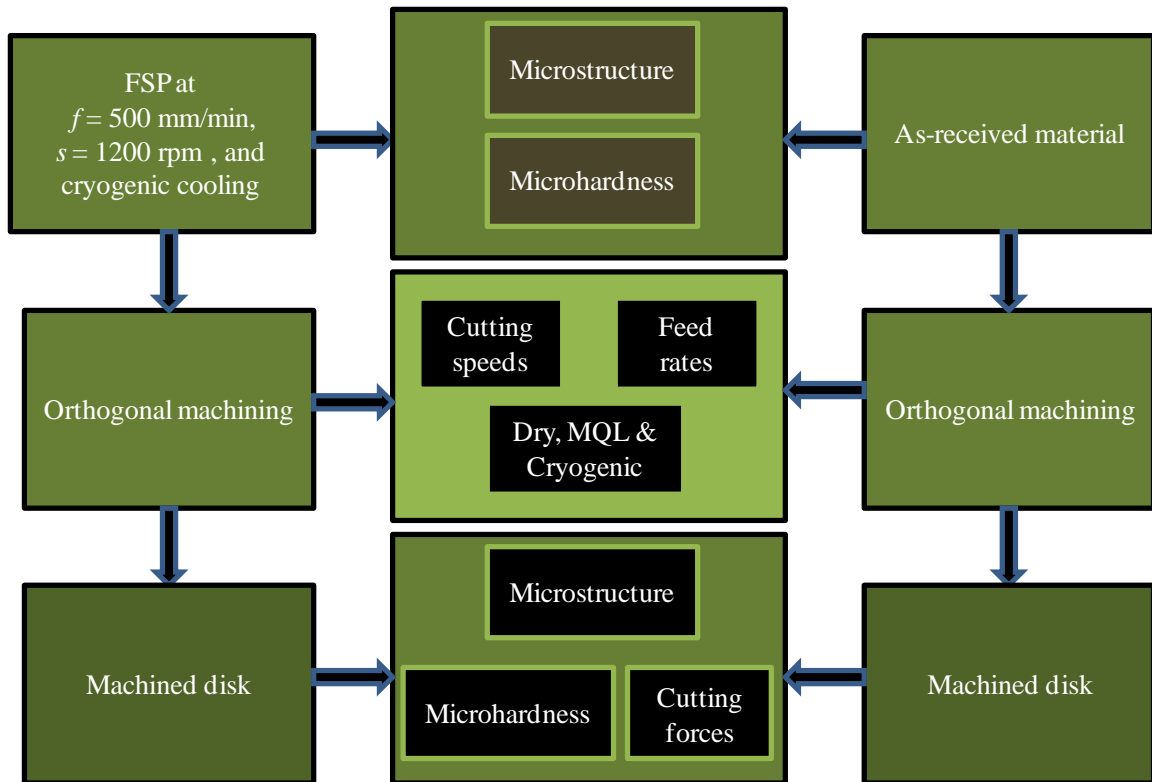
Figure 3.1: Research plan for the machining of FSP and AR *Mg AZ31B-O* alloy

3.3 Experimental setup

Fully annealed magnesium alloy, *Mg AZ31B-O* is used in the experimental work. Specimens of dimensions 115 mm X 115 mm X 3 mm are cut using a shearing machine from 1200 mm X 1200 mm X 3 mm sheet purchased from Magnesium Elektron North America, Inc. The fixture used to hold the sheets is made out of hardened steel and is shown in Figure 3.2 (a). It consists of a special made 'S' shaped cooling channel located at the back side of the fixture shown in Figure 3.2 (b). This process uses a very simple tool with a shoulder and a pin on one end. A flat-pin tool for FSP made of H13 tool steel as shown in Figure 3.3 (a). Its dimensions are 19.1 mm shoulder diameter, 6.4 mm pin diameter, and the height of the pin is 2.5 mm (slightly shorter than the 3 mm thickness of the sheet). Eight overlapping passes are made on the sheet, with 50% tool overlap between consecutive passes. The real challenge lies in achieving the homogeneous and refined grain structure throughout the sheet's thickness.

In order to achieve refined and homogeneous grain structure, different cooling techniques are used. These include cooling underneath the fixture, flood cooling on top of the sheet, cryogenic on top as well as underneath the fixture. A combination of these applications is used at different processing conditions of feed f = 300, 400, 500 mm/min and rotational speed s = 1000 and 1200 rpm. These sets of experiments are performed on a HAAS milling machine equipped with a flood cooling system and a cryogenic cooling system.
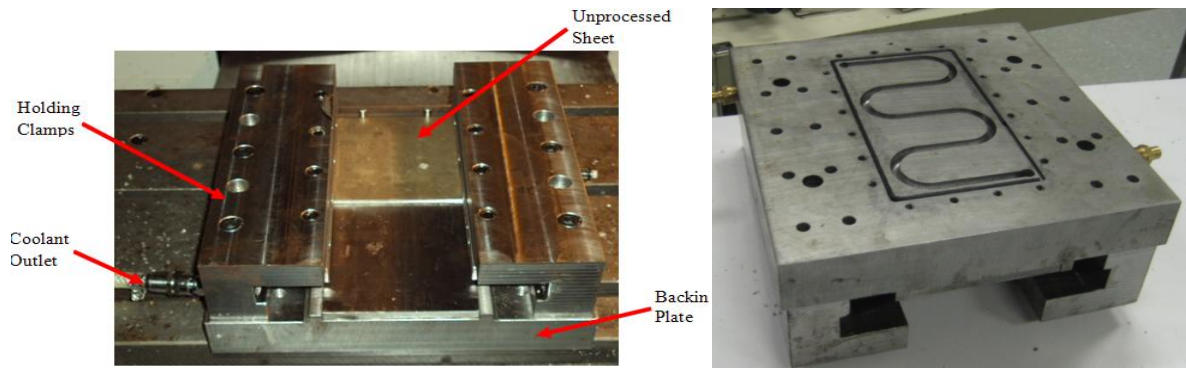
Figure 3.2: (a) Fixture with sheet   (b) Fixture cooling channel

Figure 3.3: (a) Flat pin-   (b) FSP passes
tool used for the experiments
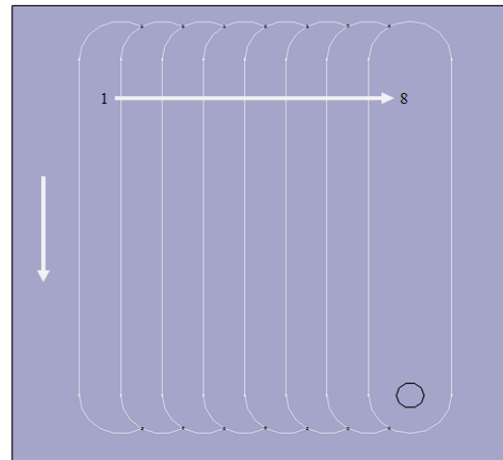
The selection of translation feed f and rotational speed s is made using the results obtained by Darras [1] in his PhD dissertation on the same Mg alloy. According to his results, a smaller grain size and a processed sheet without any cavities and good surface

28

finish was obtained using certain conditions. The results of this process are very sensitive to the stirring conditions used and their effects change from material to material. The stirring conditions which may have a positive influence on *MgAZ31B H* alloy which is partially annealed, may have a negative influence on *Mg AZ31B-O* alloy. As seen from the Table 3.2 from Darras [1], the smaller grain sizes are obtained from f = 300, 400 and 500 mm/min and s = 1000 and 1200 rpm. Hence, a combination of these processing parameters are used herein.

Table 3.2: Average grain size from different processing conditions [1]

Rotational speed (rpm)	Translational speed (mm/min)	Average grain size (µm)
1000	300	5.2
1200	300	6.1
1750	300	8.1
2500	300	14.4
1200	200	5.8
1200	400	5.4
1200	500	4.7

Figure 3.4 shows a pictorial view of the eight multiple pass, MP, FSP process with 50% overlap between consecutive passes. The face of the sheet in contact with the tool is denoted as Face 1 (top surface) and the other face (bottom surface) of the sheet as Face 2. The tool is rotated in the spindle by means of a tool holder and when it plunges into the sheet, a translational feed is given to complete the process. The 50% overlap between successive passes was selected to ensure that the sheet is processed fully. A, B, C in Figure 3.4 denotes three different sample positions for the observation of material microstructure and microhardness after FSP. Some burrs are formed on the sheet during FSP. Those burrs are removed in a later stage by the grinding machine when the circular disks are cut out from these processed sheets. For the ease of explanation, multiple pass is abbreviated to MP in the following sections.
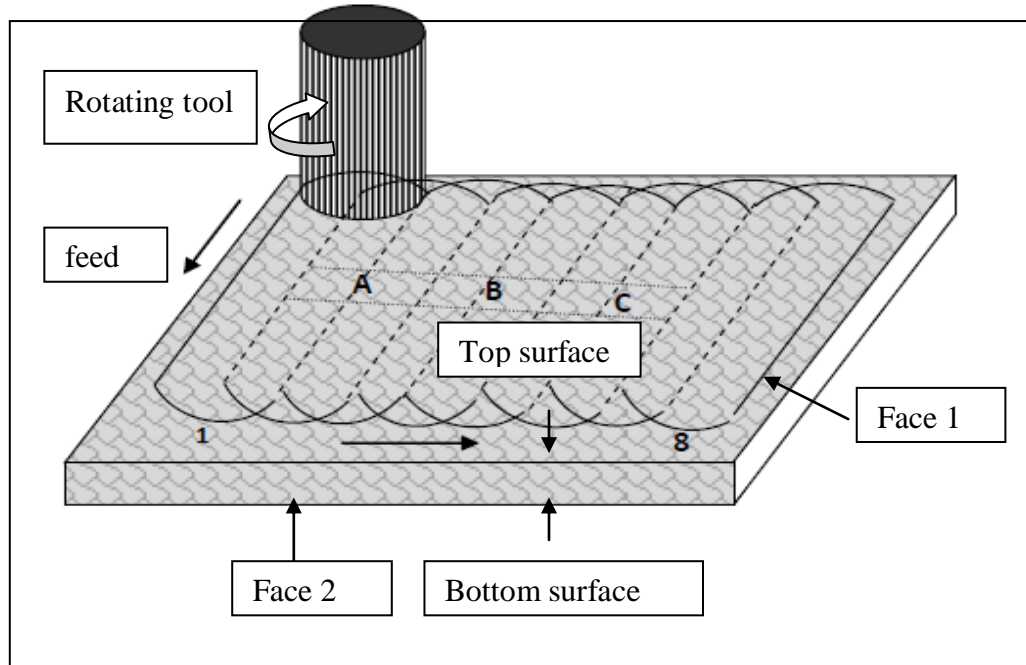
Figure 3.4: Pictorial view of multiple-pass (eight-pass) friction stir processing

3.4 Description of the metallographic examination

The following describes the different steps involved in the metallographic examination of the samples. First, the equipment used is listed and then the procedure is described in detail.

3.4.1 Equipment used

A Struers-Discotom-5 grinding wheel is used for cutting a small portion from the machined sheet for mounting as a specimen in order to study the metallurgical microstructure. Struers cold mounting with acrylic epofix resins with epofix hardener is used for preparing the mould for holding the sample, while a Struers grinding and polishing machine (Rotoforce-3, Multi Doser, Rotopol-25) is used for grinding and polishing the specimens. A Nikon Epihot microscope is used for microstructural observation at various magnifications.

3.4.2 Description of procedure

In order to observe the microstructure, the following steps are taken for all specimens:

1. The sheet is cut into small samples by using Struers sample cutting machine using the prescribed grade of cutting disk, which is 36 TRE grade for cutting the Mg alloys. The sample is cleaned of all impurities using the ultrasonic cleaning machine.

2. The sample is removed from the ultrasonic machine and cold mounted using Struers epoxy resin and epoxy hardener. The resin is thoroughly mixed with epoxy hardener for 3 minutes and is left for 2 minutes. It is then poured into the sample mould. The mould is left to dry for 24 hours. Then, the sample is removed from the mould and cleaned using the ultrasonic machine.

3. Four samples at a time are placed on a horizontal plane using a Struers sample holder on a Struers sample positioning instrument to maintain the horizontal level of the samples.

4. The samples are polished on Struers grinding and polishing machine using sand papers ranging in grades from 320, 500, 800, 1200, 2000 and 4000 with water as a lubricant to eliminate surface scratches which are found in this kind of soft material.

5. MD largo is used for grinding the surface using 3 µm abrasive without any water.

6. MD mol is used for polishing with 1 µm abrasive without any water.

7. The samples are washed clean with soap water and alcohol after each grinding and polishing step, followed by drying using high pressure air.

8. After finishing and polishing, it is etched using picral solution for 30 seconds for original material and 45 seconds for FSP material. The different etching times are used because the etching time of 30 seconds does not work on the FSP sample.

9. The microstructure is observed under the optical microscope at a magnification of 500X. A Nikon Epihot microscope is used to observe the microstructure at 200X and 500X magnifications and capture the microstructure images.

The sample preparation is discussed in detail in the following section and these activities can be classified as:

- Mounting
- Grinding
- Polishing
- Etching

Samples are cut using the Struers Discotom-5 cut off wheel which uses abundant water based coolant so as to not change the microstructure and properties of the material. Compatible grade of cutoff disk is to be selected based upon the hardness of the materials to be cut. (e.g., Mg alloys require Grade 36TRE). They are cleaned using ultrasonic cleaning equipment to remove any dirt particles accumulated during the cutting process.

(i) Mounting the specimen

Specimens of 30 mm diameter are cold mounted since Mg alloy is a soft material with a melting temperature around 672 ºC and the temperature in hot mounting goes up to 550 ºC which may affect the properties of the alloy. Hence, cold mounting is used to eliminate possible effects of high temperature. Cold mounting takes 24 hours for the sample to dry. The resin used is epofix resin with a hardener. They are mixed in the ratio of 25:3 by weight where 25 parts are of resin and 3 parts are of hardener. The mixture is thoroughly stirred for 3 minutes and left to stabilize for 2 minutes. Then, Struers vacuum unit is used to eliminate the air bubbles, by creating a vacuum and then the liquid is

poured into the mould. The specimens are removed from the mounting after 24 hours, when it has dried out. They are then prepared for the next stage of operation.

(ii) Grinding and polishing the specimen

Four specimens are firmly held in Struers sample holder using the Struers positioning instrument in order to have all the specimens on the same horizontal level which is required for proper grinding and polishing of the specimens. These specimens are then coupled to the spindle of the Struers Rotoforce equipment that rotates and holds the specimen on various grinding and polishing papers. Sand papers are held on the rotating grinding disk using a cover, and magnetic disks are held magnetically on the rotating grinding disk. The procedure for grinding and polishing of this alloy is selected from Struers apparatus which has separate procedures for the different materials that are to be examined. These procedures are stored in the automated program of Multidoser and Rotopol that are a part of the equipment and that controls the lubrication during the actual polishing process. The program is retrieved, the bottles with necessary lubricants are set up, and the various grades of grinding and polishing paper are made available in the order specified. At the end of use of each grinding or polishing step, the specimens are cleaned with soap water and alcohol and then dried using compressed air. The forces and the polishing times can be changed in the system before the process starts using auto or manual modes depending upon the number of samples, as mentioned by the Struers website. The force value used for grinding these four samples is 200N and the grinding and polishing time is 2 minutes each. The program for Mg alloy is retrieved and used for all the samples reported herein.

(iii) Etching the sample

The samples are etched using the picric acid and alcohol solution which is the specified etchant for Mg alloys. The etching time is fixed at 30 seconds for AR material sample and 45 seconds for FSP sample and after etching, they are washed and cleaned with alcohol and water. The compressed air is used to dry the sample after etching.

The original microstructure of unprocessed *Mg* alloy sheet is observed throughout the thickness of the sheet and it has an average grain size of 10 µm, and is found to be uniform throughout the sheet thickness. Figures 3.5 (a) and 3.5 (b) show the original microstructure obtained at a magnification of 500 X at different positions across the sheet thickness. In the micrograph, we can see the black spots which are the *Al*, *Zn* and *Si* alloying elements. The average grain size was obtained by using *ImagePro* software by taking the measurements at different positions in the sample.
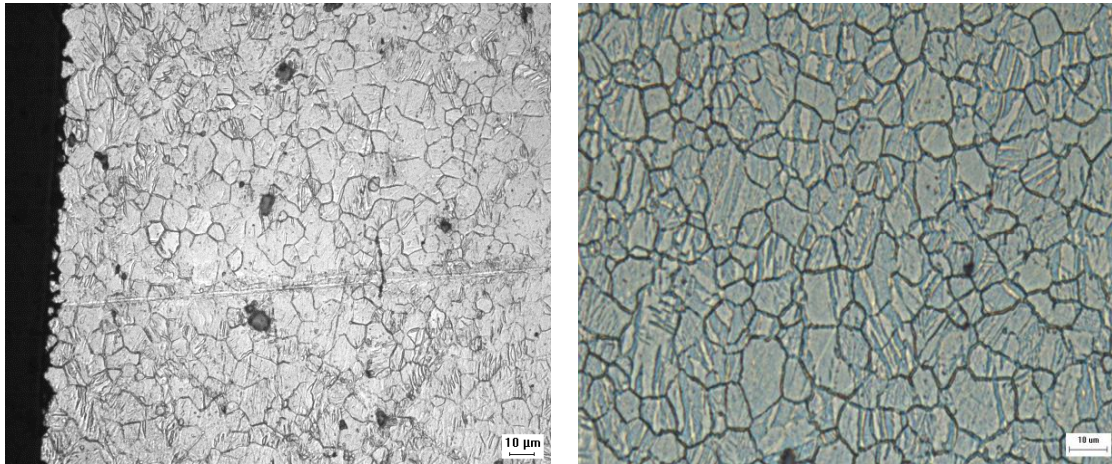
Figure 3.5: (a) Original microstructure at 500 X magnification near the top region of *Mg AZ31B-O* alloy sheet

(b) Original microstructure at 500 X magnification near the middle region of *Mg AZ31B-O* alloy sheet

3.5 Experimental work

FSP experiments are carried out at different cooling conditions on the *Mg* sheet and for different processing parameters. Experiments designated as MP (1-sided) and MP (2-sided) with cooling underneath the fixture, flood cooling, and cryogenic cooling at different positions of top and underneath the fixture are investigated for their microstructure and the microhardness results.

3.5.1 MP (1-sided) with Swiss Lube coolant underneath the fixture

The sheet is fully processed with multiple passes (8) and processing on one side of the sheet (1- sided). It is processed by applying the Swiss Lube coolant to the S-channel (under the central portion of the fixture) as shown in Figure 3.2(a). During the process, the condition of sheet material is observed during each subsequent pass. Large magnesium chips are formed, which is an indication of high heat being generated at the tool and sheet interface due to friction or due to the large contact force between the tool and the sheet at the interface. The processed sheet is shown in Figure 3.6. The metallographic examination is done by cutting the sample from the center of the pass at sections shown in Figures 3.4 and 3.7. The microstructure is observed across the thickness of the sheet to analyze the effect of the process. The microstructure images are obtained using a Nikon Epithot microscope at a magnification of 500 X as shown in Figure 3.8. The observation of the microstructure indicates that the increase in grain size from an average 10 µm in the original material to an average 14 µm in Figures 3.8(a)-(d). There is a grain growth due to the heat generated during the process with a non-homogeneous grain structure through the thickness. The grain size of the sheet is refined by the process of dynamic recrystallization, DRX as described in Chapter 1, but due to the unavailability of enough cooling in the sheet surface the grain size increases. The grain size variation from bottom to top shows an increase, at the bottom the average grain size is 12 µm and 20 µm at the top. The variation in grain size across the thickness of the sheet is likely due to the temperature gradient which exists due to the non uniform temperature distribution and the varying strain-rate distribution across the thickness of the sheet.

Figure 3.6: Processed sheet at $f = 500$ mm/min and $s = 1200$ rpm

Three different samples are cut from sheets at different positions throughout the cross section as shown in Figure 3.7 at positions denoted by numbers 1, 2 and 3.

Figure 3.7: Samples 1, 2, 3 taken from the processed sheet at the locations indicated

(a)

(b)

(c)

(d)

Figure 3.8: Microstructure throughout the depth of the sheet from bottom to top surface at 500 X magnification and the stirring conditions of f = 500 mm/min and rotational speed s = 1200 rpm (a) Bottom region, (b) Middle region- 1, (c) Middle region- 2, (d) Top region

3.5.2 MP (2-sided) with Swiss Lube coolant underneath the fixture

The sheets are processed on both sides. First, the sheet is fully processed on one side as described above in process MP (1-sided) with Swiss Lube coolant and it is then flipped and processed on the other side using the same stirring conditions. The resulting grain size is shown in Figure 3.10. The resulting grain size is larger than that obtained through Section 3.5.1 MP (1-sided) with Swiss Lube coolant and highly inhomogeneous as well. The average grain size is 12 µm average on the top and 10 µm on the bottom surfaces, but, in the middle section it has an average grain size of 20-25 µm. The sheet is processed in three different ways on the other side: in the same direction as the first side, in the opposite direction of the first side and in transverse direction. However, the grain size is similar in all three of these processes.

Figure 3.9: (a) Multiple pass two sides, side 1   (b) side 2

(a)   (b)

(c)   (d)

Figure 3.10: Microstructure throughout the depth of the sheet from bottom to top surface at 500 X magnification and the stirring conditions of $f = 500$ mm/min and rotational speed of $s = 1200$ rpm (a) Bottom region, (b) Middle region- 1, (c) Middle region- 2, (d) Top region

3.5.3 MP (1-sided) with flood coolant on top and underneath the fixture

Swiss Lube is applied as a flood coolant on top, as well as underneath the fixture for a better grain size as shown in Figure 3.11. Such a process was used in order to take away the heat generated during the process, and in attempting to create a homogeneous and refined grain structure. There is no melting of material observed during the process and the observed microstructure results are shown in Figure 3.12, which shows that there is some change in grain size compared to Section 3.5.1 MP 1-sided with Swiss Lube coolant and Section 3.5.2 MP (2- sided) with Swiss Lube coolant, but it is not a

significant change. The surface temperature is measured approximately in this case to roughly estimate the time the sheet takes to return to room temperature after each pass using a thermocouple as a sensor. It takes approximately 45 seconds for the sheet to return to normal room temperature after each processing pass when flood cooling is applied. Therefore, the next pass is made after a waiting time of 45 seconds. The grain size in the bottom region is more refined than in the top region and it is of 7 µm average, in the middle region it is 9 µm and in the top region it is 10 µm average.
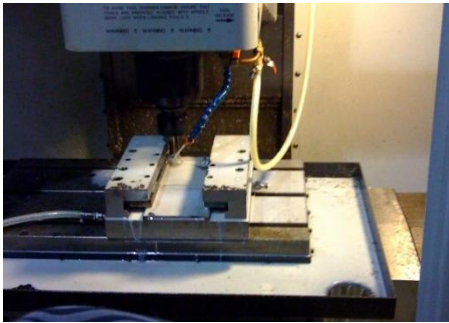
Figure 3.11: (a) Experimental set up of flood cooling

(b) Processed sheet

(a)   (b)

(c)   (d)
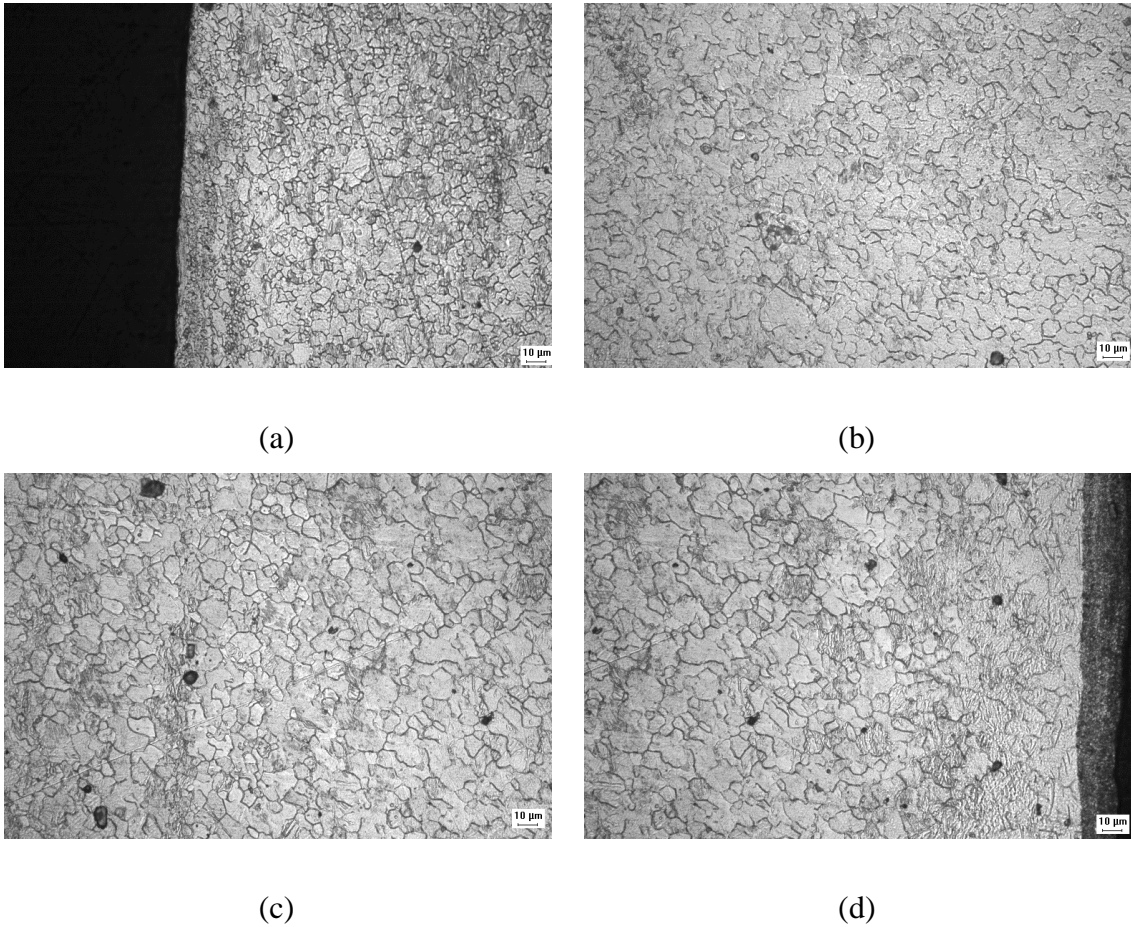
Figure 3.12: Microstructure throughout the depth of the sheet from bottom to top surface at 500 X magnification and the stirring conditions of $f = 500$ mm/min and rotational Speed of $s = 1200$ rpm (a) Bottom region, (b) Middle region- 1, (c) Middle region- 2, (d) Top region

3.5.4 MP (1-sided) with flood coolant and 45 seconds waiting time between successive passes

The sheets are processed with a waiting time of 45 seconds after each pass in order to allow the sheet to return to room temperature. There was no melting and no visible surface defects observed and the processed sheet appears to have a smooth surface finish. Smaller size grains when compared to those of Section 3.5.3 MP (1-sided) with flood coolant on top and underneath the fixture are obtained on the top region of the sheet which received the flood cooling, even though the microstructure is not homogenous through the thickness as shown in Figure 3.13. The grain size in the bottom region is

more refined than in the top and the middle region and it is 3-5 µm average there, while in the middle region it is 7-10 µm and in the top it is 10 µm on average.
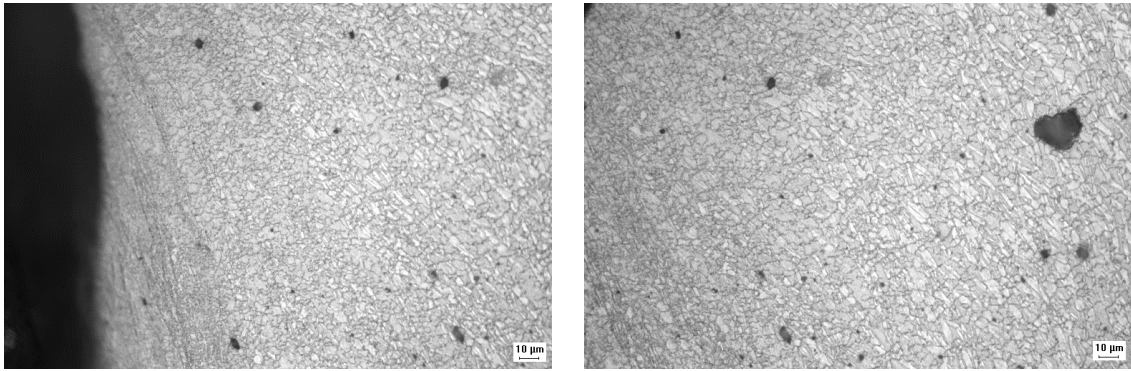
(a)

(b)
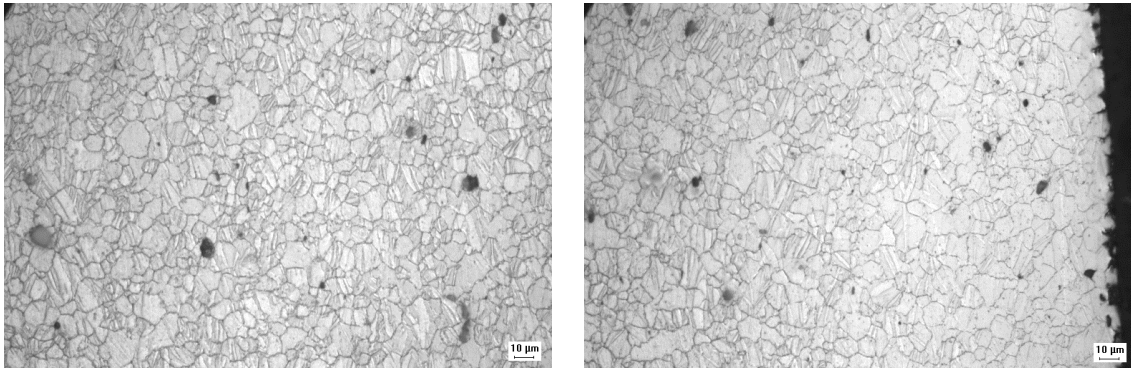
(c)

(d)

Figure 3.13: Microstructure throughout the depth of the sheet from bottom to top surface at 500 X magnification and the stirring conditions of $f = 500$ mm/min and rotational speed $s = 1200$ rpm (a) Bottom region, (b) Middle region- 1, (c) Middle region- 2, (d) Top region

3.5.5 MP (2-sided) with Swiss Lube flood coolant and 45 seconds waiting between passes

The sheet is processed on both sides under the same stirring conditions and same waiting time of 45 seconds between passes and using flood cooling on both surfaces. No melting is observed and the sheet obtained is apparently free from defects and cavities with a

smooth surface finish. A small grain structure is obtained near the bottom region which experienced flood cooling, but the grain structure is similar to that observed in specimens processed as described in Section 3.5.4 MP (1-sided) with flood coolant and 45 seconds waiting time between each pass, as shown in Figure 3.14.
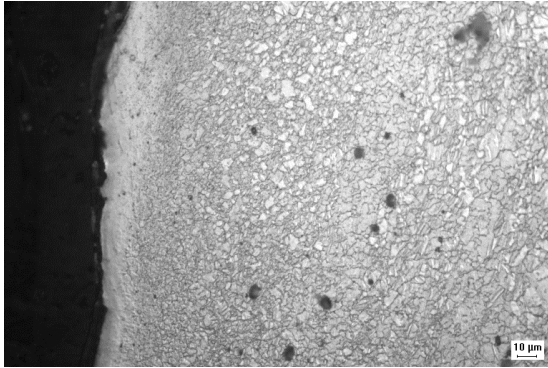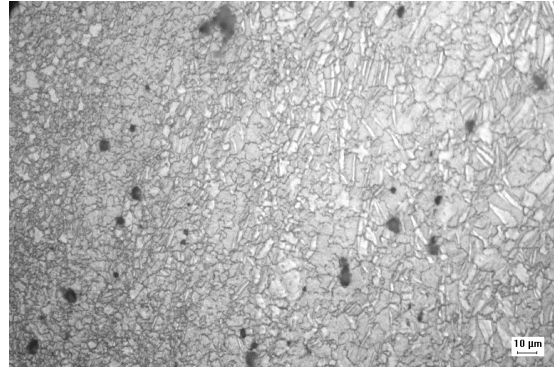
(a)   (b)
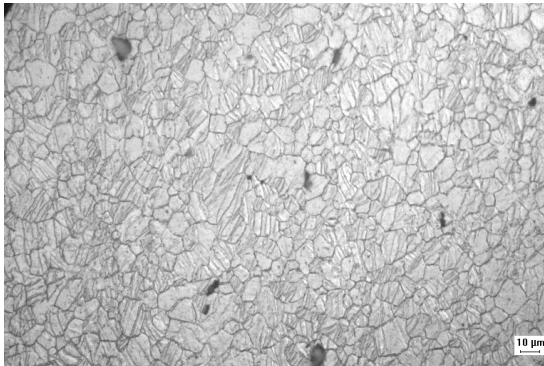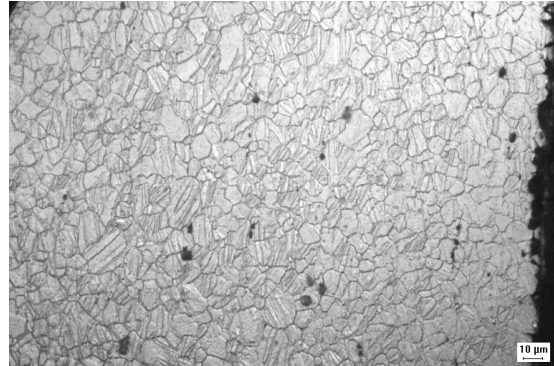
(c)   (d)

Figure 3.14: Microstructure throughout the depth of the sheet from bottom to top surface at 500 X magnification and the stirring conditions of $f = 500$ mm/min and rotational speed of $s = 1200$ rpm (a) Bottom region, (b) Middle region- 1, (c) Middle region- 2, (d) Top region

3.5.6 MP with cryogenic cooling on top and Swiss Lube coolant underneath the fixture

Liquid nitrogen is applied only on the tool-sheet interface via a nozzle. The jet is applied at the back of the tool sheet interface, at the front and also on the side, on different sheets shown in Figure 3.15. No melting of the sheet is observed and the processed sheet is free from observable defects and has a nice surface finish. The observed grain size is not better than that obtained using Section 3.5.5 MP (2-sided) conditions with Swiss Lube coolant and 45 seconds waiting between each pass and is more inhomogeneous, as shown in Figure 3.16. This is due to insufficient quantities of liquid nitrogen cooling actually reaching the critical points in the plate in order to retain the refined grain structure. Restricting and applying the jet exactly at the interface of the tool and sheet is a challenge. The cryogenic cooling on top and the Swiss Lube underneath the fixture was not enough to reduce the growth of the recrystallized grains, and hence, the grain size obtained is large. The grain size is in the range of 10-20 µm at different positions. Therefore, for the next process, the cryogenic cooling is applied only underneath the fixture to check and compare the results. The fixture is cooled before being used to process the material by letting the liquid nitrogen pass underneath the fixture for 15 minutes.

(a)   (b)   (c)
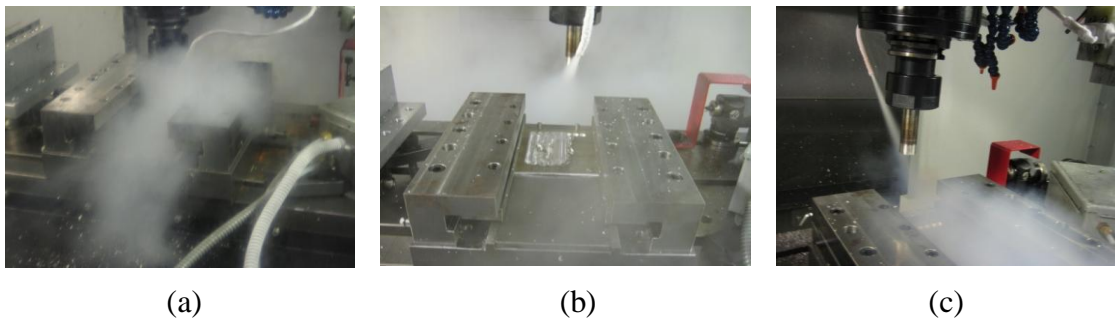
Figure 3.15: Cryogenic cooling applied at (a) side, (b) front, and (c) back of the tool sheet interface
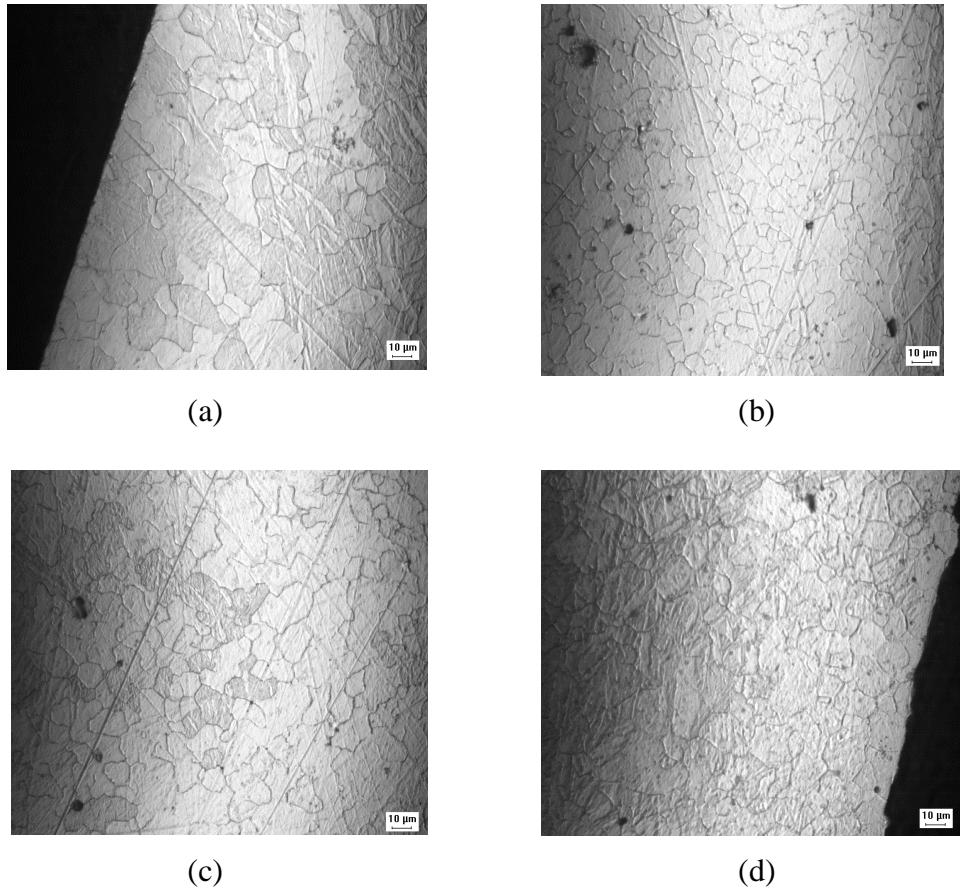
Figure 3.16: Microstructure throughout the depth of the sheet from bottom to top surface at 500 X magnification and the stirring conditions of f = 500 mm/min and rotational speed of s = 1200 rpm (a) Bottom region, (b) Middle region- 1, (c) Middle region- 2, (d) Top region

3.5.7 MP with cryogenic cooling underneath the fixture (bottom)

Liquid nitrogen is only applied underneath the fixture and the experimental setup is shown in Figure 3.17(a). The coolant is passed using a system of low temperature-resistant tubing through the inner S-channel underneath the fixture. The fixture is precooled for 15 minutes and the resulting grain size and microhardness show a better trend than in Section 3.5.6 MP process which uses the cryogenic cooling on top and Swiss Lube coolant underneath the fixture, as shown in Figure 3.18. Very small grains in the range of 0.5-2 µm are observed in the bottom region of the specimen, about 150 µm from the surface and microhardness values in the range of 80-90 HV are also obtained in

that region. However, the overall sheet grain structure is not homogeneous in the thickness direction, and hence, a hybrid technique of using flood cooling on top and cryogenic cooling on the bottom surface is attempted next.

Figure 3.17: (a) Cryogenic cooling applied underneath   (b) processed sheet
the fixture

(a)   (b)
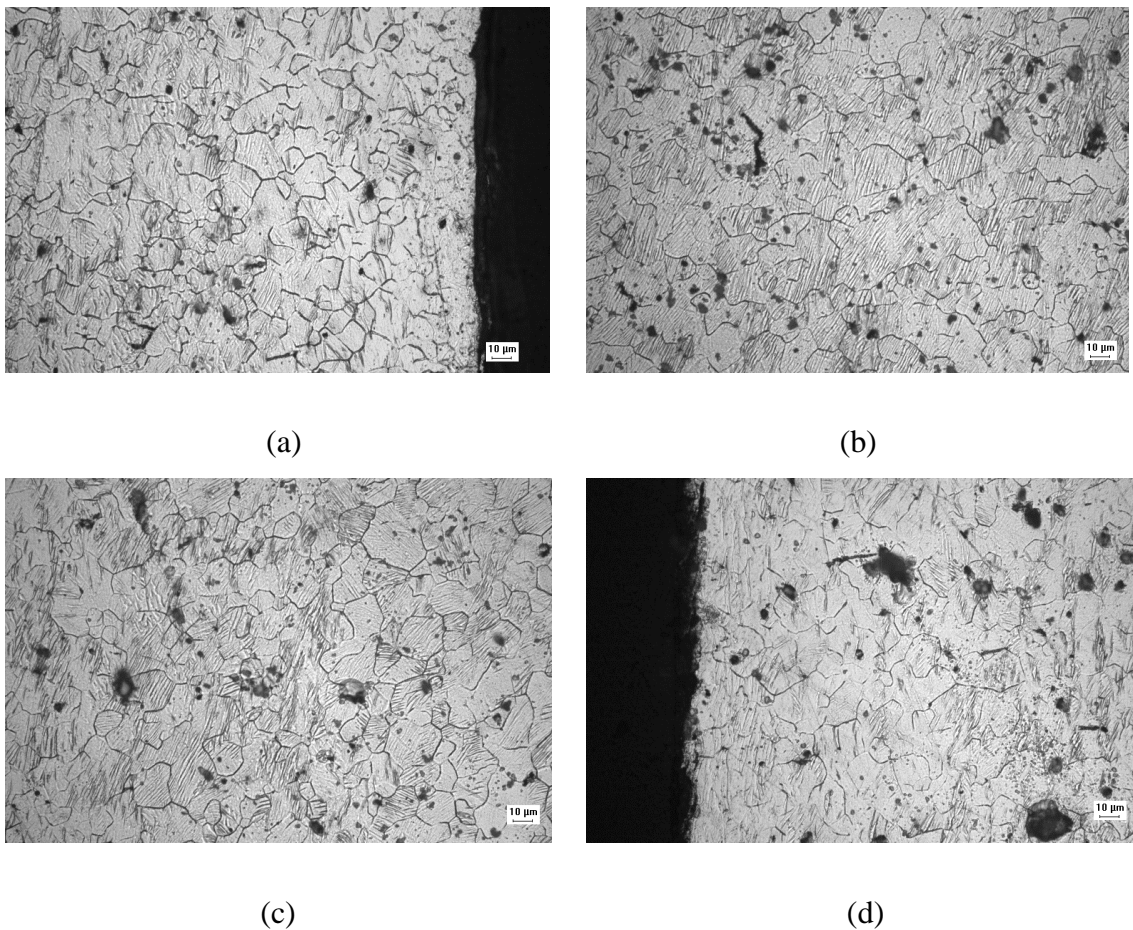
(c)   (d)
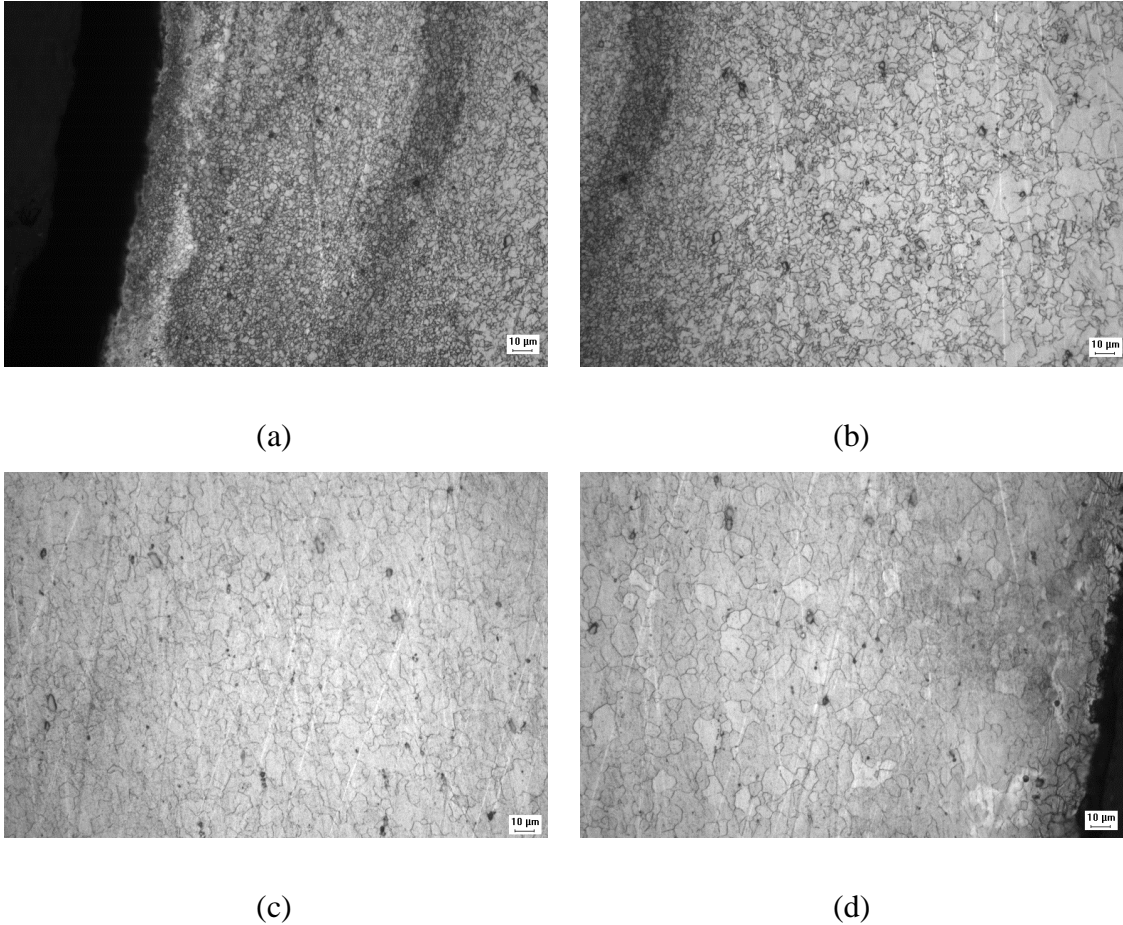
Figure 3.18: Microstructure throughout the depth of the sheet from bottom to top surface at 500 X magnification and the stirring conditions of $f = 500$ mm/min and rotational speed of $s = 1200$ rpm (a) Bottom region, (b) Middle region- 1, (c) Middle region- 2, (d) Top region

3.5.8 MP with flood cooling (Swiss Lube) on top and cryogenic cooling underneath the fixture (bottom)

Flood coolant was used on the top surface and cryogenic cooling on the bottom surface, which is underneath the fixture, as shown in Figure 3.19. The resulting grain size of this hybrid cooling process gives an average of 4.5 µm. The grain size is not as small as previously obtained in Section 3.5.7 MP process with cryogenic cooling underneath the fixture (bottom) but it is more uniform in the thickness direction.
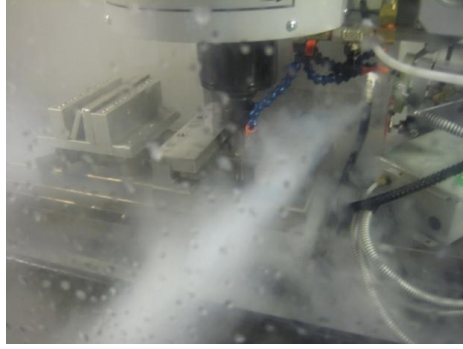
Figure 3.19: (a) Cryogenic cooling applied underneath the fixture (bottom) and flood cooling on the top surface

(b) processed sheet
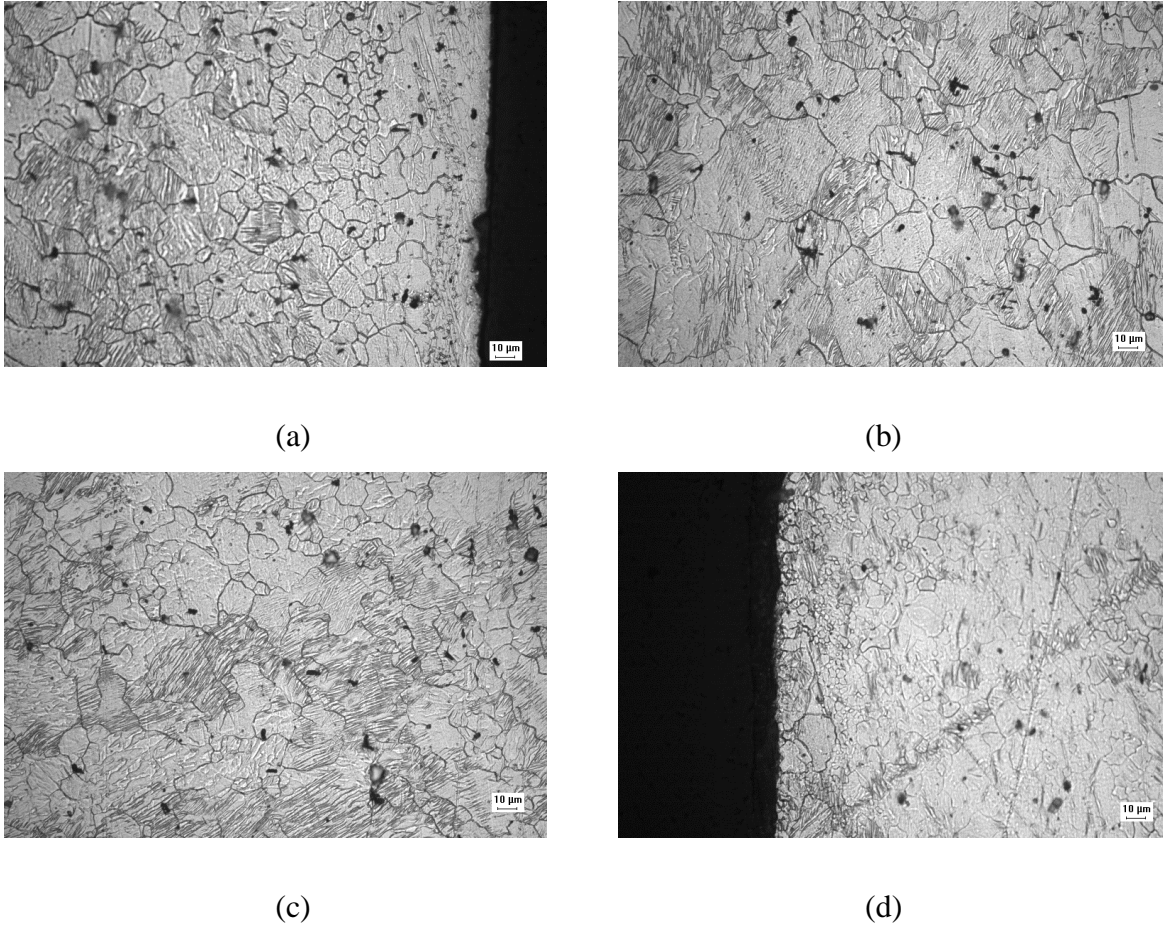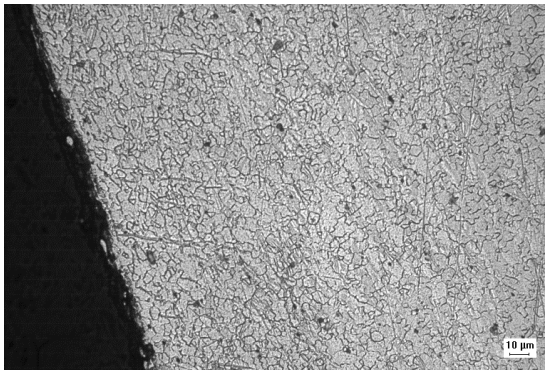

(a)
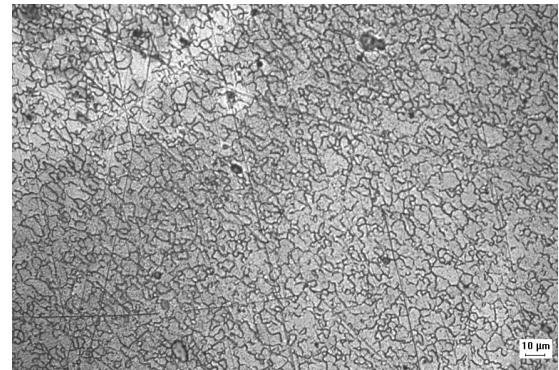
(b)
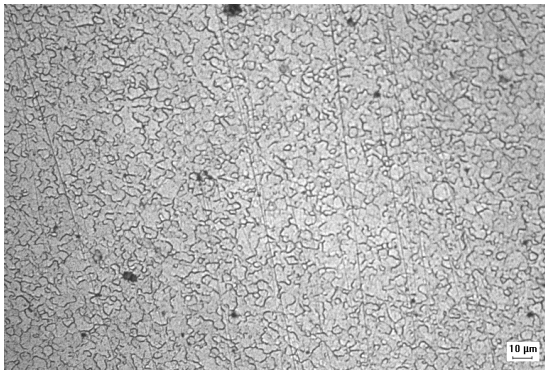
(c)
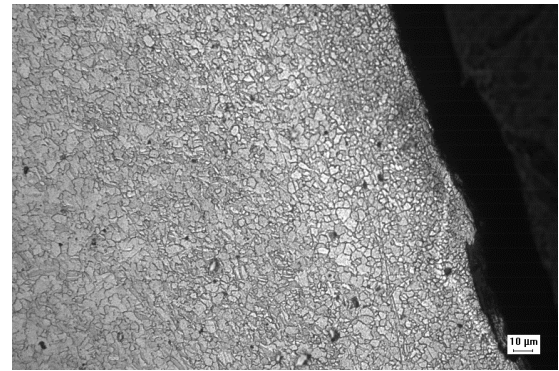
(d)

Figure 3.20: Microstructure throughout the depth of the sheet from bottom to top surface at 500 X magnification and the stirring conditions of $f = 500$ mm/min and rotational speed of $s = 1200$ rpm (a) Bottom region, (b) Middle region- 1, (c) Middle region- 2, (d) Top region

3.5.9 MP with cryogenic cooling on top as well as underneath the fixture (bottom)

Liquid nitrogen is applied on the top surface as well as at the bottom of the fixture by freezing the fixture for 15 minutes prior to use, in an attempt to produce more uniform and smaller grain size. Figure 3.21 shows the experimental setup and the processed sheet surface. The resulting microstructure is shown in Figure 3.22. The grain size is large at the stirring conditions of f = 300, 400 mm/min and s = 1000 rpm, while a small and homogeneous grain structure is observed at a stirring condition of f = 500 mm/min and s = 1200 rpm. As shown in Figure 3.22, the obtained grain size is much smaller and more refined, and also more homogenous than what was obtained in Section 3.5.8 MP with Flood Cooling (Swiss Lube) on Top and Cryogenic Cooling Underneath the Fixture (bottom). The grain size near the bottom region for about 150 µm from the bottom surface is very fine, and is about 0.5-1 µm, and the average grain size in the middle region is about 3-5 µm while at the top region it is 8-10 µm.
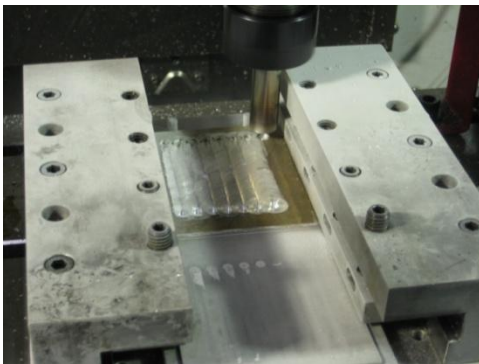
| (a) | (b) |

Figure 3.21: (a) Experimental setup for the cryogenic cooling
on top and bottom FSP with the frozen fixture, (b) Processed sheet at stirring conditions
of f = 500 mm/min and s = 1200 rpm

(a)

(b)

(c)

(d)
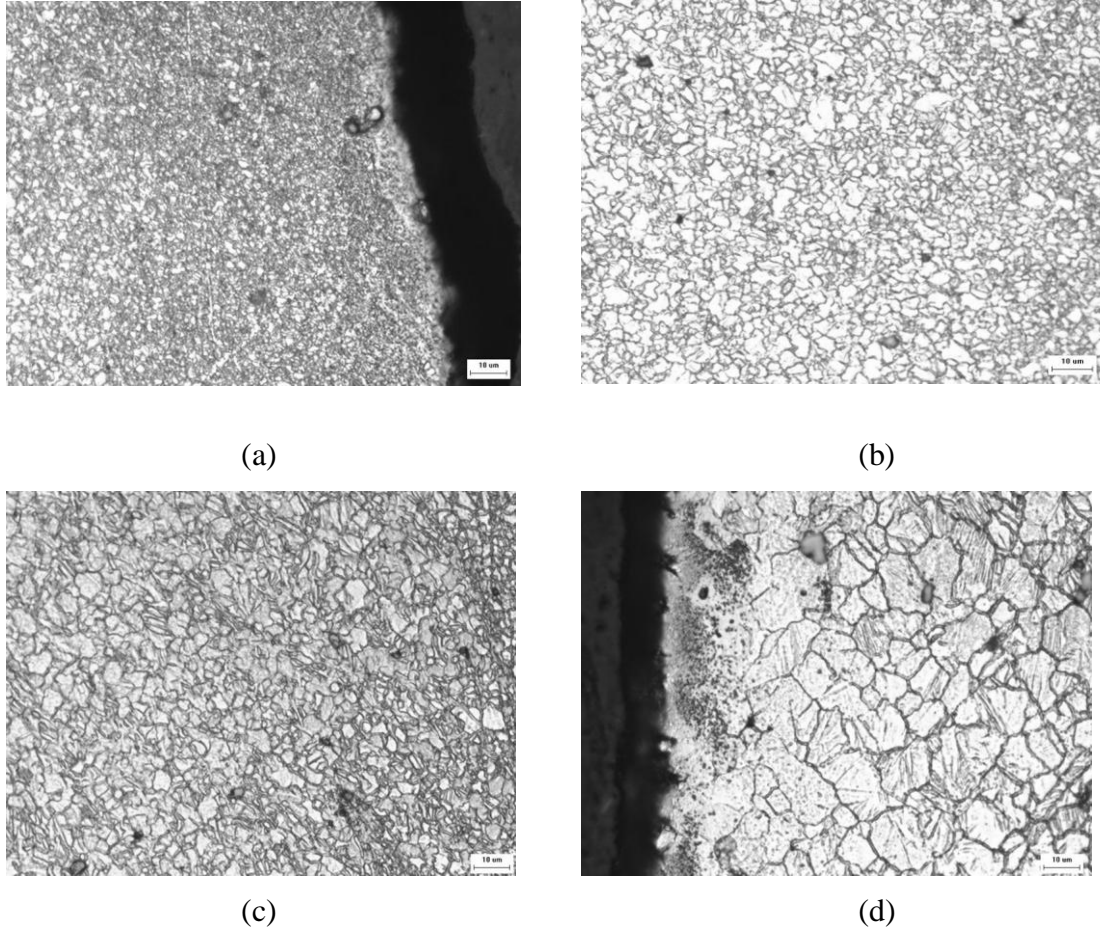
Figure 3.22: Microstructure throughout the depth of the sheet from bottom to top surface at 500 X magnification and the stirring conditions of f = 500 mm/min and rotational speed of s = 1200 rpm (a) Bottom region, (b) Middle region- 1, (c) Middle region- 2, (d) Top region

Table 3.3 summarizes the average grain size values obtained at different locations in the 3 mm thick *Mg AZ31B-O* alloy sheet for all the cooling conditions tested.

Table 3.3. Average grain size values for all the FSP cooling conditions tested

S.No.	Conditions	Location	Average grain size (µm)
1	MP (1-sided) with Swiss Lube coolant underneath the fixture	Bottom	12
		Middle	15
		Top	20
2	MP (2-sided) with Swiss Lube coolant underneath the fixture	Bottom	10
		Middle	20-25
		Top	12
3	MP (1-sided) with flood coolant on top and underneath the fixture	Bottom	7
		Middle	9
		Top	10
4	MP (1-sided) with flood coolant and 45 seconds waiting time between successive passes	Bottom	3-5
		Middle	7-10
		Top	10
5	MP (2-sided) with Swiss Lube flood coolant and 45 seconds waiting between passes	Bottom	3-5
		Middle	7-10
		Top	10
6	MP with cryogenic cooling on top and Swiss Lube coolant underneath the fixture	Bottom	10-20
		Middle	10-20
		Top	10-20
7	MP with cryogenic cooling underneath the fixture (bottom)	Bottom	0.5-2
		Middle	5-10
		Top	8-10
8	MP with flood cooling (Swiss Lube) on top and cryogenic cooling underneath the fixture (bottom)	Bottom	4.5
		Middle	6-8
		Top	5
9	MP with cryogenic cooling on top as well as underneath the fixture (bottom)	Bottom	0.5-1
		Middle	3-5
		Top	8-10

3.6 Microhardness

3.6.1 Measurement of microhardness

The hardness testing apparatus used in the experimental work consists of a CLARK Digital Microhardness Tester CM-700 AT with a minimum measuring unit and minimum graduation of 0.1 µm and 200X magnification. This equipment was used for microhardness measurements on the FSP samples at various locations across the thickness of the sheet. The loads and the indent size used during the microhardness testing are very small, 50 gf and the indent size of 30 µm respectively. A square-based pyramid indenter is used to make the hardness measurements at varying loads from 15 to 1000 gf across the sample and the impressions are precisely located using the microscope. The length of the diagonals of the rhombus-shaped indentation made by the indenter is measured microscopically, and the relative test loads are used to obtain a hardness value. The microhardness values obtained are useful as an indicator of the grain size obtained using FSP process.

Vickers hardness test is used and the formula used to calculate the microhardness value is [47]:

$$HV = 1.854 * (F/d^2)$$
(3.1)

where: F = Load in kgf

and $d = (d_1 + d_2)/2$ (Arithmetic mean of the two measured diagonals of the indent, d_1 and d_2 in mm) while HV = Vickers hardness. The obtained data is tabulated in Tables 3.3 – 3.7.

3.6.2 Measurement of microhardness on the FSP sheet

The measurement specifications used for performing microhardness test on this material are:

Load: 50 gf

Dwell time: 12 seconds

d_1 and d_2 were measured to give the average diagonal diameter.

Microhardness measurements are made across the thickness on the samples obtained using the FSP process and the different cooling conditions. Three sets of readings are recorded for each sample at the same distance below the surface and at different positions. These are then plotted against distance from the processed face, as described in Chapter 2. Initial microhardness measurements are made on the original magnesium sheet sample and the average hardness value was found to be 53 HV as shown in Table 3.4.

Equation 3.2 represents the Hall-Petch (H_v) equation which shows the direct relationship between the microhardness value and the grain size diameter. The microhardness value is high for smaller grains.

$$H_v = 40 + 72\ d^{-1/2} \qquad\qquad (3.2)$$

H_v is the microhardness value on the Vickers scale
d is the diameter of the grain size

3.6.3 Microhardness for samples obtained from MP (1-sided) and MP (2-sided) with Swiss Lube coolant underneath the fixture

The microhardness values of MP (1-sided) and MP (2-sided) with Swiss Lube coolant as explained under Sections 3.5.1 and 3.5.2 respectively underneath the fixture are recorded. These values are found to be low compared to the original microhardness value due to the increase in grain size due to the high temperature involved in this FSP process as no direct cooling is used to dissipate the heat. The average hardness value for MP (1-sided) is 50 HV and for MP (2-sided) it is 52 HV. These values are found to be different when

to the original microhardness which is 53 HV due to the grain size increase because of the high temperature involved in this FSP process and no coolant is used to dissipate the heat. The data are plotted against the distance at thickness positions shown in Figure 3.23. The plot shows that the microhardness is modestly reduced in FSP sample due to the increase in grain size to 14 µm from the initial value of 10 µm, and hence the average hardness value is slightly smaller than the AR material's microhardness. From the graph, we can see that there is no real trend in the variation of microhardness and one assumes that this is due to the inhomogeneity of the grain size due to the uncontrolled heat dissipation and varying strain-rates involved in the FSP process. The error values shown in the graph is the difference between the average and the actual microhardness values. The numbers 1-10 on the x-axis denote the depths below the bottom surface of the sheet i.e. 30 µm, 300 µm etc.

Table 3.4: Initial, MP (1-sided) Section 3.5.1 and MP (2-sided) Section 3.5.2 with Swiss Lube coolant underneath the fixture microhardness values

Distance (µm)	Initial Hardness (HV)	MP (2-sided) (HV)			MP (1-sided) (HV)		
		Set 1	Set 2	Set 3	Set 1	Set 2	Set 3
30	49.4	53	60	74.1	55.2	51	51.9
300	49.4	50.2	48.5	49.7	44.6	48	52.8
600	50.2	43.1	54.4	53.9	50	48	50.9
900	52.6	47.4	49.9	52.8	44.1	50.7	50.2
1200	51.5	41	50.6	50.6	51.2	43.9	53.3
1500	55.4	47.1	44.8	53.3	43.3	47.7	50.7
1800	51.3	48.5	51.3	51.3	45.4	49.3	50.8
2100	54.7	44.7	52.4	51.9	50.2	49.3	48.2
2400	48.9	43.9	65.4	53.3	50.6	52.5	51.2
2700	57.6	56.1	57.6	57.6	51.6	53.5	52.1
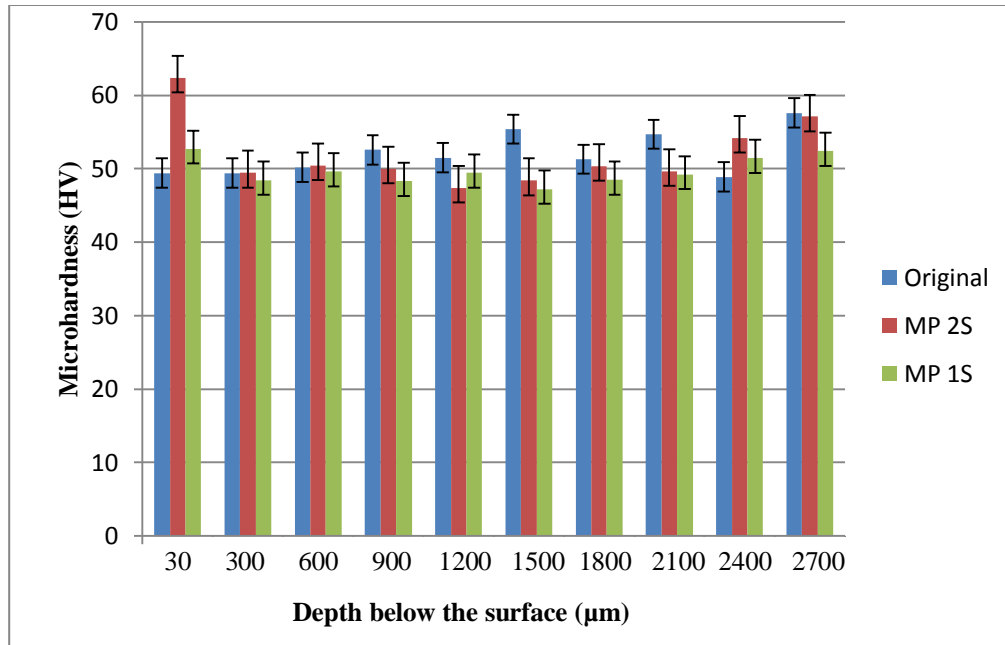
Figure 3.23: Microhardness data at different depths below the top surface of the sheet for the original material and for MP (1-sided) Section 3.5.1 and MP (2-sided) Section 3.5.2 with Swiss Lube cooling underneath the fixture

3.6.4 Microhardness data for processed samples obtained from MP (1-sided) with cryogenic cooling underneath the fixture section 3.5.7

Microhardness values for the case MP (1-sided) with cryogenic cooling underneath the fixture show high microhardness values in a region of fine grains at a distance of 150 µm from the bottom face of the FSP sheet. The microhardness values are in the range of 75-90 HV in that region. Cryogenic cooling helps dissipate the heat at a higher rate than the Swiss Lube cooling, which in turn helps in retaining the small recrystallized grains and hence, higher microhardness values are obtained.

The microhardness values obtained for these cooling conditions are plotted against the distance from the bottom face of the sheet. Results shown in Figure 3.24 indicate that there are high hardness values in the bottom region of MP (1-sided) with cryogenic cooling underneath the fixture sample. That section received the highest rate of cooling with the fixture being frozen using liquid nitrogen. The microhardness values vary across

54

the plate thickness with the inhomogeneous grain structure. The microhardness plots obtained for MP with cryogenic cooling on top and Swiss Lube coolant underneath the fixture sample is shown in Figure 3.25. The graph shows a homogeneous trend of micro hardness values even though the highest hardness value is only 68 HV which is less than the 90 HV obtained using MP (1-sided) with cryogenic cooling underneath the fixture.

Table 3.5: Microhardness values near the bottom face of the sheet obtained using MP (1-sided) with cryogenic cooling underneath the fixture

Microhardness values				
Distance (µm)	Set 1 (HV)	Set 2 (HV)	Set 3 (HV)	Average (HV)
25	89.4	88.5	88.5	88.8
60	87.2	86.7	86.1	86.7
90	85.4	85.1	85	85.2
120	79.7	76.7	76.4	77.6
150	74.4	73.3	73.3	73.7

Table 3.6: Microhardness values for MP (1-sided) (Section 3.5.7) with cryogenic cooling underneath the fixture sample along the thickness of the sheet

	Sample 1			Sample 2			Sample 3		
Top region to bottom region									
Distance (μm)	Set 1 (HV)	Set 2 (HV)	Set 3 (HV)	Set 1 (HV)	Set 2 (HV)	Set 3 (HV)	Set 1 (HV)	Set 2 (HV)	Set 3 (HV)
30	67.9	67.1	69.4	66.6	67.9	68.8	68.1	66.2	69.6
300	70.1	67	68.6	68.8	67.8	68	70.3	66.1	68.8
600	65.2	61.9	63.3	63.9	62.7	62.7	65.4	61	63.5
900	56.1	61.2	58.6	54.8	62	58	56.3	60.3	58.8
1200	67.5	60.9	58.5	66.2	61.7	57.9	67.7	60	58.7
1500	59.1	54.6	59.2	57.8	55.4	58.6	59.3	53.7	59.4
1800	58.3	53.8	53.5	57	54.6	52.9	58.5	52.9	53.7
2100	51.8	56.2	50.1	50.5	57	49.5	52	55.3	50.3
2400	52.4	54.2	51.4	51.1	55	50.8	52.6	53.3	51.6
2700	50.8	50.9	50.1	49.5	51.7	49.5	51	50	50.3
3000	50.2	50.2	50.3	48.9	51	49.7	50.4	49.3	50.5
3170	88.5	89.4	86.7	87.2	90.2	86.1	88.7	88.5	86.9

Table 3.7: Microhardness values for MP (1-sided) with cryogenic cooling on top and Swiss Lube coolant underneath the fixture sample along the thickness of the sheet (Section 3.5.6)

	Sample 1			Sample 2			Sample 3		
	Top region to bottom region								
Distance (μm)	Set 1 (HV)	Set 2 (HV)	Set 3 (HV)	Set 1 (HV)	Set 2 (HV)	Set 3 (HV)	Set 1 (HV)	Set 2 (HV)	Set 3 (HV)
30	60.8	64.5	67.5	61.5	63.6	67.8	60.1	65	68
300	65.7	61.1	57.5	66.4	60.2	57.8	65	61.6	58
600	65	54.6	61.7	65.7	53.7	62	64.3	55.1	62.2
900	61.9	56.8	56.5	62.6	55.9	56.8	61.2	57.3	57
1200	60.1	55.9	56.5	60.8	55	56.8	59.4	56.4	57
1500	53.3	57.5	53	54	56.6	53.3	52.6	58	53.5
1800	55.6	55.2	69	56.3	54.3	69.3	54.9	55.7	69.5
2100	58.6	57.2	63.2	59.3	56.3	63.5	57.9	57.7	63.7
2400	59.2	50.8	67.5	59.9	49.9	67.8	58.5	51.3	68
2700	57.7	58.6	58	58.4	57.7	58.3	57	59.1	58.5
3000	58.5	62.7	59.8	59.2	61.8	60.1	57.8	63.2	60.3
3170	60.1	60.8	61.2	60.8	59.9	61.5	59.4	61.3	61.7
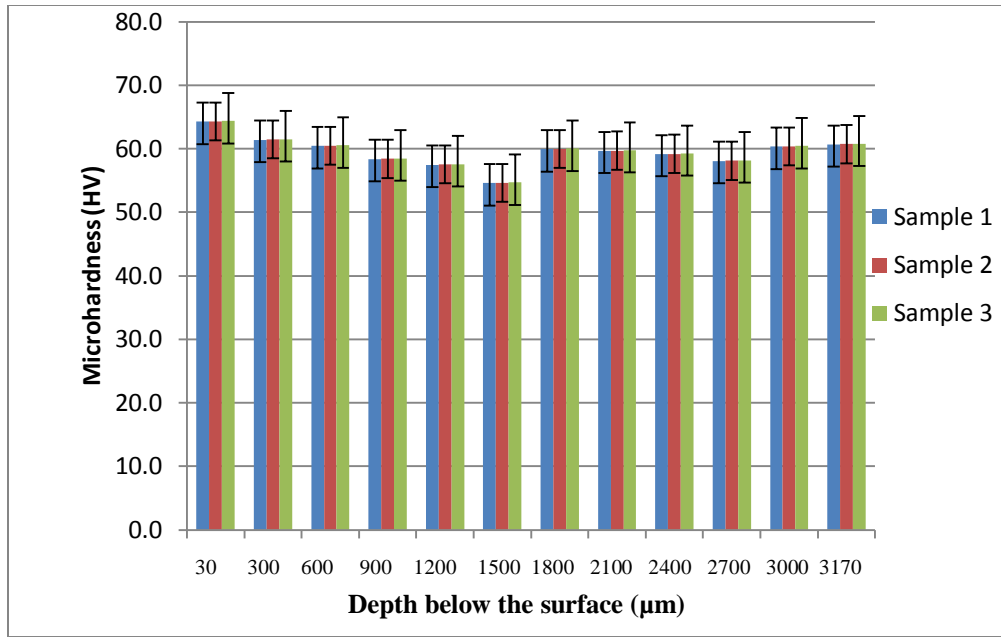
Figure 3.24: Microhardness plot for MP (1-sided) with cryogenic cooling underneath the fixture (Section 3.5.7)
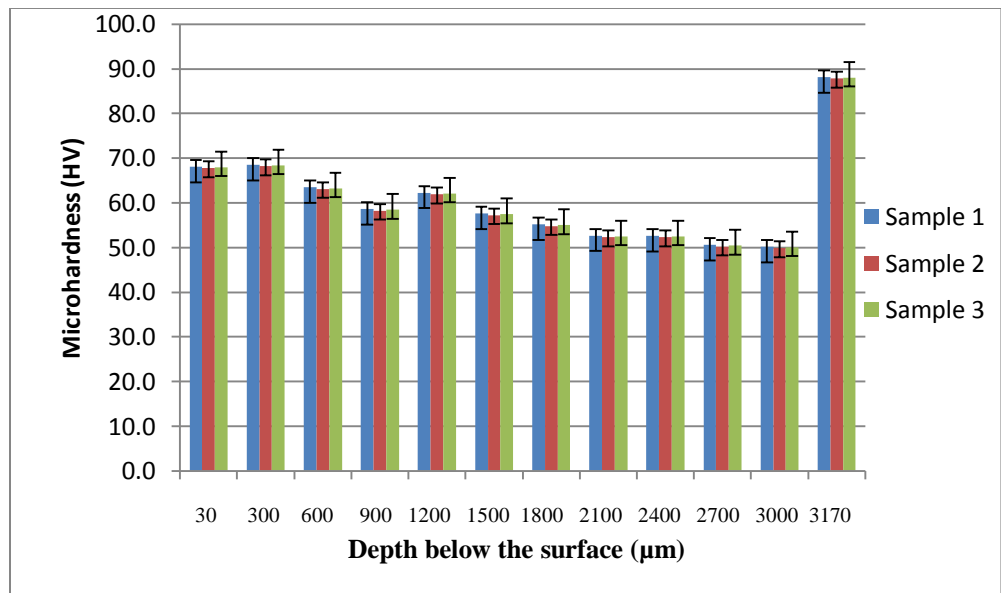
Figure 3.25: Microhardness plot for MP (1-sided) with cryogenic cooling on top and Swiss Lube coolant underneath the fixture

Figure 3.26 shows the microhardness plot for MP (1-sided) with cryogenic cooling underneath the fixture Section 3.5.7, 150 µm fine grain region. The microhardness values

decrease as we move from bottom to top due to the effect of cryogenic cooling under the fixture.
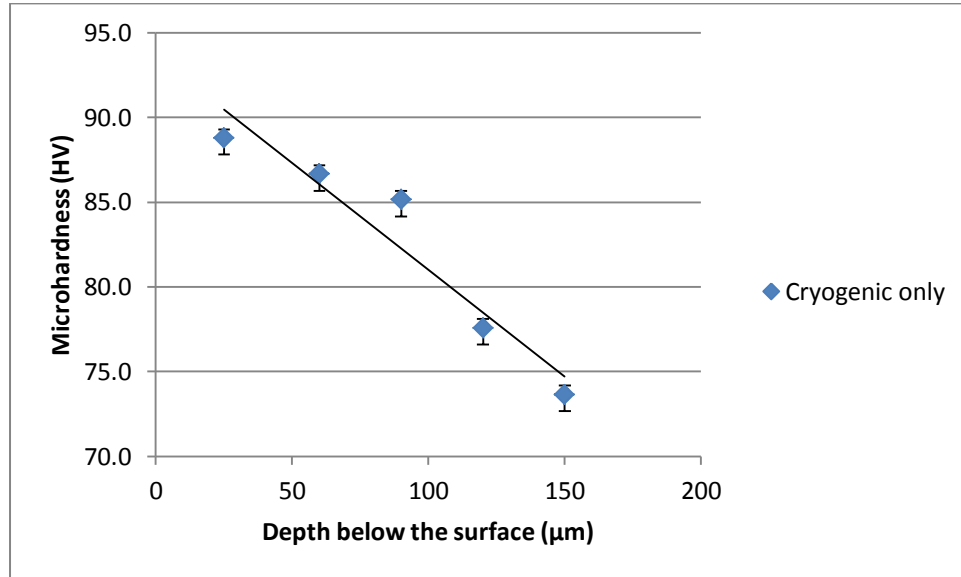
Figure 3.26: Microhardness plot for the MP (1-sided) with cryogenic cooling underneath the fixture, 150 μm fine grain bottom region (Section 3.5.7)

Table 3.8 shows the microhardness values for the original sheet and the cryogenic fluid applied on the top of the sheet Section 3.5.8 as well as on the bottom of the sample at stirring conditions of f = 500 mm/min and speed s = 1200 rpm. From the Table 3.8, we can see that maximum value of microhardness is 125 HV which is approximately 2.5 times the microhardness of as-received material i.e., 53 HV.

Table 3.8: Microhardness values for MP (1-sided) with cryogenic on top as well as bottom at f = 500 mm/min and speed s = 1200 rpm (Section 3.5.8).

Distance (μm)	Original sheet microhardness (HV)			MP (1-sided) with cryogenic cooling on top as well as at bottom (HV)		
	AR 1	AR 2	AR 3	FSP 1	FSP 2	FSP 3
25	44.6	54.8	44.5	124.8	112.9	114.1
50	47.7	51.5	53	96.4	91.6	95.2
75	49.9	48.7	50.7	89.4	85.1	85.1
100	46.4	50	48.2	83.3	84.8	82.1
125	42.8	47	48.9	76.5	79.7	75
150	46.8	52.9	49.5	79.5	76.5	79.7
175	54.4	53.3	50.4	69.5	64.8	60.9
200	50.2	50.9	53.4	65.1	63	61.1

From Figure 3.27, we can see the microhardness value decreases with the distance from the bottom face of the FSP sheet, and it is 125HV at a distance of first 25 µm from the bottom face, which is approximately 2.5 times the microhardness of as-received material i.e., 53 HV. This proves the significant effect of pre-cooling the fixture using cryogenic cooling and applying cryogenic fluid under the fixture, as well as on the top surface, during the FSP.
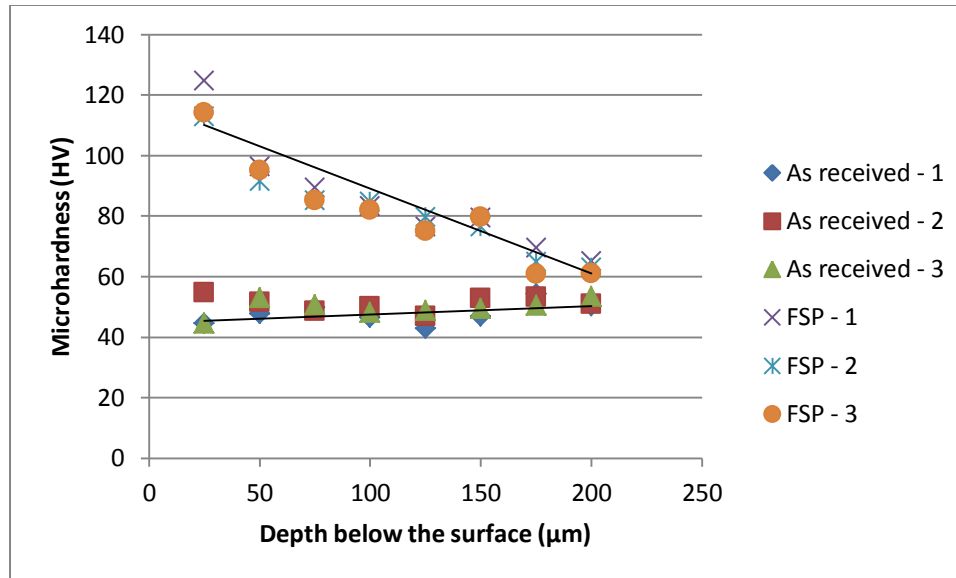
Figure 3.27: Microhardness plots for as-received material sample 1, 2 & 3 and FSP material sample 1, 2 & 3 (Section 3.5.8)

From the Figure 3.27, we can see that the highest values of microhardness are found, in the case of MP (1-sided) with cryogenic cooling applied on top as well as at the bottom. The highest among them are in the bottom region, being located at around 150 µm, in the sheet processed using cryogenics on top as well as at the bottom. Hence, as we see from the above results, the high microhardness values and smallest grain sizes with better homogeneity are achieved in the case of MP (1-sided) with cryogenic cooling on top as well as at the bottom and at the stirring conditions of $f = 500$ mm/min and rotational speed $s = 1200$ rpm. These conditions are fixed and 36 FSP disks of 75 mm diameter are obtained from the 115 mm X 115 mm FSP sheets. All the specimens used during the machining experiments will be processed in this manner.

CHAPTER 4

MACHINING EXPERIMENTAL TECHNIQUES

4.1 Introduction

The following sections present details of the work material, cutting tools, machine tool, equipments and tool insert used during the experiments, cutting tool edge radius measurement using Zygo, experimental set up for dry, MQL and cryogenic machining, measurement of cutting forces, and different types of chips collected during the experiments.

4.2 FSP and AR disk material

FSP *Mg* disks used in the machining experiments are obtained from a fixed set of processing conditions of translational feed, f = 500 mm/min and rotational speed, s = 1200 rpm. After the FSP, the sheets are cut on a milling machine into 36 disks of 75 mm diameter each. The AR material sheet is also cut into another 36 disks of 3 mm thickness for identical orthogonal machining experiments as used for the FSP material. The dimensions of the disk are as shown in Figure 4.1, and they are selected based upon the design of the mandrel to hold the disk in the turning center chuck. Three different holes are made in the disk to screw it to the mandrel.
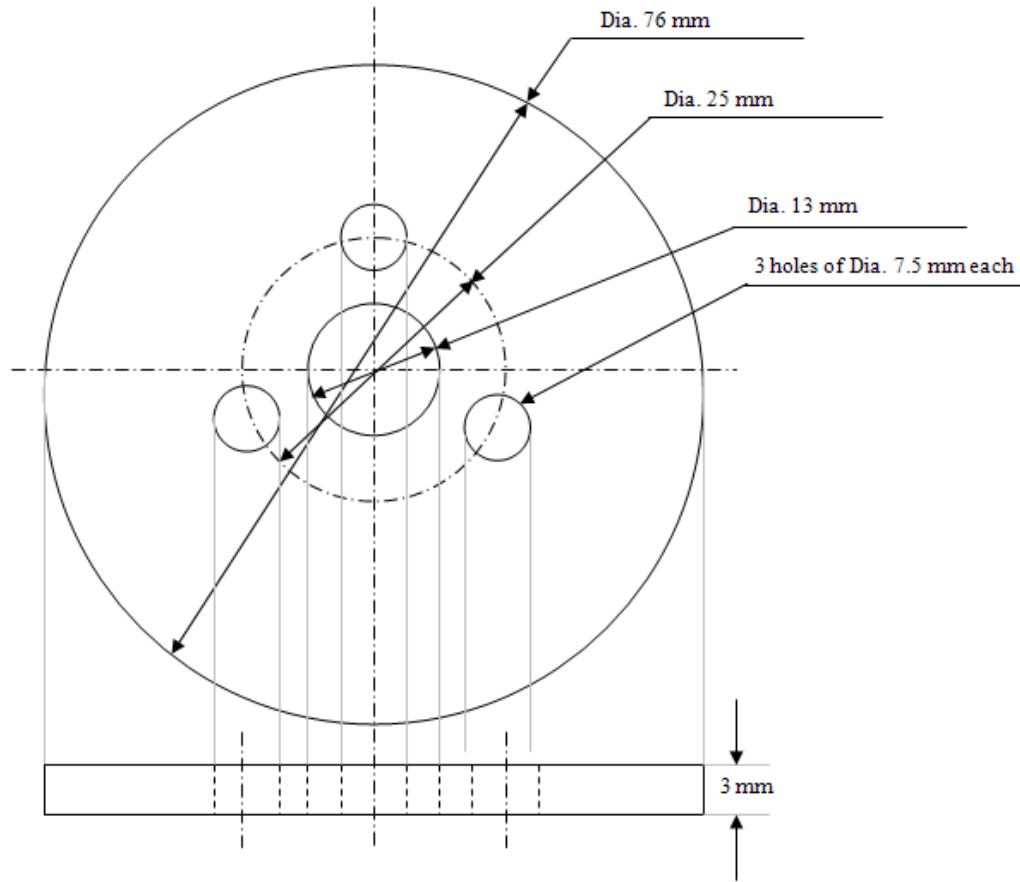
Figure 4.1: Specifications of the disk used in the machining experiments

4.3 Cutting tools and experimental equipment

The Mazak turning center shown in Figure 4.2 is used for the orthogonal machining experiments. Its specifications are: turning speed 4000 rpm, turning diameter 320 mm and turning length 800 mm. It can be programmed for the orthogonal machining and turning operations.

Figure 4.2: Mazak Quick Turn 10 turning machine

4.4 Cutting tool insert

Magnesium alloy is an easy to cut material and hence a simple cutting tool insert is used which is based upon ASM standards. It is an uncoated flat carbide tool insert, TNMG432, K-grade from Kennametal inc. with a positive rake angle of 7°. The tool dimensions are as shown in Table 4.1.

Table 4.1: Cutting tool insert nomenclature

	D (mm)	$L10$ (mm)	S (mm)	R_ε (mm)	D_1 (mm)
	12	22	4.76	0.8	5.16

4.4.1 Cutting tool edge radius measurements using Zygo

Cutting tool edge radius plays an important role in machining of any material. It heavily influences the machined surface microstructure, microhardness, surface integrity, chip properties and work material surface properties.

In this study, the tool edge radius value is kept constant to permit a better comparison of the experimental results obtained from different machining conditions and different initial material properties. Hence, it is important to actually measure the edge radius and select the ones with the values near the median.

The edge radius of the uncoated carbide tool insert represents the measure of roundness of the insert between the rake face and the flank face at the cutting edge of the insert. The edge radius of these inserts is measured using a Zygo Interferometric Microscope, which is a 3D Optical Surface Profiler along with Metropro 8.0 analysis software, as shown in Figure 4.3. It is a white light interferometer system which offers fast, noncontact, high-accuracy, 3D metrology of surface features. The inserts are selected based upon an acceptable range of edge radius values. A total of 106 tool edge radii are measured, from which 72 values close to the mean, 45 µm are selected for use in the orthogonal machining experiments.

Figure 4.3: Zygo interferometric microscope with Metropro software system

4.4.2 Technique and the procedure to measure the edge radius

The tool insert is placed on a fixture that allows the light source from the Zygo microscope to impinge directly on the cutting edge. After capturing the surface of the cutting edge, a screen shot of the cutting edge profile is taken using Metropro analysis software. The three dimensional surface of the cutting edge involved in the machining

process whose edge radius is to be determined is captured at 50X magnification. Figure 4.4 shows an oblique plot of the cutting edge of a typical uncoated carbide tool insert, surface map and surface profile of the insert. The surface profile is plotted using Matlab software to determine the accurate value of the cutting edge radius.
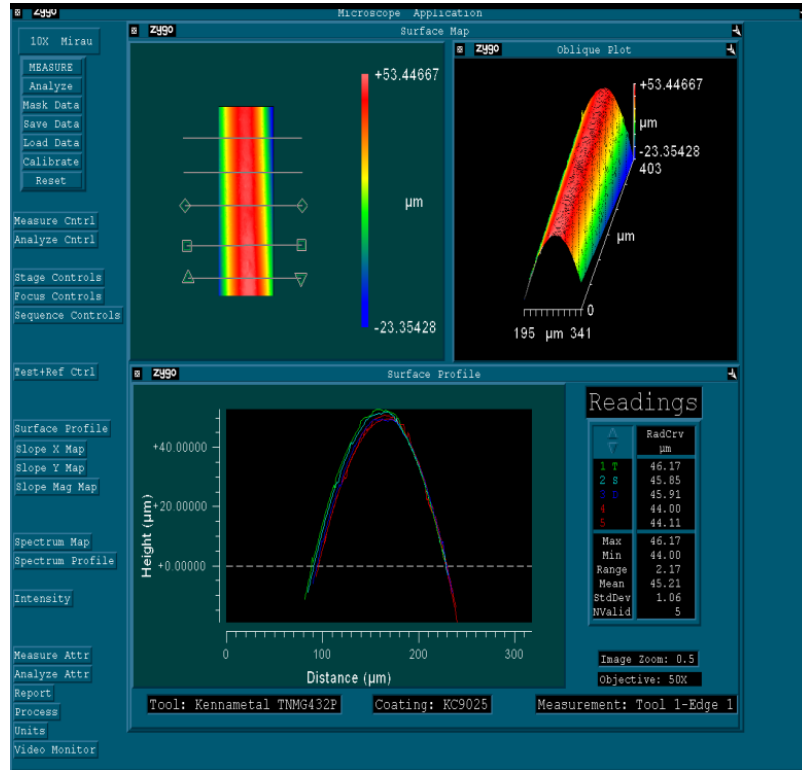
Figure 4.4: Screen shot of edge radius profile of uncoated carbide tool insert taken using Zygo interferometric microscope at 50X magnification

Five different measurements are made on each edge of the insert and an average value is obtained by using Metropro software. In this way the edge radius values are measured for all 106 tool inserts and their cutting edge radii are accurately calculated by using Matlab software. An average of all these edge radius values is taken and the edge radius values near the median range are selected for the experiments, and the values which are far away from the median are discarded. The average value of the edge radius is found to be 45 µm. The minimum measured edge radius value used is 42 µm and the maximum is 48 µm.

4.5 Experimental setup

The experimental set up is as shown in Figure 4.5 and consists of:

1. A Mazak CNC turning machine
2. FSP and AR magnesium alloy disks
3. Uncoated carbide tool inserts (TNMG432, Tool Grade: K)
4. Kistler 9121 3D Dynamometer for obtaining force measurements
5. Infrared camera for temperature measurement (A FLIR Systems ThermaCam PM695)
6. Spray lubrication system for minimum quantity lubrication (Unimax Serv-O-Spray Model Number 25-03)
7. Liquid nitrogen setup for cryogenic cooling (ICEFLY® cryogen delivery system from Air Products Inc.)
8. Chip disposal tank

Figure 4.6 shows the pictorial top view of this orthogonal machining process set up. The mandrel is attached to the chuck which holds the workpiece. The infrared camera and the dynamometer are positioned as shown in Figures 4.5 and 4.6., a feed is given to the tool insert and the cutting process is performed. The infrared camera lens is covered with a protection lens screen and the camera position is fixed at a distance of 0.5 m from the machining disk.
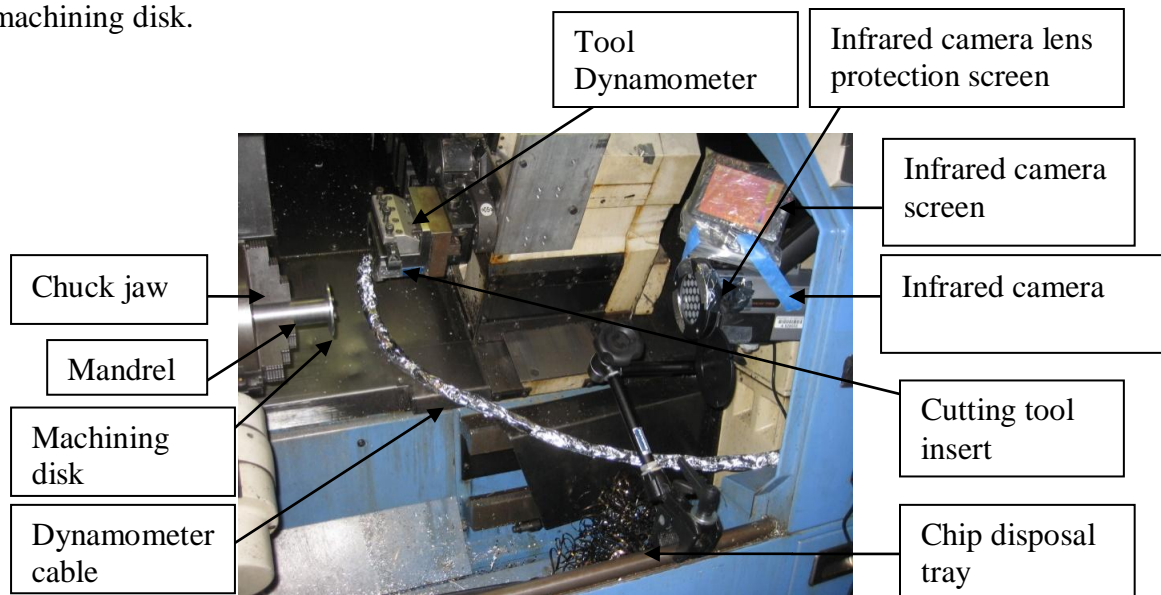
Figure 4.5: Experimental setup for the machining experiments
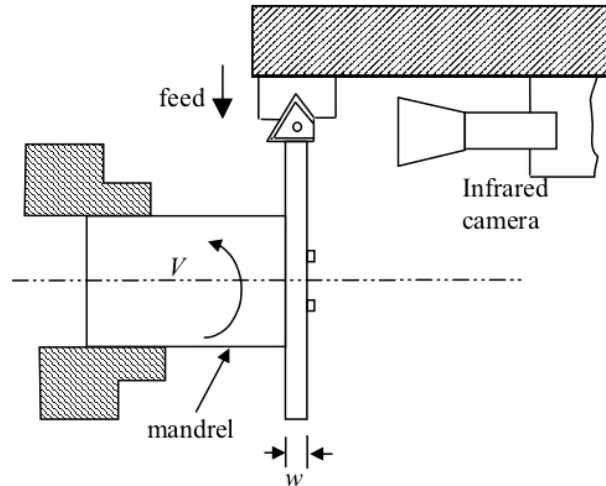
Figure 4.6: Pictorial view of the orthogonal machining process

A total of 72 disks are machined using dry, MQL and cryogenic cutting conditions. Twenty four disks are machined (12 AR and 12 FSP) from the previously prepared specimens. Four different cutting speeds and three different feed rates are used to generate data on the cutting force, microstructure and microhardness variations generated under the experimental machining conditions given in Table 4.2.

At the beginning of each series of experiments, a new cutting edge of the insert is mounted onto the tool-holder, and a new work material disk is fixed to the mandrel. During the experiments, chips are collected and labeled with their various cutting conditions. The cutting force components and the cutting temperature values are recorded on Kistler 9121 3D Dynamometer and FLIR Systems ThermaCam PM695 Infrared camera, respectively during the experiments.

Table 4.2: Cutting parameters

Cutting speed (m/min)	50, 150, 250, 350
Feed (mm/rev)	0.1, 0.2, 0.3
Width of cut (mm)	3 mm
Work material	*Mg AZ31B-O* alloy
Microhardness	50-55 HV
Disk diameter (mm)	75 mm
Disk thickness (mm)	3 mm
Tool insert type	TNMG432
Tool material	Uncoated carbide
Tool grade	K
Mean tool edge radius (μm)	45 μm

4.6 Machining

Machining experiments are performed on the FSP and AR disks under dry, MQL and cryogenic cooling conditions using the cutting conditions listed in Table 4.2. The following section explains it in detail.

4.6.1 Dry machining

Dry machining is a sustainable process because no coolant is used during the cutting. However, the disposal of chips is a problem. A typical tool insert and the workpiece after the cutting process are shown in Figure 4.7.

Figure 4.7: Tool insert and workpiece after dry machining

4.6.2 MQL conditions

The MQL conditions reported herein use a vegetable oil based coolant and the oil used here is called UltraLube purchased from MSC Industrial Supply. Spray lubrication in the form of a fine mist is applied at the interface between tool insert and the workpiece. A small flow rate of 50 ml/hour is used during the experiments. The MQL set up is shown in Figure 4.8. It consists of an air compressor pushing the lubricant through the MQL system to the nozzle near the tool and the workpiece interface as shown in Figure 4.8 b.

MQL oil system   Tube for oil outlet
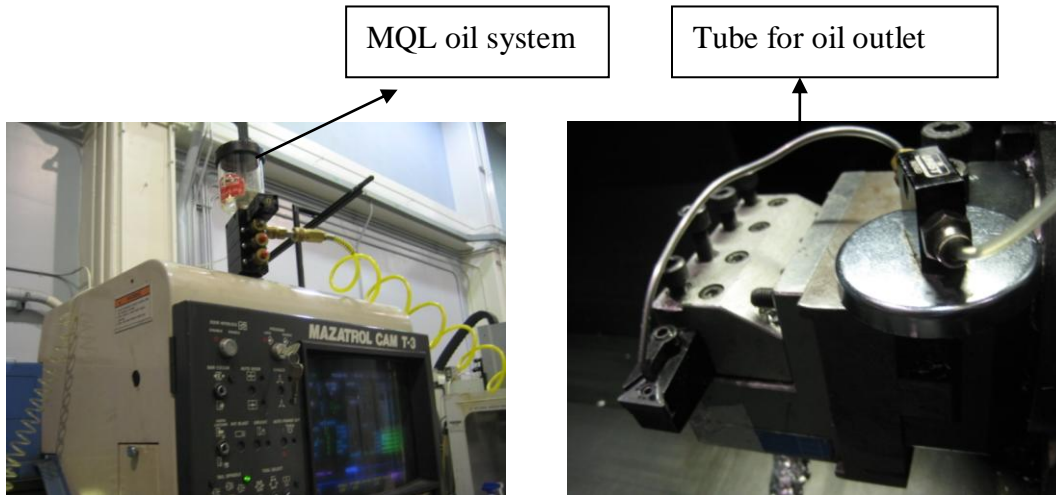
Figure 4.8: (a) Spray lubricant MQL system   (b) Delivering nozzle of MQL, near the cutting edge

4.6.3 Cryogenic conditions

The cryogenic setup consists of the liquid nitrogen tank and the copper tubing for the delivery of the liquid nitrogen. A flow rate of 0.3 kg/min of the liquid nitrogen is applied at the interface between the cutting tool edge and the disk. Figure 4.9(a) shows the application of liquid nitrogen jet at the flank face of the tool insert, and Figure 4.9(b) shows the liquid nitrogen storage tank.

Figure 4.9: (a) Liquid nitrogen jet application   (b) Liquid nitrogen tank

4.7 Measurement of cutting forces

A Kistler 9121 three-component tool dynamometer is used to measure the force components: the feed force (F_t) and the cutting force (F_c). Calibration of the dynamometer was done initially by using a load of known value. For each machining experiment, the dynamometer was set to record the cutting and feed force data and the files were analyzed later. The average force with the standard deviation was recorded in order to get a variation in force amplitude due to the cyclic nature of the forces. In order to eliminate the signals from any likely chatter or instability, several initial experiments are performed. A total of 72 experiments are conducted and the force data was collected and analyzed for 72 test conditions. The dynamometer set up consists of a data acquisition system used to record the force signals from three different channels, as shown in Figures 4.10 (a) and 4.10 (b).

Figure 4.10: (a) Force signal values in three channels   (b) Force data acquisition system

Tables 4.3 - 4.8 show the measured force values for all 72 test conditions. Since *Mg* alloy is an easy to cut material, the force values recorded are in the range of 100-360 N, which is quite small when compared to the forces obtained during machining of materials such as steel and titanium alloys which are in the range of 1000 N. Not much difference is observed for the force (cutting force and feed force) values between the AR and the FSP

processed disks under the same machining conditions. However, there is a slight variation in the forces obtained under different cooling conditions of Dry, MQL and Cryo.

The cutting and feed forces are recorded and plotted for six different sets denoted as Dry AR, Dry FSP, MQL AR, MQL FSP, Cryo AR, Cryo FSP machining respectively. Graphs are plotted for the force values against the cutting speed at constant feed values of 0.1, 0.2 and 0.3 mm/rev. Figures 4.11- 4.17 show the cutting and feed force plots. From the graphs it is shown that the forces increase with an increase in the cutting speed at fixed feed values. The feed force values are found to be smaller than the cutting force values. The force values under cryogenic conditions for both FSP and AR conditions are slightly higher than Dry and MQL because larger forces are required at low cutting temperatures. Between Dry and MQL there is a small difference in the force values when compared to those found between Dry and Cryo or Cryo and MQL forces.

Table 4.3: Measured forced values F_t and F_c for dry machined AR disks

Cutting speed (m/min)	Feed rate 0.10 mm/rev		Feed rate 0.20 mm/rev		Feed rate 0.30 mm/rev	
	F_t(N)	F_c(N)	F_t(N)	F_c(N)	F_t(N)	F_c(N)
50	118	153	169	233	162	282
150	141	186	179	289	181	339
250	146	191	187	304	197	351
350	156	191	175	290	192	367

Table 4.4: Measured forced values F_t and F_c for dry machined FSP disks

Cutting speed (m/min)	Feed rate 0.10 mm/rev		Feed rate 0.20 mm/rev		Feed rate 0.30 mm/rev	
	F_t(N)	F_c(N)	F_t(N)	F_c(N)	F_t(N)	F_c(N)
50	112	150	141	227	135	283
150	149	186	178	279	173	340
250	141	190	172	298	175	336
350	144	187	185	306	190	352

Table 4.5: Measured forced values F_t and F_c for MQL machined AR disks

Cutting speed (m/min)	Feed rate 0.10 mm/rev		Feed rate 0.20 mm/rev		Feed rate 0.30 mm/rev	
	F_t(N)	F_c(N)	F_t(N)	F_c(N)	F_t(N)	F_c(N)
50	115	150	143	222	151	273
150	127	180	153	270	161	329
250	129	183	174	290	169	345
350	127	184	168	291	164	337

Table 4.6: Measured forced values F_t and F_c for MQL machined FSP disks

Cutting speed (m/min)	Feed rate 0.10 mm/rev		Feed rate 0.20 mm/rev		Feed rate 0.30 mm/rev	
	F_t(N)	F_c(N)	F_t(N)	F_c(N)	F_t(N)	F_c(N)
50	102	141	120	219	135	277
150	129	182	150	271	153	323
250	132	185	159	290	171	340
350	130	183	169	297	158	331

Table 4.7: Measured forced values F_t and F_c for cryogenically machined AR disks

Cutting speed (m/min)	Feed rate 0.10 mm/rev		Feed rate 0.20 mm/rev		Feed rate 0.30 mm/rev	
	F_t (N)	F_c (N)	F_t (N)	F_c (N)	F_t (N)	F_c (N)
50	150	177	163	230	176	295
150	144	172	188	283	190	343
250	165	184	205	309	204	370
350	151	186	192	307	186	347

Table 4.8: Measured forced values F_t and F_c for cryogenically machined FSP disks

Cutting speed (m/min)	Feed rate 0.10 mm/rev		Feed rate 0.20 mm/rev		Feed rate 0.30 mm/rev	
	F_t (N)	F_c (N)	F_t (N)	F_c (N)	F_t (N)	F_c (N)
50	146	141	150	231	162	292
150	161	177	171	275	168	327
250	151	188	189	300	192	364
350	167	198	178	296	205	356
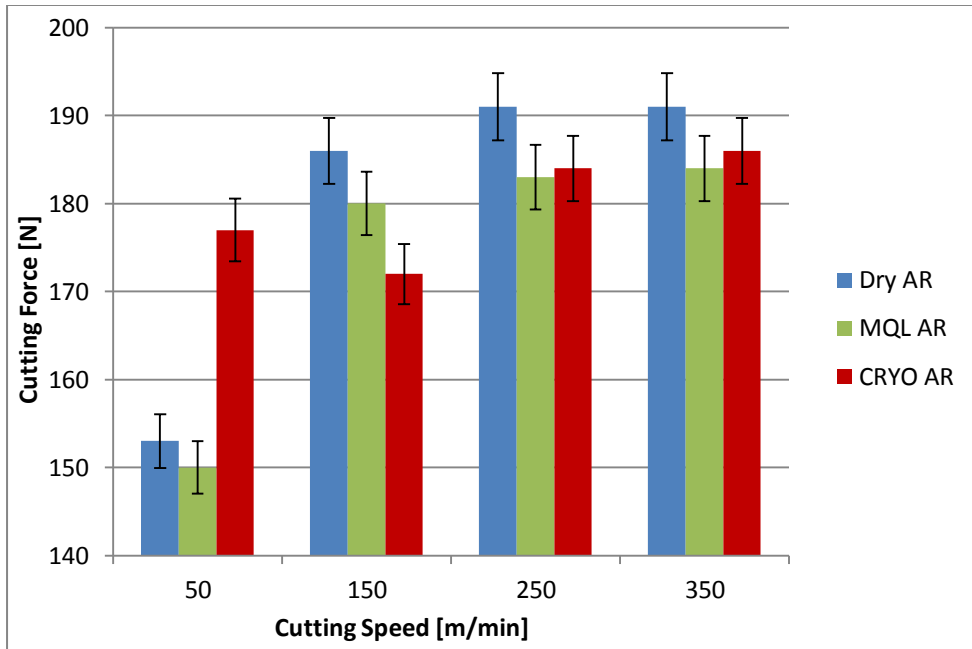
Figure 4.11 (a): Variation of cutting force with cutting speed at constant feed value of 0.1 mm/rev for AR samples
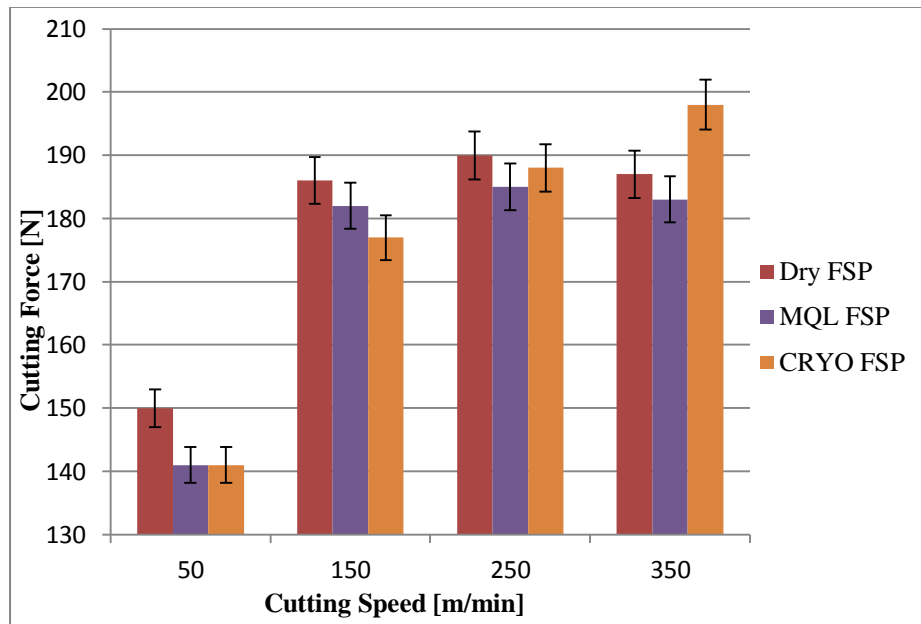
Figure 4.11 (b): Variation of cutting force with cutting speed at constant feed value of 0.1 mm/rev for FSP samples
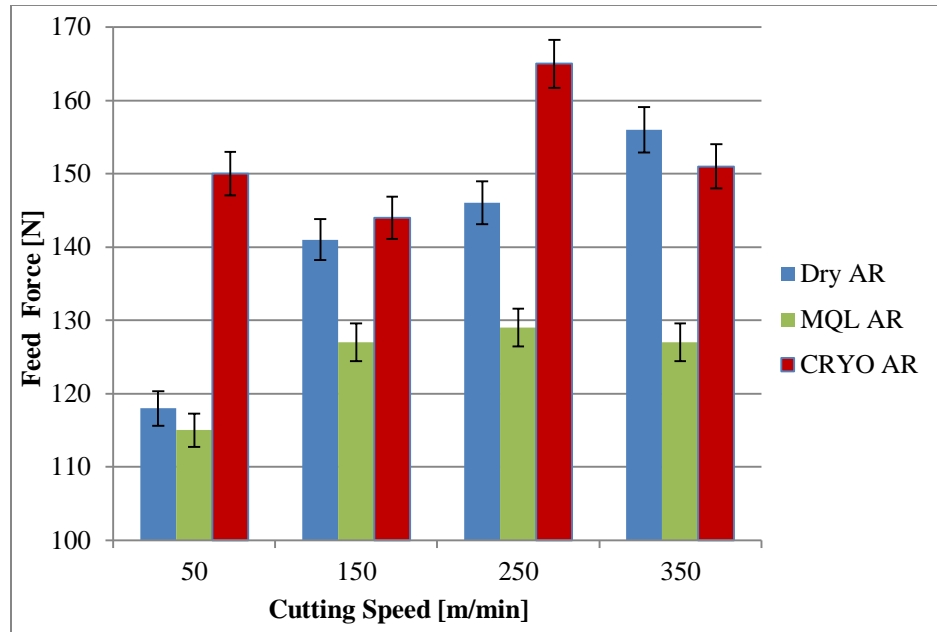
Figure 4.12 (a): Variation of feed force with cutting speed at constant feed value of 0.1 mm/rev for AR samples
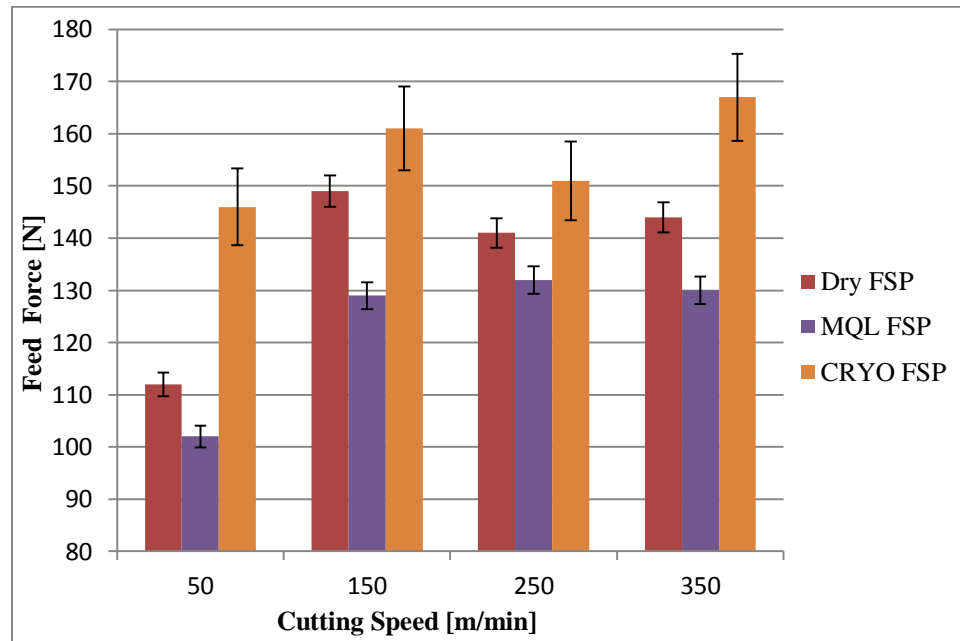
Figure 4.12 (b): Variation of feed force with cutting speed at constant feed value of 0.1 mm/rev for FSP samples
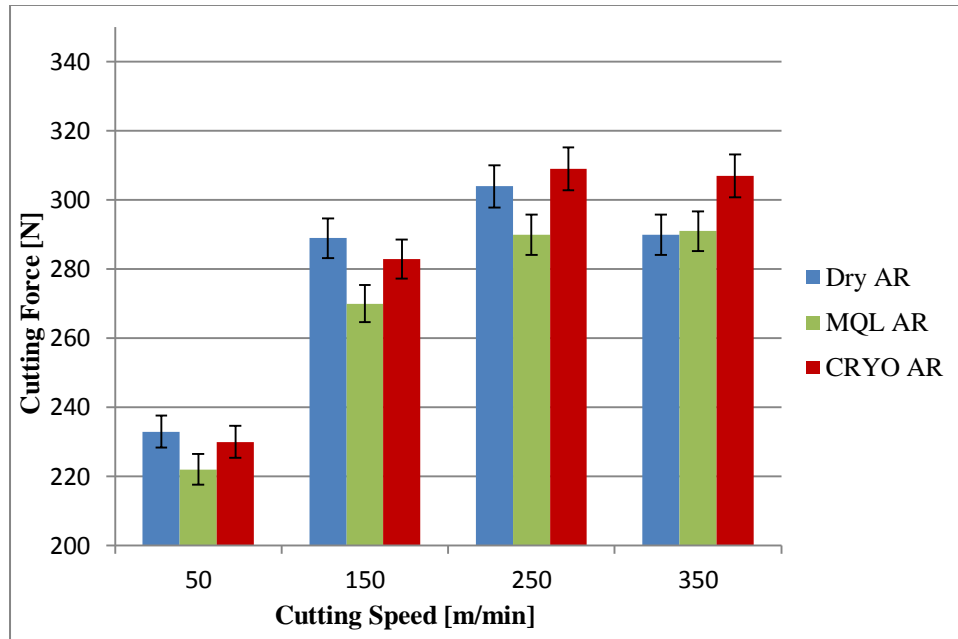
Figure 4.13 (a): Variation of cutting force with cutting speed at constant feed value of 0.2 mm/rev for AR samples
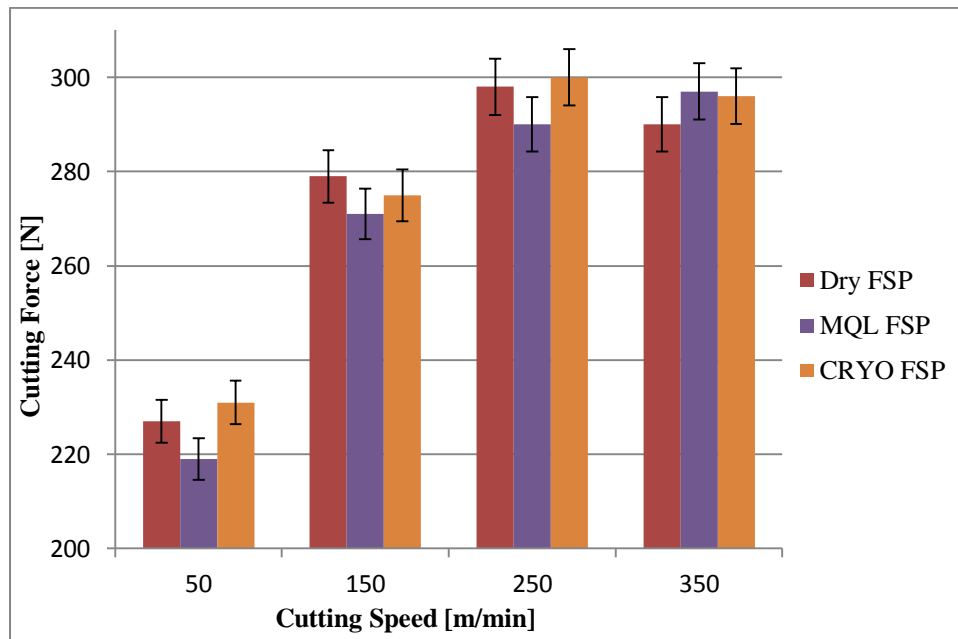
Figure 4.13 (b): Variation of cutting force with cutting speed at constant feed value of 0.2 mm/rev for FSP samples
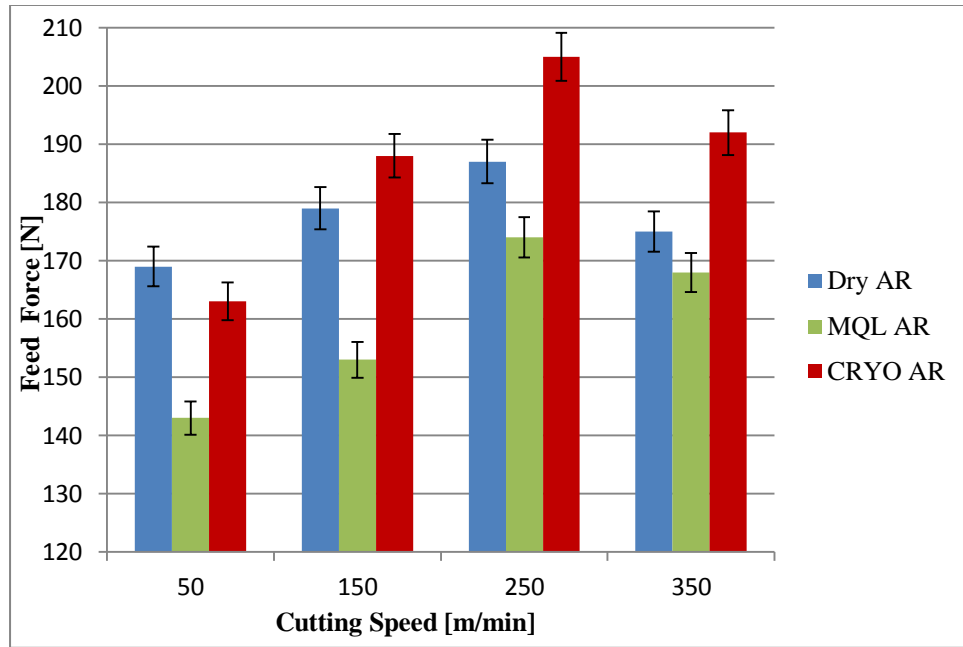
Figure 4.14 (a): Variation of feed force with cutting speed at constant feed value of 0.2 mm/rev for AR samples
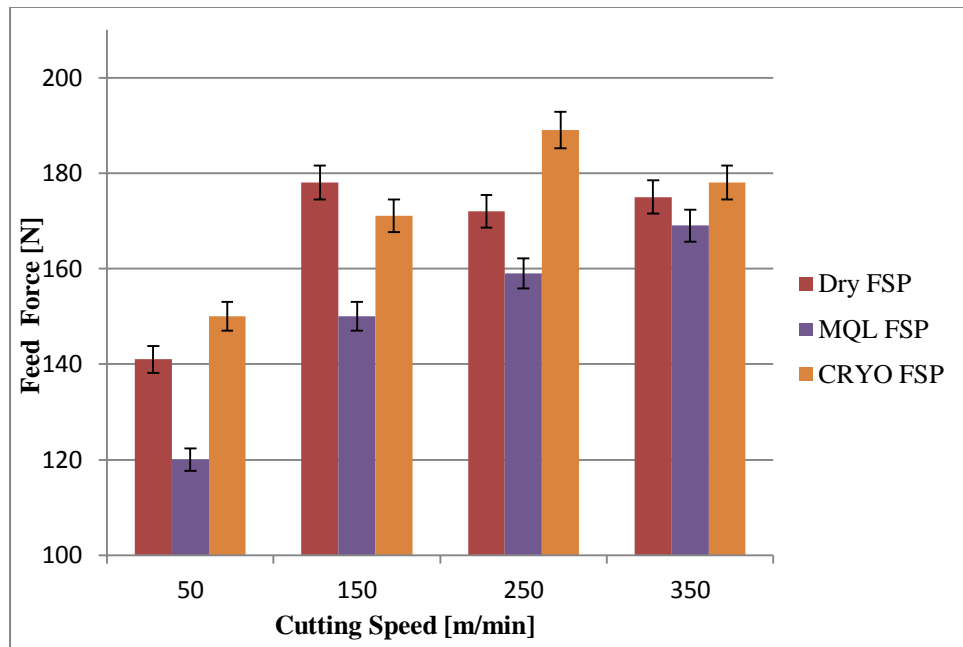
Figure 4.14 (b): Variation of feed force with cutting speed at constant feed value of 0.2 mm/rev for FSP samples
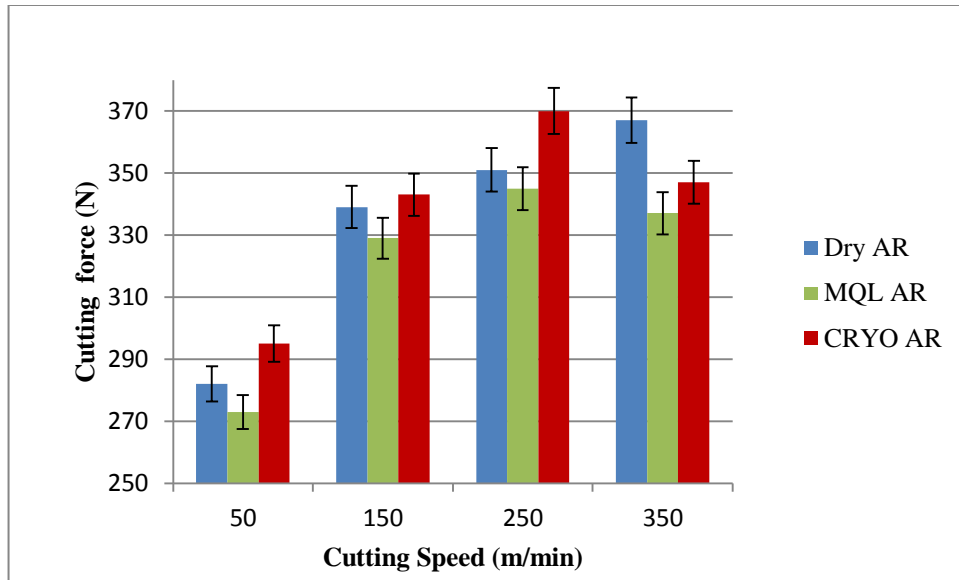
Figure 4.15 (a): Variation of cutting force with cutting speed at constant feed value of 0.3 mm/rev for AR samples
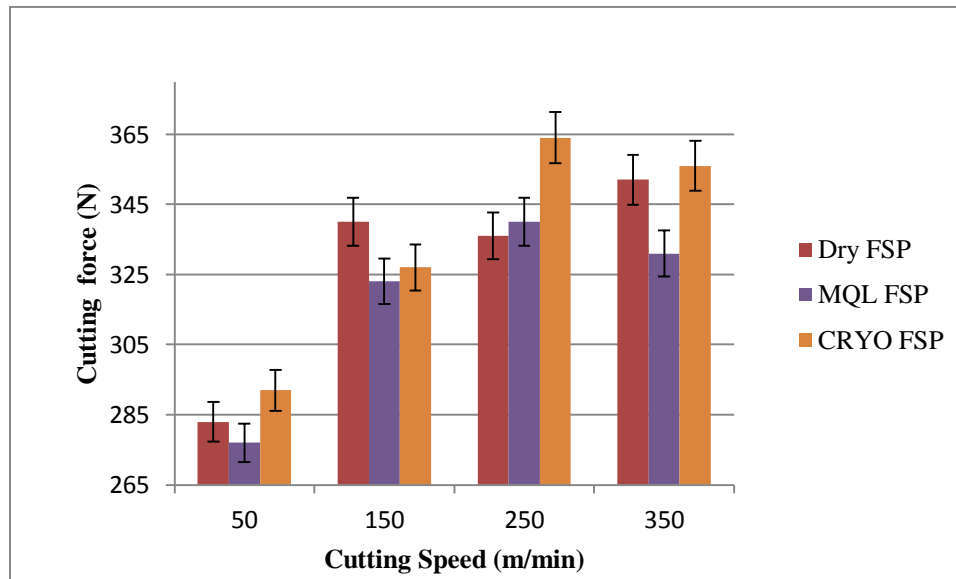
Figure 4.15 (b): Variation of cutting force with cutting speed at constant feed value of 0.3 mm/rev for FSP samples
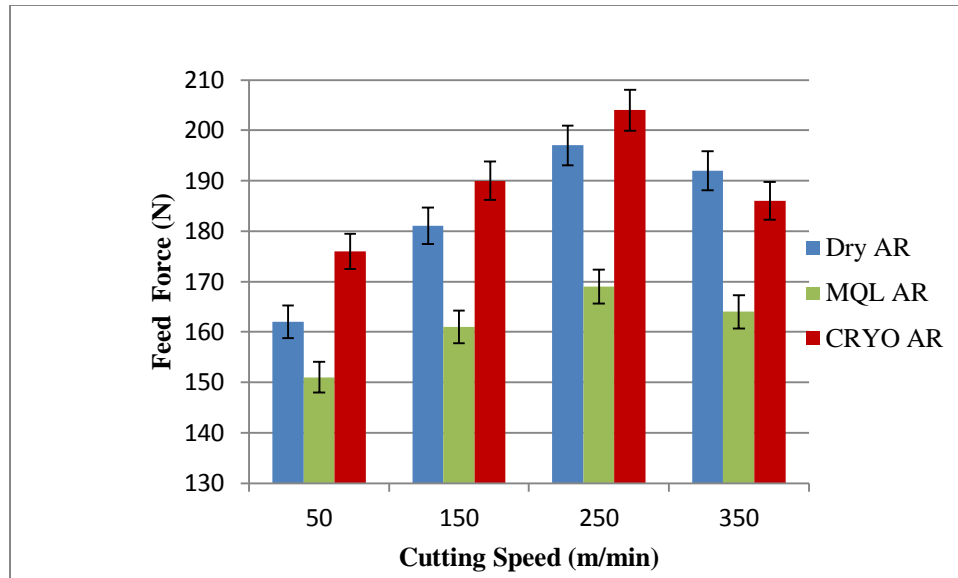
Figure 4.16 (a): Variation of feed force with cutting speed at constant feed value of 0.3 mm/rev for AR samples
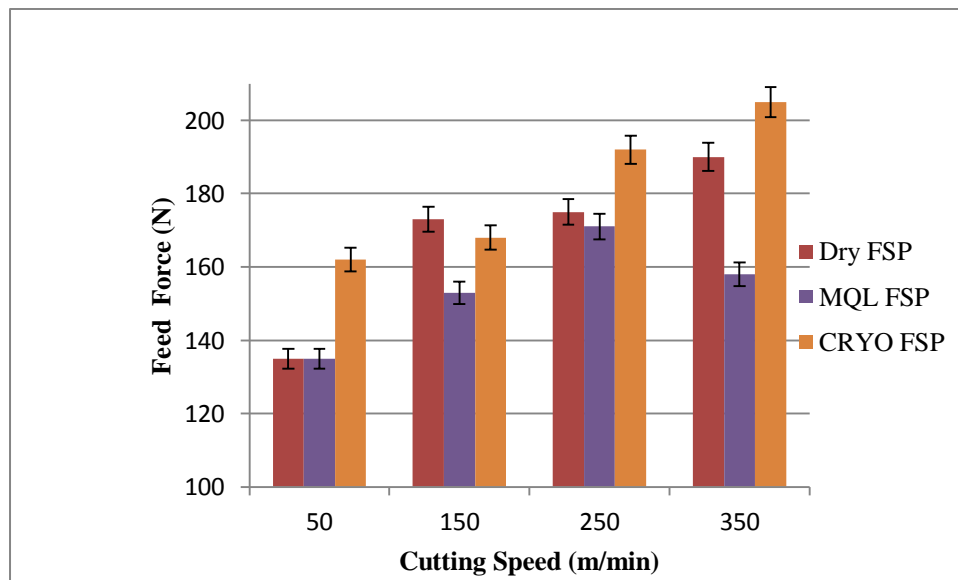
Figure 4.16 (b): Variation of feed force with cutting speed at constant feed value of 0.3 mm/rev for FSP samples

4.8 Chip formation

The different types of chips generated during the machining experiments reported above are discussed in the following section.

4.8.1 Importance of studying chip formation

Chip formation affects the surface finish, cutting forces, temperature, tool-life and dimensional tolerance. Effective machining speeds, feed rates, depth of cuts, and increased tool-life can be determined by proper understanding of the chip formation process for specific materials. Hence, it is important to study the chip formation process during the machining.

4.8.2 Different types of chips

During the machining process, three basic types of chips are formed. They are discontinuous chips, continuous chips, and continuous chips with built-up edge [48]. Chip formation depends upon the properties of the work material such as the yield strength, shear strength under compressive loading, strain-hardening characteristics, friction behavior, hardness, and ductility. Different types of chips are shown in Figure 4.17.
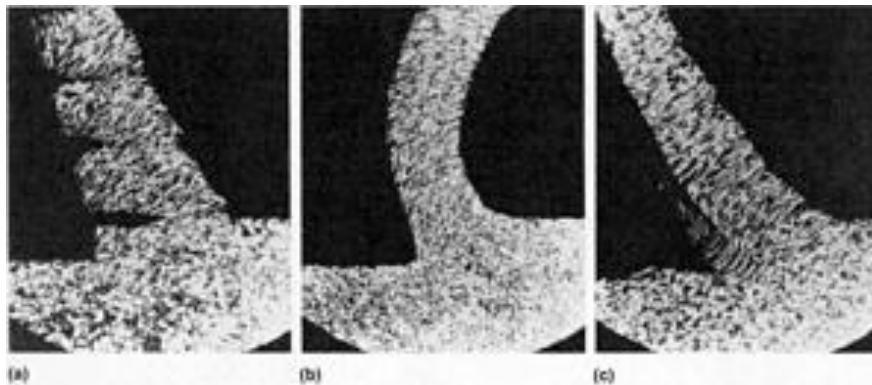
Figure 4.17: Three characteristic types of chips: (a) Discontinuous (b) Continuous (c) Continuous with built-up edge [48].

Cutting parameters such as tool materials, tool angles, edge geometries, which change due to tool-wear, cutting speed, feed, depth of cut, and the cutting environment (machine

tool deflection and cutting fluids) heavily influence the chip formation process. The built-up edge on the cutting tool further complicates the chip formation process.

A built-up edge is work material that is deposited on the rake face near the cutting edge as shown in Figure 4.17 (c). It is formed due to the localized high temperature and extreme pressure at the tool-chip interface and when the work material adheres to the cutting edge of the tool. The cutting edge is protected by this material, but the geometry of the tool is modified. Built-up edges are not stable and their formation can often be minimized by decreasing the depth of the cut, increasing the cutting speed, using positive rake tools, or applying a coolant. The application of all these techniques greatly makes the chip formation more complex. This type of chip formation is observed in softer non-ferrous metals and low carbon steels. It decreases the tool-life and final surface finish quality. Studies on the built-up edges have shown that the chip material is welded, deformed, and then deposited onto the rake face of the tool layer by layer. Improved lubrication conditions and sharp tools could be used to reduce the built-up edge.
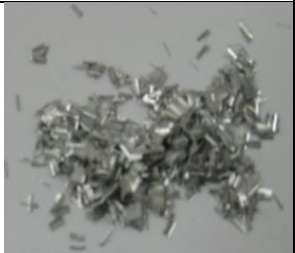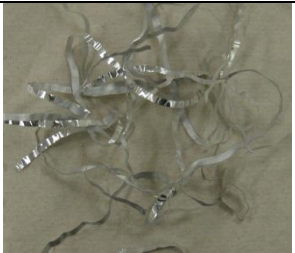
4.8.3 Chips from the machining experiments

The chips obtained for AR and FSP cases under the same machining conditions are similar. Chips obtained under Dry and MQL are similar, but the chips from Cryo at some cutting parameters differ slightly from their Dry and MQL counterparts. Examples of the different types of chips obtained under Dry FSP are shown in Table 4.9.

Three different types of chips obtained in the experiments conducted during this study are shown in Table 4.9. At a cutting speed of 50 m/min and a feed of 0.1 mm/rev, discontinuous chips are obtained, there is no change in the type of chip when increasing the feed from 0.1 to 0.3 mm/rev. When the cutting speed is increased to 150 m/min with feed, $f = 0.1$ mm/rev, a continuous chip in the form of ribbon is obtained. But, as the feed increases at a constant speed of 150 m/min, discontinuous chips are obtained at feeds 0.2 and 0.3 mm/rev. These chips are less fragmented than those obtained at cutting speed 50 m/min and feeds 0.2, 0.3 mm/rev. At the cutting speed of 250 m/min the continuous chip

is obtained and with an increase in feed to 0.2 mm/rev, the chips become less fragmented than those at cutting speed 150 m/min and feeds 0.2, 0.3 mm/rev. The chip at a cutting speed 250 m/min and a feed 0.3 mm/rev is more fragmented than at a cutting speed of 250 m/min and a feed 0.2 mm/rev. At a cutting speed 350 m/min and a feed 0.1 mm/rev, the chips are continuous and as the feed increases to 0.2 mm/rev, the chip becomes discontinuous and it is more fragmented at a feed of 0.3 mm/rev. This observation shows that discontinuous chips with more fragmentations are formed at high feed values of 0.3 mm/rev. At a cutting speed greater than 50 m/min and a low feed value of 0.1 mm/rev, a continuous chip is formed. At the feed value of 0.2 mm/rev, the chips are discontinuous, but less fragmented than those obtained at 0.3 mm/rev. The Dry and MQL machining produced similar type of chips.

Table 4.9: Different types of chips obtained at different cutting parameters during dry machining of FSP specimens

Cutting speed (m/min)	Feed rate (mm/rev)		
	0.1	0.2	0.3
50			
150			
250			
350			

Dry AR, Dry FSP, MQL AR and MQL FSP specimens have similar chip types at the same cutting parameters, whereas cryogenically machined disks frequently generate different chip types at the same conditions as shown in Table 4.10. At a cutting speed of 150 m/min and a feed of 0.1 mm/rev, the chips are discontinuous, unlike those obtained

in dry machining which are continuous. No continuous chips are obtained during cryogenic machining in current experiments. At cutting speeds of 250 m/min, 350 m/min and feed of 0.1 mm/rev, the chips are cyclic in nature as shown in Table 4.10. At a cutting speed 350 m/min and feed, $f = 0.2$ mm/rev, the cryogenically machined chips are discontinuous and more fragmented when compared to the chips obtained from dry machining.

Table 4.10: Different types of chips obtained at different cutting parameters during cryogenic machining of FSP specimens

Cutting speed (m/min)	Feed rate (mm/rev)		
	0.1	0.2	0.3
50	Same as dry	Same as dry	Same as dry
150		Same as dry	Same as dry
250		Same as dry	Same as dry
350			Same as dry

Hence, in this chapter the orthogonal machining experiments carried out on the disks are explained in detail. The force values for different AR and FSP specimens machined under dry, MQL and cryogenic conditions and using different cutting speeds and feeds are studied. The chips obtained under different machining experiment are also briefly discussed.

CHAPTER 5
RESULTS FROM MACHINING EXPERIMENTS

5.1 Microstructure and microhardness results

The results obtained from 72 different disks machined using different cutting conditions at different cutting parameters are collected and safely stored for later examination. As shown in Figure 5.1, microstructural specimens are removed from the machined disks by taking a sector from each of the 72 AR and FSP machined disks. The machined surface layer region is sliced and a cold mounted sample is prepared for each disk. The samples are washed in an ultrasonic cleaner, ground, polished and etched for metallographic examination and for the measurement of microhardness at various depths below the machined layer.

Microstructures are observed and microhardness measurements are made for the samples. Microhardness values are measured at different depths below the machined layer.The results obtained are tabulated and explained in detail under specific sections below. Parameters such as the thickness of the severe plastically deformed (SPD) surface layer, surface layer grain size, the microhardness values and the bulk grain size values at different depths are measured for each of the samples and the results are then analyzed. The micrographs are captured at 400 X magnification using an optical microscope. The microhardness values are measured using a Vickers hardness tester.
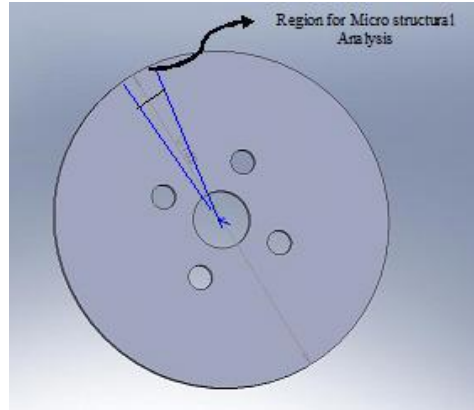
Figure 5.1: Sector sliced from the disk for the microstructure and microhardness observation

5.2 Nomenclature of micrographs

The different samples and cutting conditions are given in a nomenclature for an easier explanation of the results, as shown in Table 5.1 and 5.2.

Table 5.1: Abbreviated labels used for the different samples

Abbreviated form	Complete form
AR	As-received
FSP	Friction stir processed
Dry	Dry machining
MQL	Minimum quantity lubrication machining
Cryo	Cryogenic machining

Table 5.2: Nomenclature for the cutting parameters

Cutting speed (m/min)	Feed rate (mm/rev)		
	0.10	0.20	0.30
50	1	2	3
150	4	5	6
250	7	8	9
350	10	11	12

By combining the nomenclature of Tables 5.1 and 5.2 the used nomenclature is established. For example Dry AR 1 would mean the AR sample machined using dry machining at speed of 50 m/min and feed 0.1 mm/rev.

5.3 Microstructure classification

The microstructure results are analyzed in groups as Dry AR, Dry FSP, MQL AR, MQL FSP, Cryo AR, and Cryo FSP. Each group contains 12 microstructures obtained for the 12 cutting conditions given in Table 5.2. The results discuss the effects of changes in the cutting speed and the feed rates on the microstructure and microhardness values of the machined surface and a layer just beneath it. The results are also discussed according to the different lubrication applications of Dry, MQL and Cryo, as well as the prior processing conditions, AR and FSP.

5.4 Microstructure results

The microhardness values are measured at a distance of 10 µm shown in Tables 5.3 – 5.8 from the surface for all the samples. Due to the limitation of the microhardness tester used, it is impossible to obtain data closer to the machined surface. *Imagepro* software is used to measure the surface layer thickness, surface layer grain size and bulk grain size. For a curved surface layer boundary, the average value of surface layer thickness is taken across the width of the sample. The surface layer grain size is measured by further enlarging the image 5 times beyond the normal 400X magnification of the microscope by using the *Imagepro* software. The bulk grain size is measured at a distance of 100 µm below the machined surface.

5.4.1 Measuring the surface layer thickness

The thickness of the surface layer is measured using the *Imagepro* software. The thickness value is measured for three different micrographs obtained at different positions in the same sample and the average value is obtained. The *Imagepro* software has a feature of tracing the curvature on the image, in this case it is used for locating the machined surface layer and it plots an average over that traced path. The average of the layer thickness from the three micrographs is taken as the surface thickness layer value for that sample. The surface layer boundaries are straight for some of the samples and are

curved for others. Hence, the values are accordingly measured with the help of this software. Some of the sample figures showing the measurement of the surface layer thickness value are shown in Figure 5.2. Figure 5.2(a) shows a white line representing the value after taking an average over 3 micrograph values. Figure 5.2(b) illustrates how *Imagepro* traces over the curved machined surface layer boundary and plots an average over this boundary. The surface layer boundary is traced manually by observing the grain size variation below the machined surface.
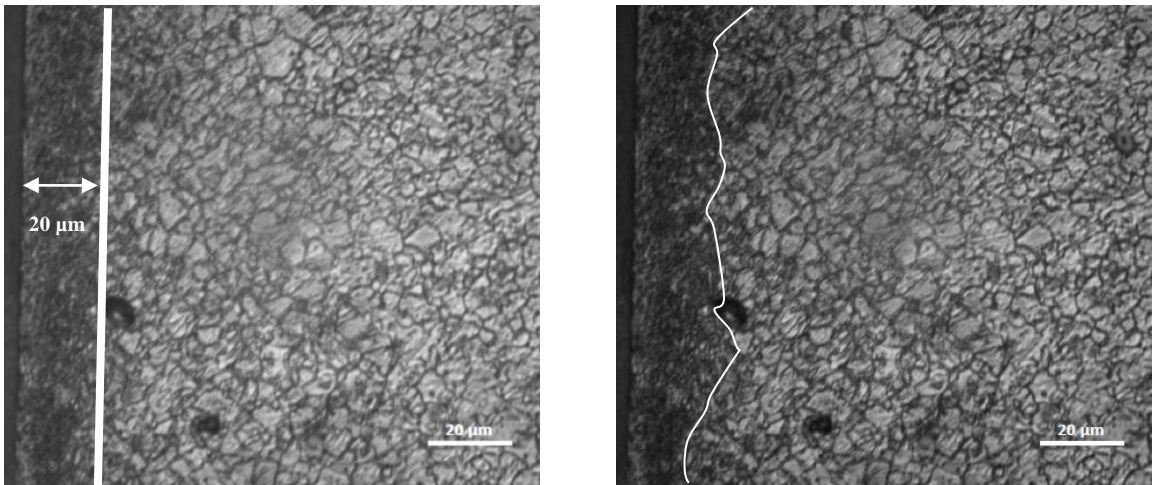
Figure 5.2: (a) Dry AR 2 average value calculated for three different microstructure images using *Imagepro* software

(b) Dry AR 2 curved surface layer traced using *Imagepro* software

Figure 5.3 shows how *Imagepro* is used to enlarge the image an additional 5 times and the surface layer grain size is measured. A portion near the surface layer is selected and *Imagepro* has a feature to trace the grain boundaries in that domain and using this data, it calculates a grain size for that region. It also measures the maximum and minimum grain size in the region and finally gives an average value grain size for the region. On each sample, three different spots are selected for calculating the grain size and then their average value is generated. This process is repeated on three different micrographs of the same sample and the average value is calculated. Hence, a total of 9 different spots are actually measured on each sample when the grain size value is evaluated.
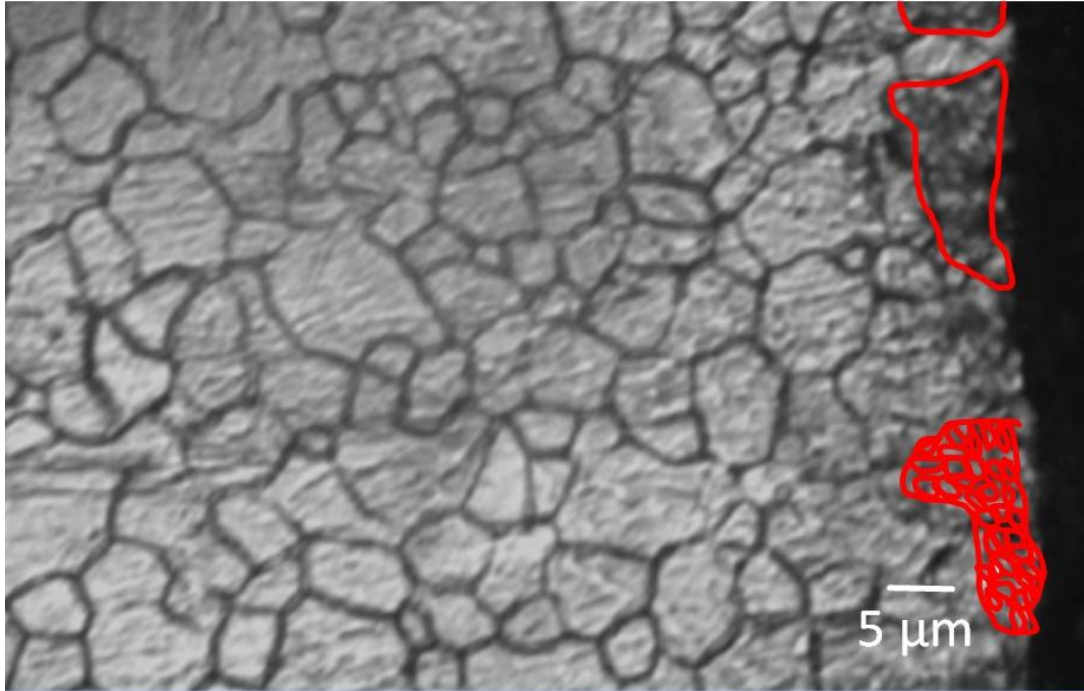
Figure 5.3: Dry AR 1 surface layer grain size calculation

5.4.2 Microstructure results for Dry AR

Dry AR microstructure and microhardness results are tabulated in Table 5.3. From Table 5.3, we see that some results are missing due to the inability in measuring those parameters due to limitation on the magnification of the optical microscope and/or bad etching. Several parameters are observed and their values are tabulated in Tables 5.3 – 5.8.

Table 5.3: Microstructure and microhardness results for Dry AR samples

Type	Surface layer thickness (µm)	Surface grain size (µm)	Microhardness at 10 µm (HV)
Dry AR 1	3	3-5	75
Dry AR 2	20	2-5	95
Dry AR 3	12	2-3	80
Dry AR 4	5	-	70
Dry AR 5	30	-	125
Dry AR 6	12	-	85
Dry AR 7	-	-	77
Dry AR 8	10	-	75
Dry AR 9	10	<1	85
Dry AR 10	5	3-5	90
Dry AR 11	10	<1.5	78
Dry AR 12	10	-	72

Figure 5.4 shows some of the sample microstructures obtained by metallographic examination of Dry AR samples. These samples are obtained for all machining conditions. Results for the parameters including surface layer thickness, surface grain size and microhardness value are obtained for different samples. The measured data is reported in Table 5.3.

Figure 5.4: Microstructure of AR samples machined under dry conditions at 400 X
magnification: (a) Dry AR 2, (b) Dry AR 5, (c) Dry AR 8, and (d) Dry AR 10

5.4.3 Microstructure results for Dry FSP

Dry FSP microstructure and microhardness results are as tabulated in Table 5.4. These
FSP samples have more variation in their microstructure between samples. Even though
Cryo FSP refines the grain size, we find that for some of the samples the grain size has
increased instead of decreasing during FSP. This is due to the uneven grain size
distribution after the FSP due to the eight multiple overlapping passes and the associated
non-uniform cooling process. The grain size also varies throughout the sheet thickness.

Table 5.4: Microstructure and microhardness results for Dry FSP samples

Type	Surface layer thickness (µm)	Surface grain size (µm)	Microhardness at 10 µm (HV)
Dry FSP 1	15	2-4	90
Dry FSP 2	10	-	70
Dry FSP 3	10	-	65
Dry FSP 4	10	1-2	70
Dry FSP 5	15	-	68
Dry FSP 6	15	3-6	63
Dry FSP 7	5	0.5-2	75
Dry FSP 8	10	-	70
Dry FSP 9	20	-	95
Dry FSP 10	10	-	78
Dry FSP 11	3	<0.5	70
Dry FSP 12	7	<0.5	75

Figure 5.5 shows some of the sample microstructures obtained by metallographic examination of Dry FSP samples.

Figure 5.5: Microstructure of FSP samples machined under dry conditions at 400 X magnification: (a) Dry FSP 1, (b) Dry FSP 9, (c) Dry FSP 10, and (d) Dry FSP 12

5.4.4 Microstructure results for Cryo AR

Microstructure and microhardness results for the Cryo AR specimens are tabulated in Table 5.5. Overall, the surface thickness values are found to be low in Cryo specimens, when compared to Dry ones, except at one value (Cryo AR 11) at the cutting speed of 350 m/min and feed 0.2 mm/rev.

Table 5.5: Microstructure and microhardness results for Cryo AR samples

Type	Surface layer thickness (μm)	Surface grain size (μm)	Microhardness at 10 μm (HV)
Cryo AR 1	7	1-2	75
Cryo AR 2	8	1-2	65
Cryo AR 3	8	-	62
Cryo AR 4	10	-	72
Cryo AR 5	8	-	62
Cryo AR 6	5	0.5-1	60
Cryo AR 7	5	<1	70
Cryo AR 8	5	<1	75
Cryo AR 9	5	<0.5	72
Cryo AR 10	5	-	75
Cryo AR 11	30	-	100
Cryo AR 12	5	-	70

Figure 5.6 shows some of the sample microstructures obtained by the metallographic examination of Cryo AR samples.
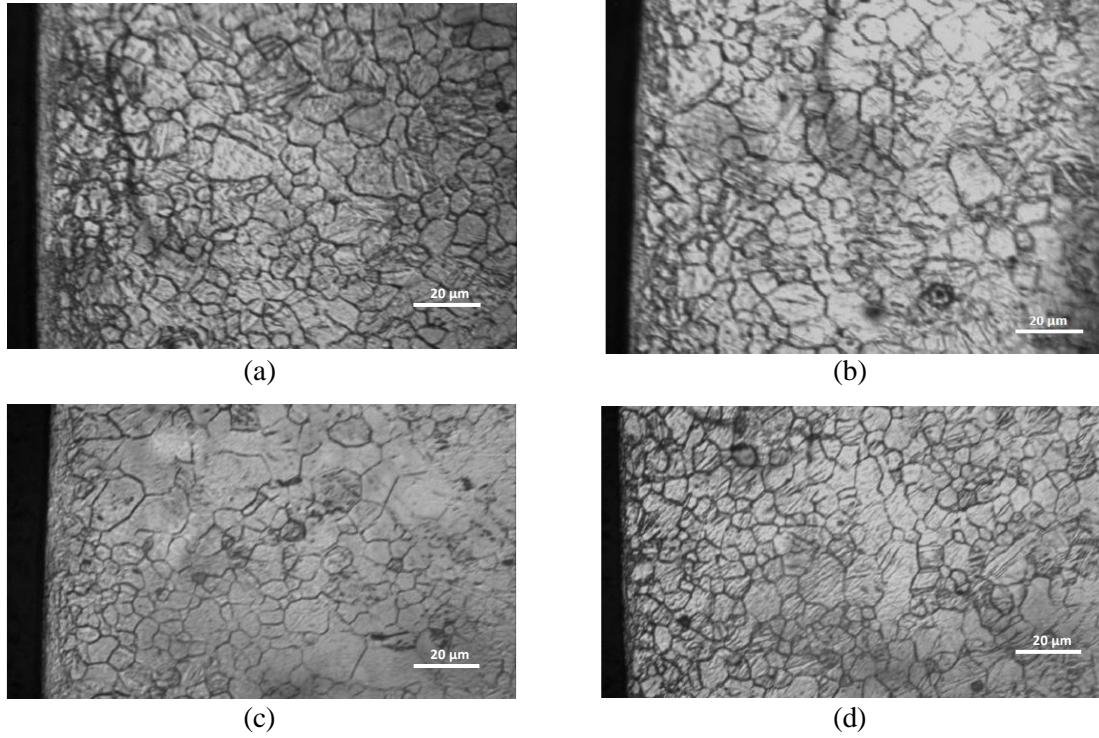
Figure 5.6: Microstructure of AR samples machined under cryogenic conditions at 400 X
magnification: (a) Cryo AR 3, (b) Cryo AR 6, (c) Cryo AR 7, and (d) Cryo AR 9

5.4.5 Microstructure results for Cryo FSP

Microstructure and microhardness results for Cryo FSP machined samples are reported in
Table 5.6.

Table 5.6: Microstructure and microhardness results for Cryo FSP samples

Type	Surface layer thickness (μm)	Surface grain size (μm)	Microhardness at 10 μm (HV)
Cryo FSP 1	6	1-1.5	70
Cryo FSP 2	6	-	75
Cryo FSP 3	10	-	80
Cryo FSP 4	5	1-2	90
Cryo FSP 5	10	1-2.5	65
Cryo FSP 6	10	-	70
Cryo FSP 7	30	-	125
Cryo FSP 8	5	4-8	76
Cryo FSP 9	5	<1	82
Cryo FSP 10	5	-	75
Cryo FSP 11	-	-	67
Cryo FSP 12	5	<0.5	95

Figure 5.7 shows some of the sample microstructures obtained by the metallographic examination of Cryo FSP samples.

(a) (b)

(c) (d)

Figure 5.7: Microstructure of FSP samples machined under cryogenic conditions at
400 X magnification: (a) Cryo FSP 5, (b) Cryo FSP 9, (c) Cryo FSP 10, and
(d) Cryo FSP 12

5.4.6 Microstructure results for MQL AR

Microstructure and microhardness results for MQL AR samples are tabulated in Table
5.7. The surface layer thickness values and hardness values are lower than those obtained
for the Dry and Cryo samples at the same cutting conditions.

Table 5.7: Microstructure and microhardness results for MQL AR samples

Type	Surface layer thickness (µm)	Surface grain size (µm)	Microhardness at 10 µm (HV)
MQL AR 1	8	2-3	80
MQL AR 2	8	2-3	82
MQL AR 3	8	-	80
MQL AR 4	7	2-3	80
MQL AR 5	5	-	75
MQL AR 6	-	-	76
MQL AR 7	5	-	81
MQL AR 8	5	0.5-2	79
MQL AR 9	5	-	76
MQL AR 10	5	1-2	72
MQL AR 11	5	0.5-2	78
MQL AR 12	3	-	77

Figure 5.8 shows some of the sample microstructures obtained by the metallographic examination of MQL AR machined samples.
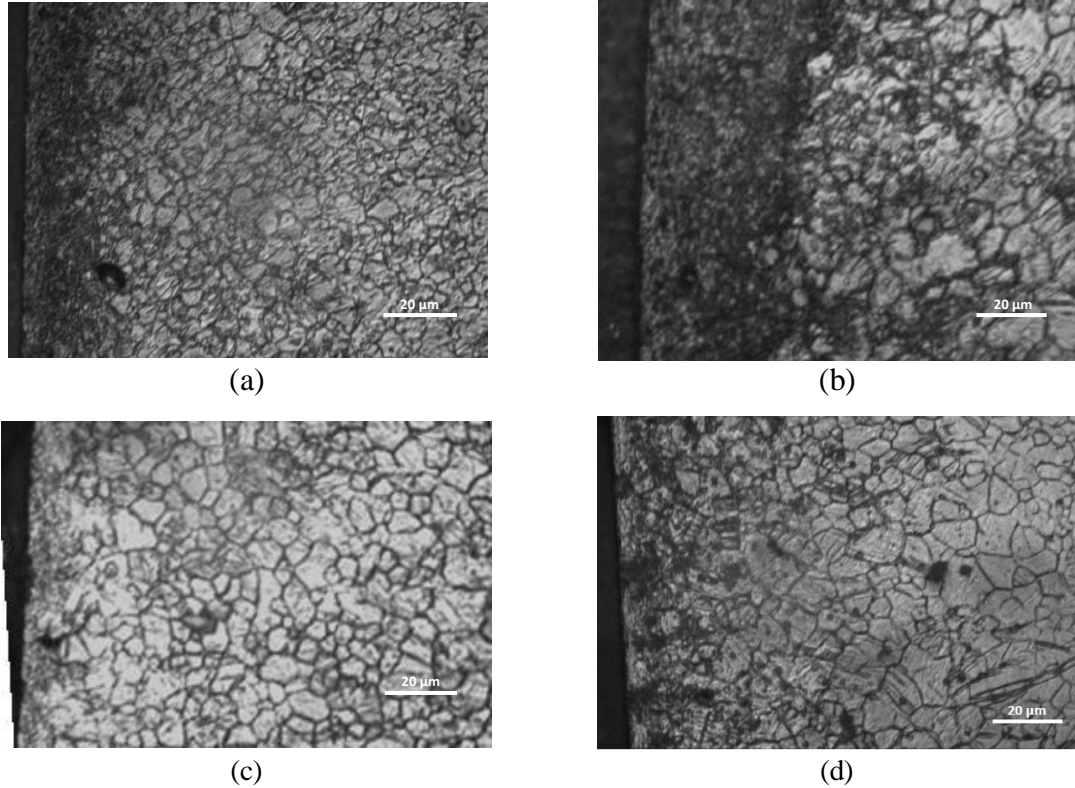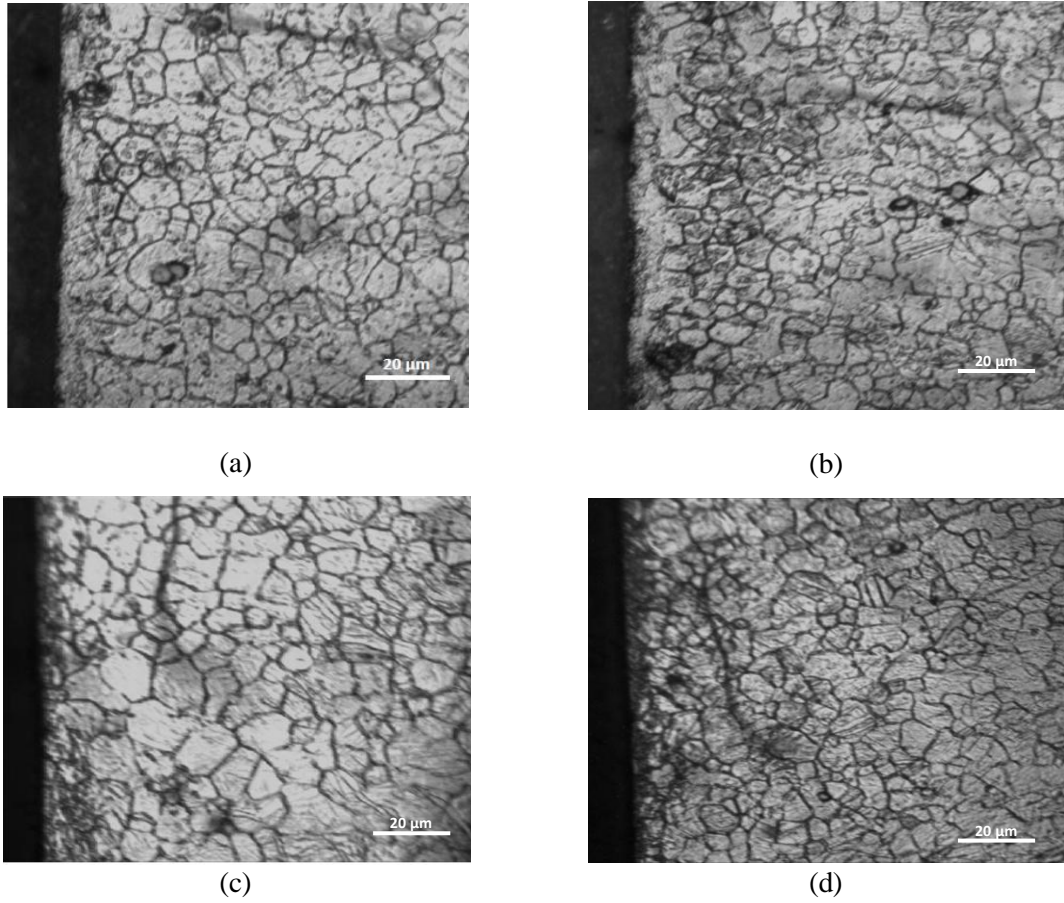
Figure 5.8: Microstructure of AR samples machined under MQL conditions at 400 X magnification: (a) MQL AR 4, (b) MQL AR 5, (c) MQL AR 8, and (d) MQL AR 9

5.4.7 Microstructure results for MQL FSP

Microstructure and microhardness results obtained from the MQL FSP machined samples are presented in Table 5.8.

Table 5.8: Microstructure and microhardness results for MQL FSP samples

Type	Surface layer thickness (µm)	Surface grain size (µm)	Microhardness at 10 µm (HV)
MQL FSP 1	-	-	72
MQL FSP 2	-	-	65
MQL FSP 3	8	-	68
MQL FSP 4	5	-	76
MQL FSP 5	7	1-2	87
MQL FSP 6	5	-	80
MQL FSP 7	5	-	90
MQL FSP 8	5	-	71
MQL FSP 9	8	2-3	70
MQL FSP 10	6	1-1.5	70
MQL FSP 11	6	0.2-1	71
MQL FSP 12	-	-	64

Figure 5.9 shows some of the sample microstructures obtained by the metallographic examination of MQL FSP samples.

<center>(a)</center>

<center>(b)</center>

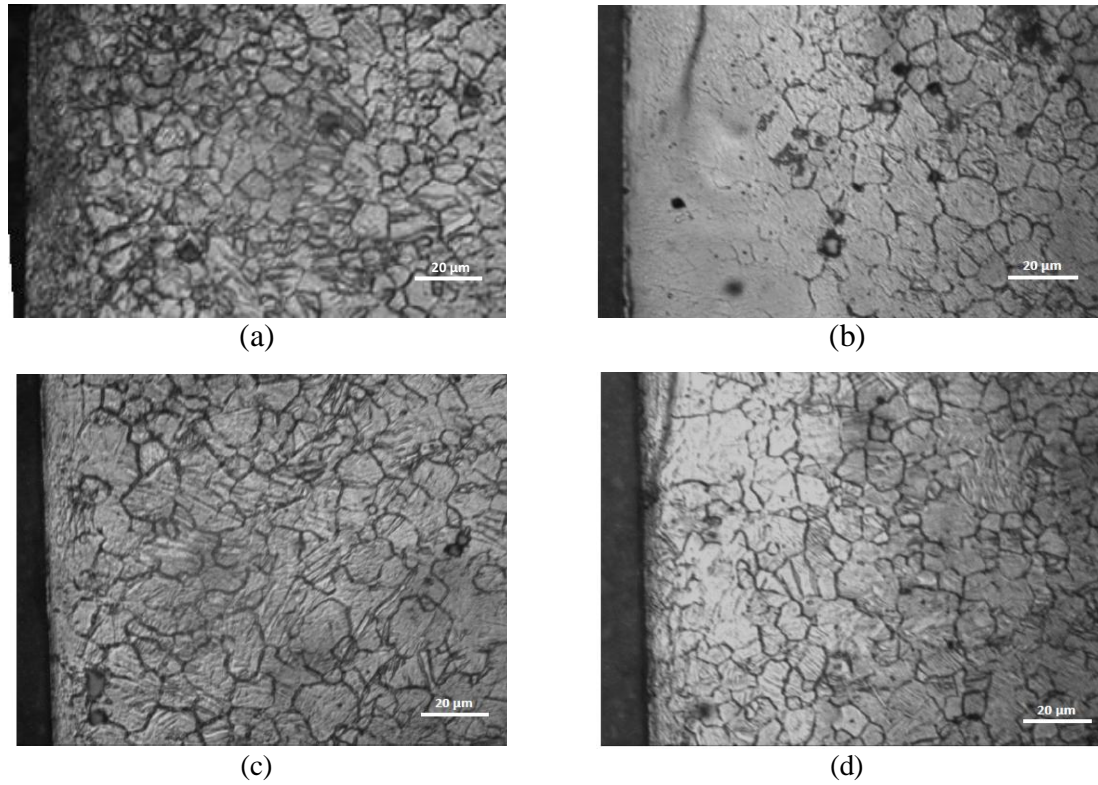<center>(c)</center>

<center>(d)</center>
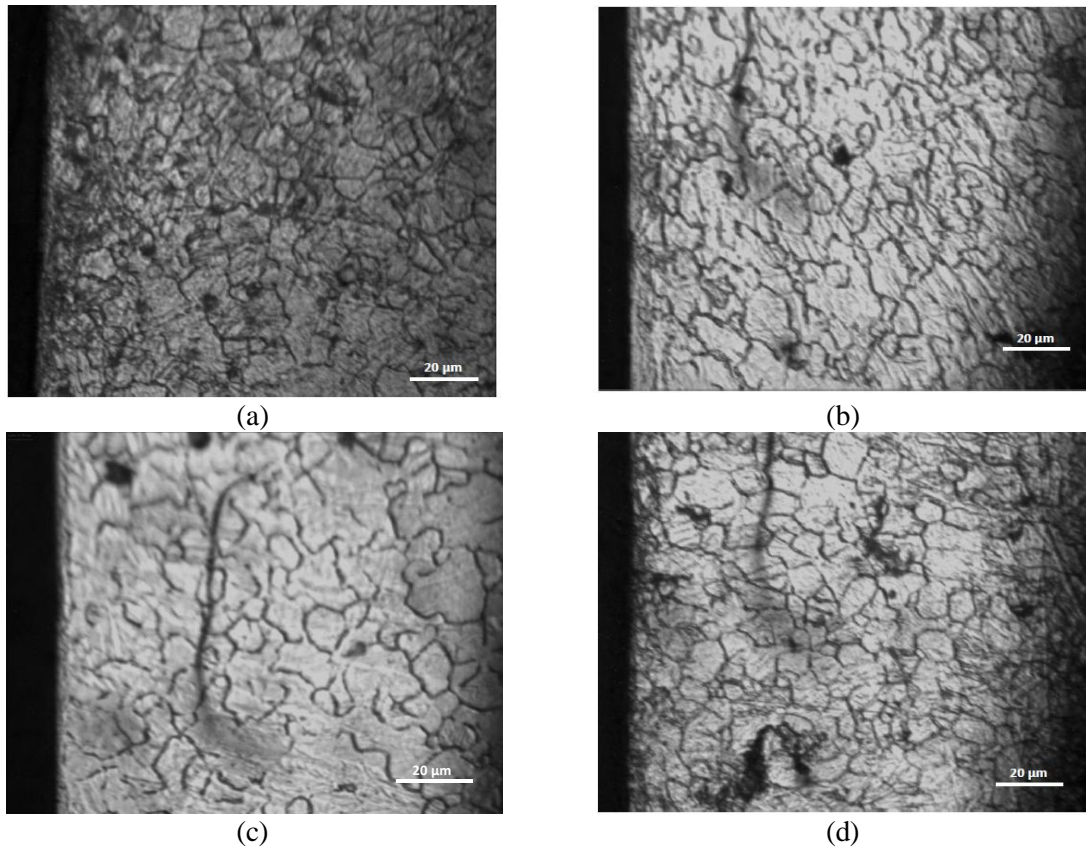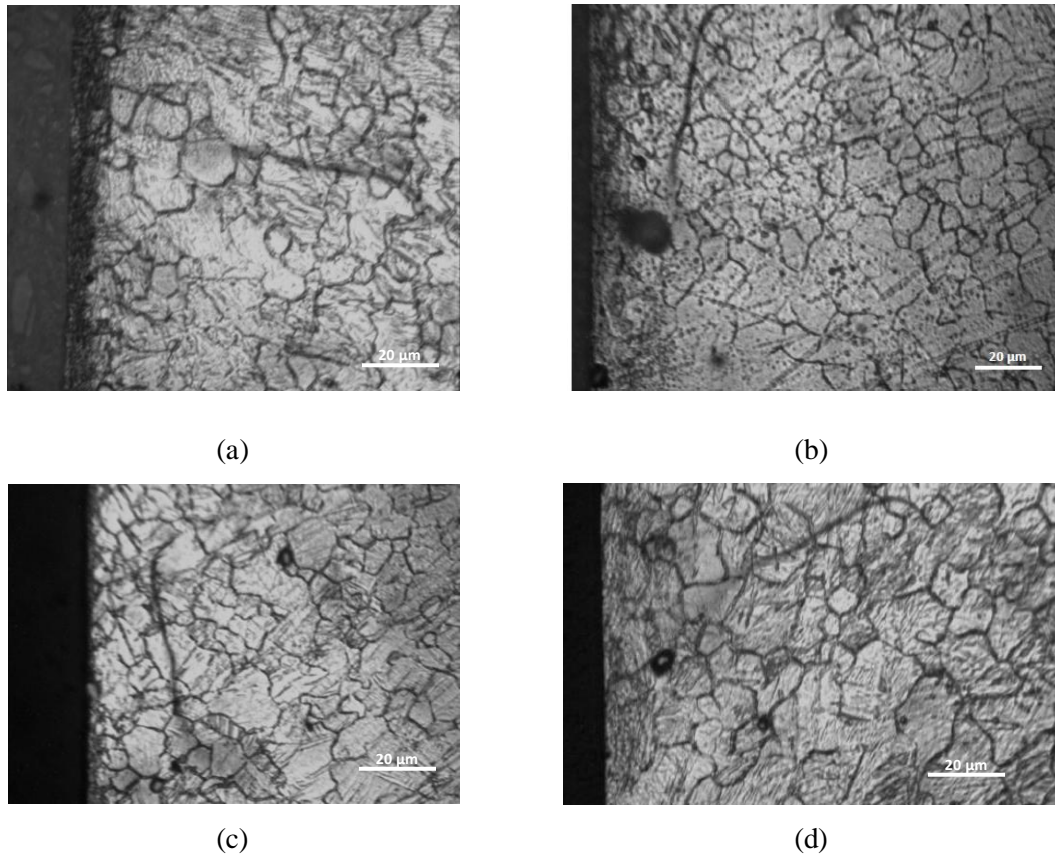
Figure 5.9: Microstructure of FSP samples machined under MQL conditions at 400 X magnification: (a) MQL FSP 3, (b) MQL FSP 5, (c) MQL FSP 8, and (d) MQL FSP 9

5.5 Microhardness results

The average microhardness values at a distance of 10 µm below the surface of all the samples are evaluated and tabulated as shown in Table 5.9.

<center>104</center>

Table 5.9: Average microhardness values at a depth of 10 µm below the machined surface for all machined samples

Microhardness values in HV						
Sample number	Dry AR	Dry FSP	Cry AR	Cry FSP	MQL AR	MQL FSP
1	75	90	75	70	80	72
2	95	70	65	75	82	65
3	80	65	62	80	80	68
4	70	70	72	90	80	76
5	100	68	62	65	75	87
6	85	63	60	70	76	80
7	77	75	70	125	81	90
8	75	70	75	76	79	71
9	85	95	72	82	76	70
10	90	78	75	75	72	70
11	78	70	100	67	78	71
12	72	75	70	95	77	64

Three different microhardness values are measured for each sample and the average hardness value is used for plotting the graphs. The graphs for AR and FSP specimens are plotted separately to better understand the data. From Figure 5.10 we see that the higher hardness values are achieved for the case of Dry AR for all 12 samples obtained at different cutting parameters. Second highest is MQL AR and Cryo AR has the lowest hardness values. This is in contrast to what we expect from cryogenic samples. This suggests that the best machining conditions for creating high hardness values in this material are achieved using dry lubrication for the used cutting conditions. Since magnesium is an easy to cut material and the temperature at the cutting interface during the machining process is low, dry cutting seems to be the best machining process in terms of microhardness values. For dry cutting, we observe that the variation of hardness with respect to change in feed and speed values amounts to a great variation in hardness values, but does not show any specific trend. Using MQL lubrication, we found almost constant hardness values when using varying speed and feed values. For cryogenically machined samples, the variation in microhardness values is small when compared to the dry machined samples.
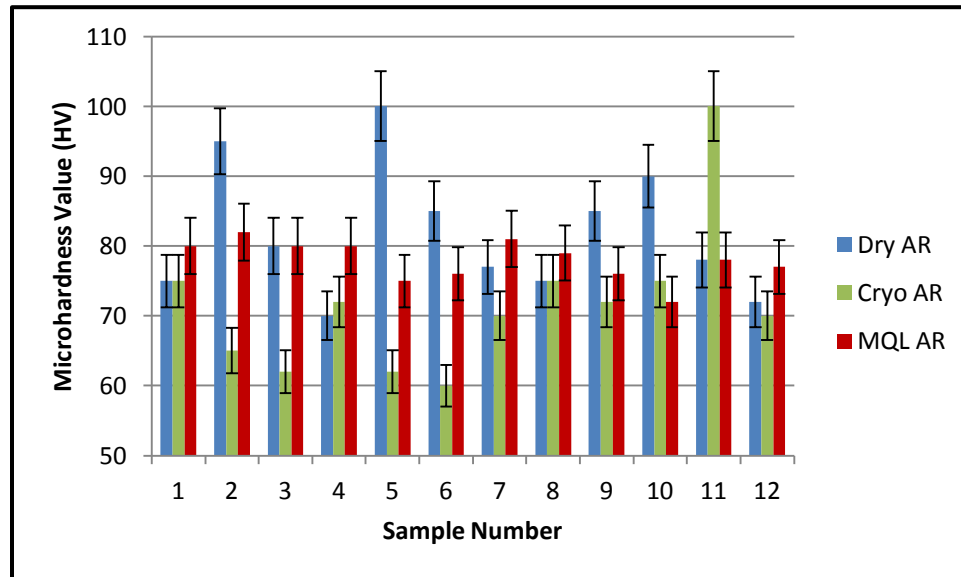
Figure 5.10: Microhardness vs. different samples for as-received specimens

From the Figure 5.11 we observe that the higher hardness values for FSP specimens are achieved for the case of Cryo FSP specimens, second highest is MQL FSP and Dry FSP samples have the lowest hardness values. The results are in contrast to what we obtained using the AR machined samples. Since the microstructure of the disk is changed by FSP, we produce different hardness values under similar machining conditions. This suggests that the best machining conditions with respect to high hardness values are achieved using Cryo cooling for the given cutting conditions in the FSP samples. The graphs does not show any specific trend, but the variation of the graphs show that changes in feed and speed values correlate with a great variation among hardness values in the Cryo machined samples. Dry machined samples have the second highest variation followed by MQL which has the least variation in microhardness values. For Cryo machined samples the microhardness variation is small when compared to the variation in the Dry machined ones.
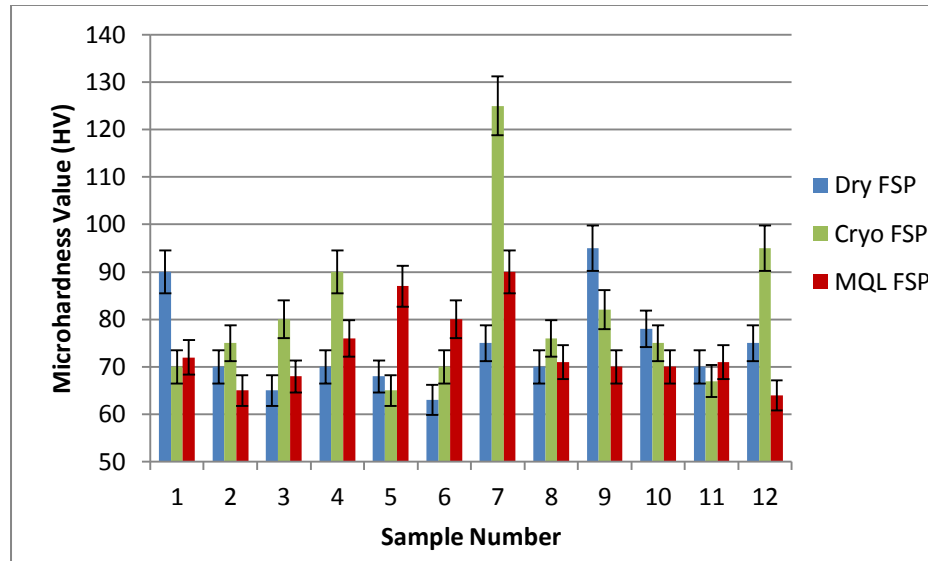
Figure 5.11: Microhardness vs. different samples for FSP specimens

5.6 Surface layer thickness figures

The machined surface layer thickness values are also measured and calculated using the *Imagepro* software and the data is presented as graphs for the different samples. Table 5.10 shows the surface layer thickness values for the different samples.

Table 5.10: Surface layer thickness values for the different samples

Surface layer thickness in µm						
Sample number	Dry AR	Dry FSP	Cry AR	Cry FSP	MQL AR	MQL FSP
1	3	15	7	6	8	-
2	20	10	8	6	8	-
3	12	10	8	10	8	8
4	5	10	10	5	7	5
5	30	15	8	10	5	7
6	12	15	5	10	-	5
7	-	5	5	30	5	5
8	10	10	5	5	5	5
9	10	20	5	5	5	8
10	5	10	5	5	5	6
11	10	3	30	-	5	4
12	10	7	5	5	3	-

From Figure 5.12 one can see the surface layer thickness value variation in the AR samples. The variation in surface layer thickness shown in Figure 5.12 is high for the case of Dry AR specimens followed by Cryo AR, and it is least for the case of MQL AR. The surface layer thickness values are high as the grain size in that region is more refined which imparts high hardness values increasing the compressive residual stress. The surface layer thickness values are small for the case of MQL whereas they are high for Dry AR samples. The values of surface layer thickness for Cryo AR are higher than those obtained by MQL AR. These variations agree with the microhardness values, suggesting that grain size has been refined in that region. With the increase in feed and speed values, one observes a constant trend for case of MQL AR and Cryo AR whereas the trend is varying for the case of Dry AR samples. This suggests that dry machining condition is better than MQL, Cryo for achieving high hardness values in AR materials.
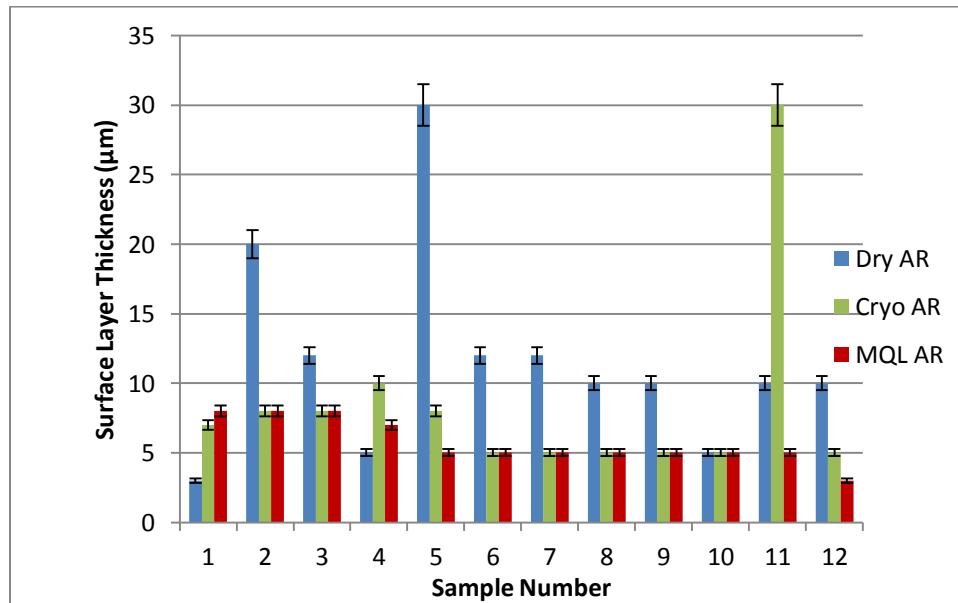
Figure 5.12: Surface layer thickness vs. different samples for as-received specimens

In Figure 5.13, we observe that the surface layer thickness value variation in Dry FSP, MQL FSP and Cryo FSP samples. The variation observed is highest for case of Cryo FSP, followed by Dry FSP, and it is least in the case of MQL FSP. The surface layer thickness values are found to be low for the case of MQL FSP where as they are high for Dry FSP specimens. The values for Cryo FSP are higher than those obtained by MQL

FSP. With the increase in feed and speed values, we observe a constant trend for case of MQL FSP and Cryo FSP where as the trend is varying for the case of Dry FSP.
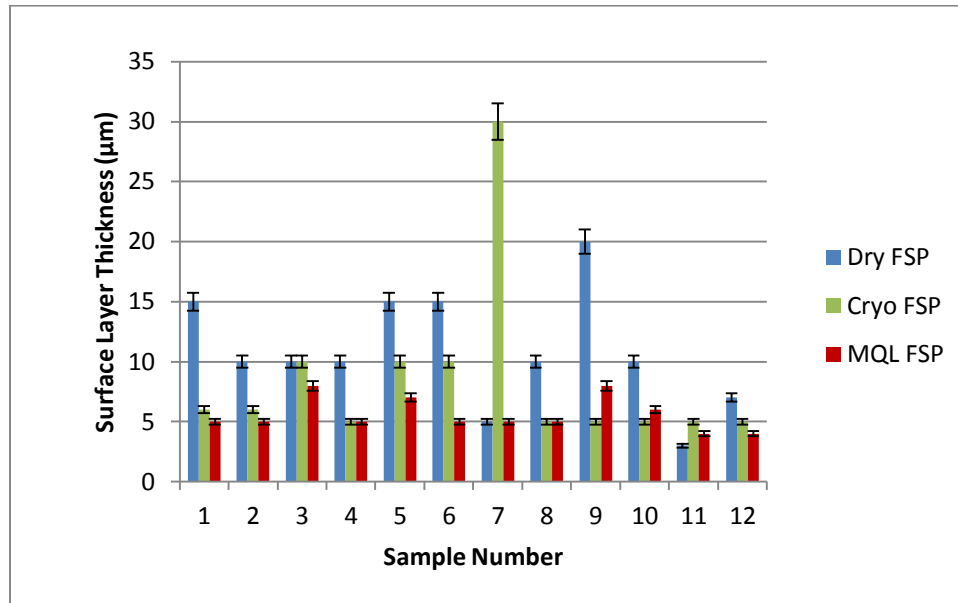
Figure 5.13: Surface layer thickness vs. different samples for FSP specimens

5.7 Microhardness values vs. cutting speed at constant feed values

Microhardness values as a function of cutting speed for different samples, which use constant feed values, are shown in Figure 5.14. In Figure 5.14, we observe that the microhardness values show an increasing trend for case of Dry AR specimens whereas they are almost constant for case of MQL AR and Cryo AR samples.
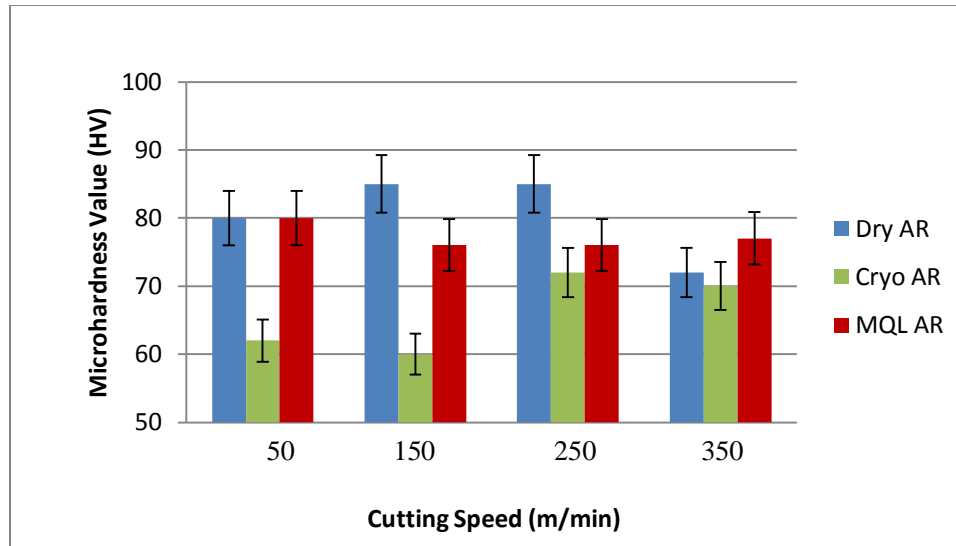
Figure 5.14: Microhardness values vs. cutting speed for AR specimens machined at constant feed of 0.1 mm/rev

Figure 5.15 shows that for FSP samples under Dry, MQL and Cryo lubrication conditions, the microhardness values show an increasing trend with increase in cutting speed for the case of Cryo AR and MQL AR specimens where as they are decreasing for Dry AR samples.
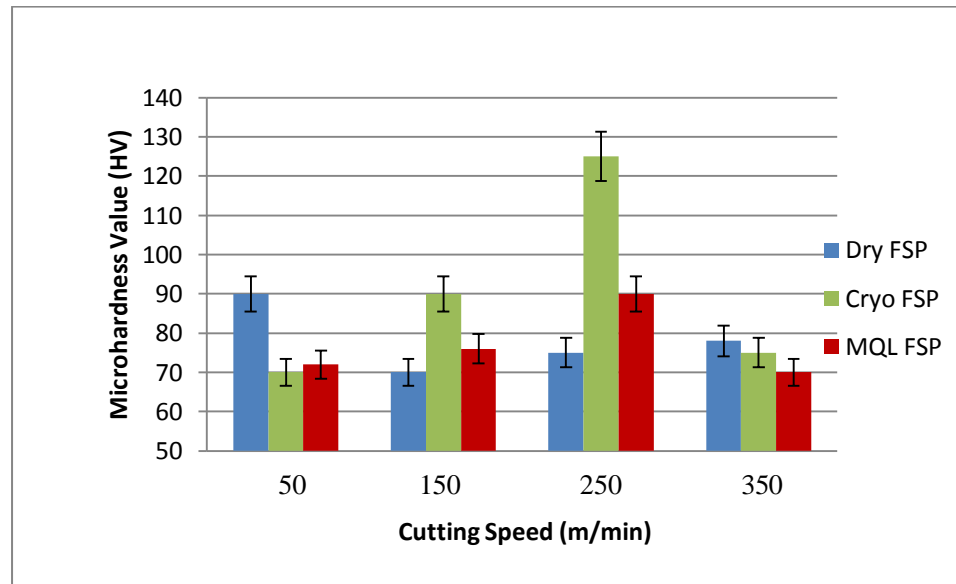
Figure 5.15: Microhardness values vs. cutting speed for FSP specimens machined at constant feed of 0.1 mm/rev

As shown in Figure 5.16, with an increase in feed value to 0.2 mm/rev, and at different cutting speeds, we observe, that the microhardness values are increasing with an increase in cutting speed for Cryo AR specimens. For the case of Dry AR samples, the values are decreasing, and they are almost constant for the case of MQL AR.
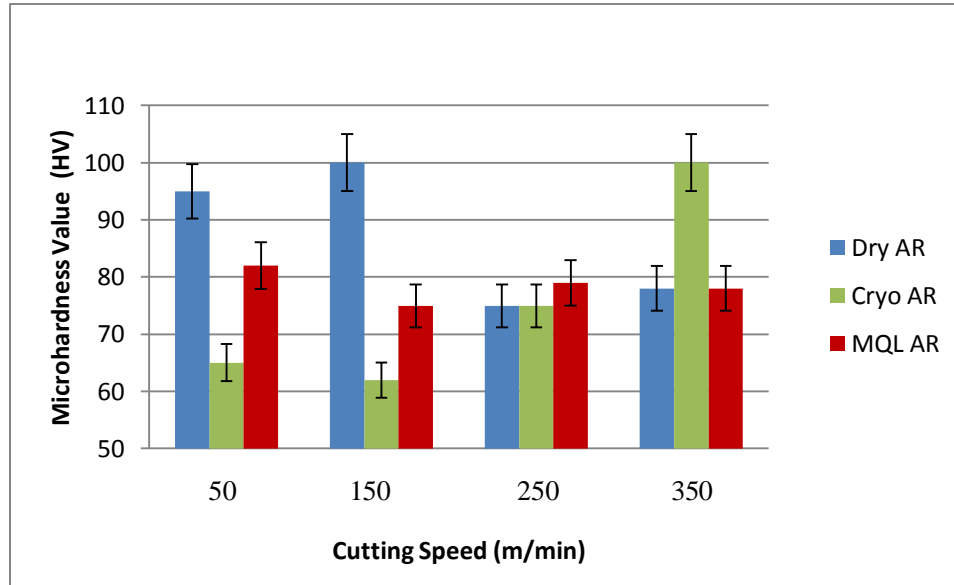
Figure 5.16: Microhardness values vs. cutting speed for AR specimens machined at constant feed of 0.2 mm/rev

With an increase in feed value to 0.2 mm/rev, and at different cutting speeds, we observe the variation in hardness for FSP samples shown in Figure 5.17. Figure 5.17 shows that there is no clear variation as we found in case of the microhardness. For the Cryo specimens, the microhardness values are first decreasing, and then increasing with an increase in cutting speed. A similar trend is observed for the case of MQL FSP samples where the microhardness values first increase to a highest value of 88 HV at a speed of 150 m/min, and then decreases when the cutting speed increases to 250 and 350 m/min. The trend is relatively constant for the case of Dry FSP samples.

111
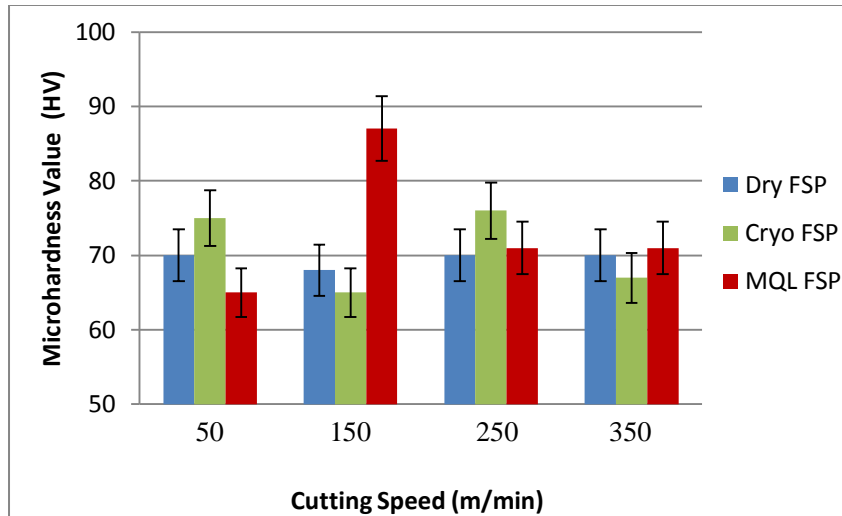
Figure 5.17: Microhardness values vs. cutting speed for FSP specimens machined at constant feed of 0.2 mm/rev

With an increase in feed value to 0.3 mm/rev, and at different cutting speeds, we observe the hardness variation shown in the Figure 5.18, which increase with an increase in cutting speed for Cryo AR specimens. For the case of Dry AR samples, the values first increase, then remain constant and finally decrease, so the trend in the case of Dry AR specimens is not clear. For MQL AR specimens the hardness at first decreases with an increase in cutting speed, and then remains constant as the speed increases in value.
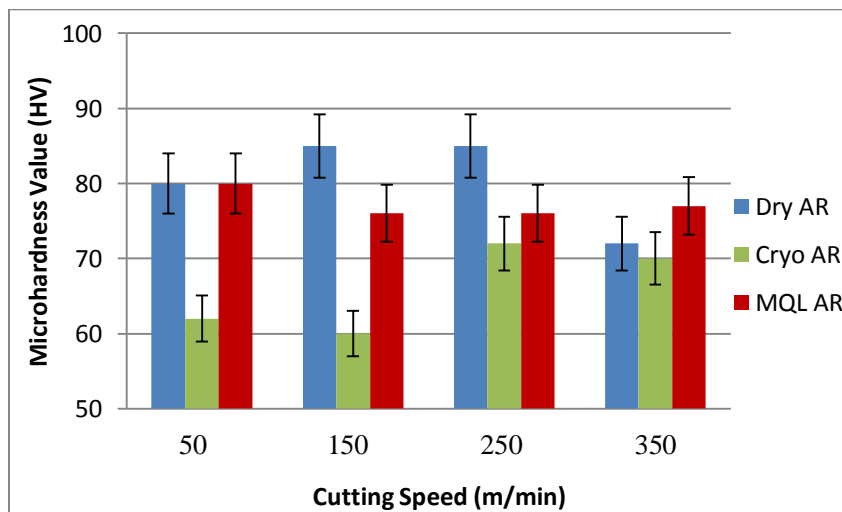
Figure 5.18: Microhardness values vs. cutting speed for AR specimens machined at constant feed of 0.3 mm/rev

For FSP samples at a feed of 0.3 mm/rev, we observe the following trend: Figure 5.19 shows that for Dry FSP specimens the microhardness values increase with a decrease of the cutting speed from 350 m/min. For MQL AR specimens the hardness values increase, and then decrease, and we see there is no clear trend. For the cryogenic machined samples, the measured hardness values first decrease, and thereafter increase with the cutting speed.
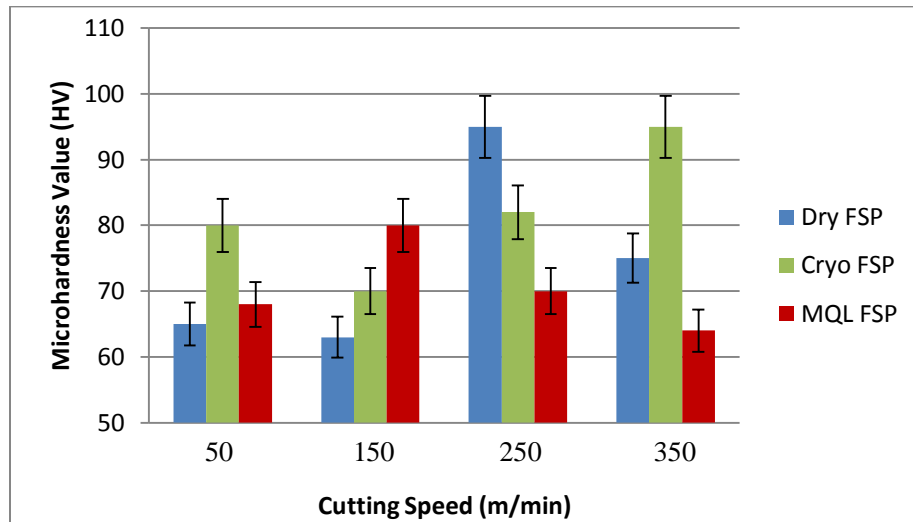
Figure 5.19: Microhardness values vs. cutting speed for FSP specimens machined at constant feed of 0.3 mm/rev

5.8 Microhardness measurements at different depths from the machined surface

Microhardness measurements are also made at several positions below the machined workpiece surface. The distances used are 10, 30, 50, 70, 90 and 110 μm below the surface. After 100 μm of depth from the machined layer the microhardness values are found to be constant as we enter the bulk material region. Table 5.11 shows the micro hardness values for 4 different AR samples obtained after each machining process. This same data is also presented in graphical form in Figures 5.20 – 5.26.

Table 5.11: Microhardness values for Dry AR machined specimens as a function of distance beneath the machined surface

Microhardness values (HV)				
Distance (μm)	Dry AR 1	Dry AR 4	Dry AR 7	Dry AR 10
10	75	70	77	90
30	65	60	68	78
50	60	55	60	65
70	58	52	55	55
90	55	50	52	54
110	52	51	48	52

Table 5.12: Microhardness values for Dry FSP machined specimens as a function of distance beneath the machined surface

Microhardness values (HV)				
Distance (μm)	Dry FSP 1	Dry FSP 4	Dry FSP 7	Dry FSP 10
10	90	70	75	78
30	80	60	58	65
50	73	50	50	54
70	67	45	45	52
90	58	48	47	48
110	59	57	48	46

Table 5.13: Microhardness values for Cryo AR machined specimens as a function of distance beneath the machined surface

Microhardness values (HV)				
Distance (μm)	Cryo AR 1	Cryo AR 4	Cryo AR 7	Cryo AR 10
10	75	72	70	75
30	62	60	65	60
50	62	60	60	60
70	59	62	60	58
90	60	60	56	59
110	62	60	55	75

Table 5.14: Microhardness values for Cryo FSP machined specimens as a function of
distance beneath the machined surface

Microhardness values (HV)				
Distance (µm)	Cryo FSP 1	Cryo FSP 4	Cryo FSP 7	Cryo FSP 10
10	70	90	125	75
30	50	80	100	70
50	45	75	80	66
70	42	70	65	60
90	40	70	60	55
110	45	68	55	57

Table 5.15: Microhardness values for MQL AR machined specimens as a function of
distance beneath the machined surface

Microhardness values (HV)				
Distance (µm)	MQL AR 1	MQL AR 4	MQL AR 7	MQL AR 10
10	80	80	81	72
30	68	75	61	65
50	61	66	58	62
70	57	63	52	60
90	55	62	50	55
110	57	55	51	55

Table 5.16: Microhardness values for MQL FSP machined specimens as a function of
distance beneath the machined surface

Microhardness values (HV)				
Distance (µm)	MQL FSP 1	MQL FSP 4	MQL FSP 7	MQL FSP 10
10	72	76	90	70
30	60	60	55	65
50	55	53	50	60
70	52	50	50	59
90	54	60	49	55
110	58	55	50	55

Figure 5.20 shows the measured microhardness as a function of distance from the
machined surface. Specimens machined using Dry, MQL and Cryo conditions are plotted
on the same graph to aid in the data comparison. As expected, we find the microhardness
values decreasing, as we move away from the machined surface. This is due to the
refinement of grain size in the region close to machined surface. Figures 5.21- 5.26 show

similar pattern, and have some variations depending upon the machining and preparation process used.

Figure 5.20: Microhardness values vs. depth beneath the machined surface for FSP specimens machined at 50 m/min cutting speed and 0.1 mm/rev feed

Figure 5.21: Microhardness values vs. distance beneath the machined surface for AR specimens machined at 150 m/min cutting speed and 0.3 mm/rev feed

Figure 5.22: Microhardness values vs. distance beneath the machined surface for FSP specimens machined at 150 m/min cutting speed and 0.3 mm/rev feed
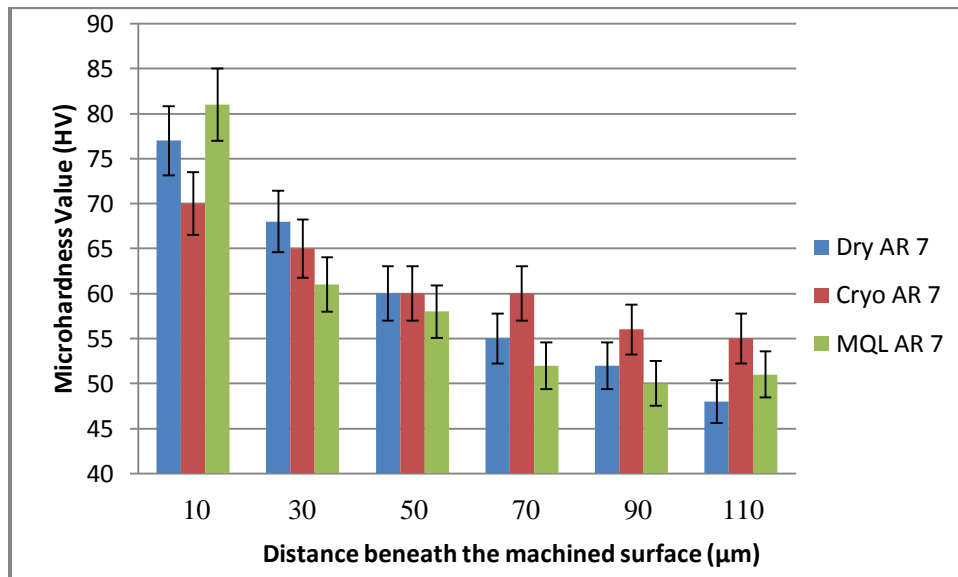
Figure 5.23: Microhardness values vs. distance beneath the machined surface for AR specimens machined at 250 m/min cutting speed and 0.1 mm/rev feed
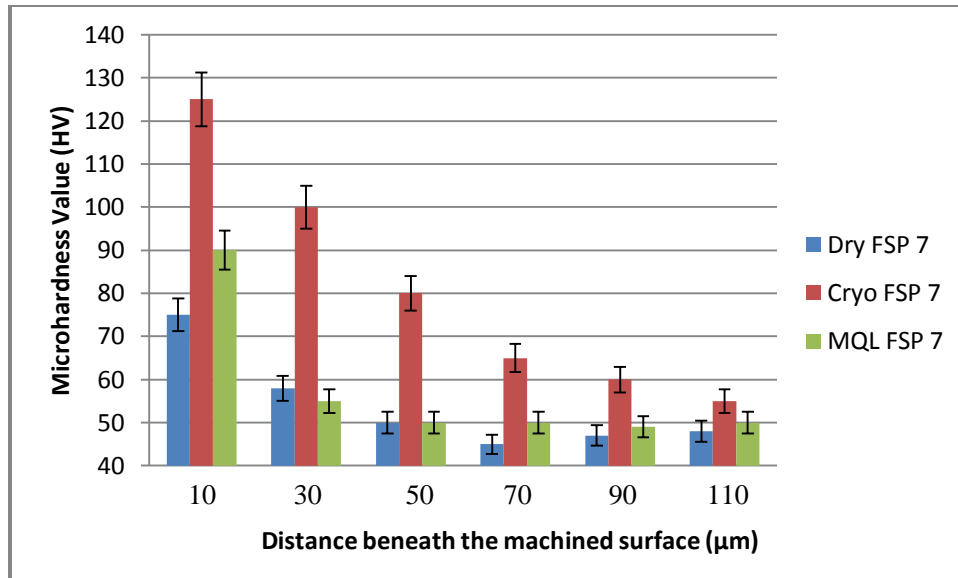
Figure 5.24: Microhardness values vs. distance beneath the machined surface for FSP specimens machined at 250 m/min cutting speed and 0.1 mm/rev feed
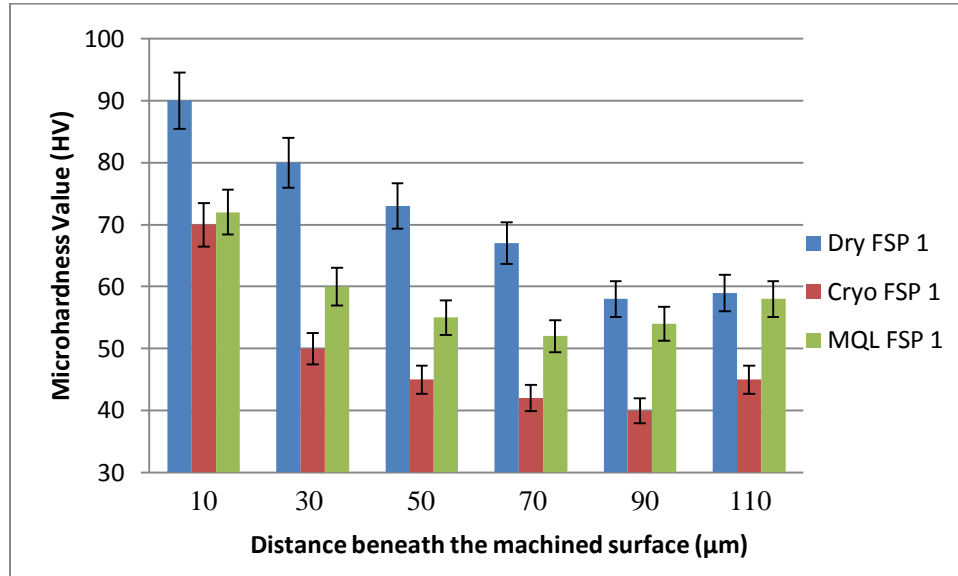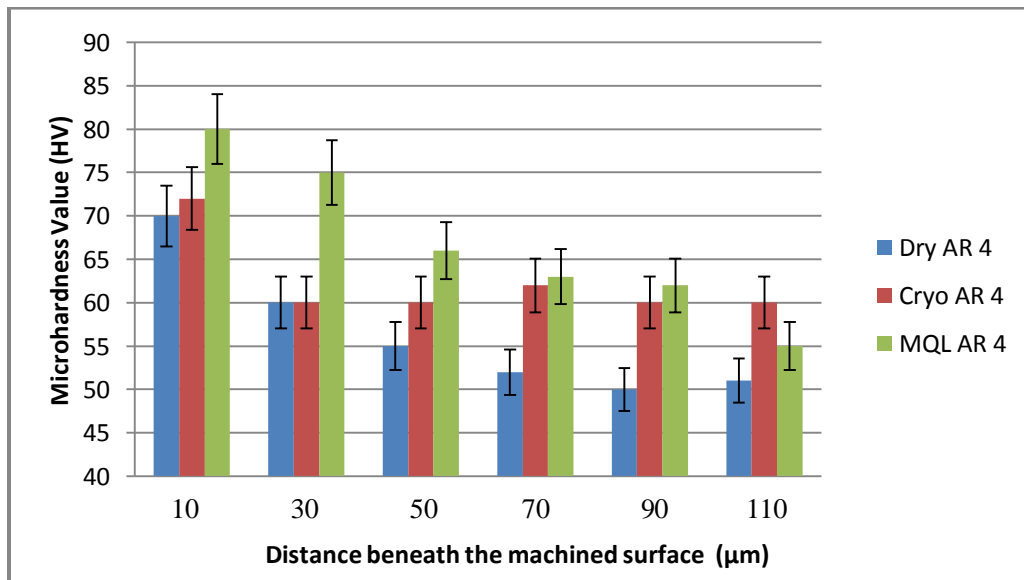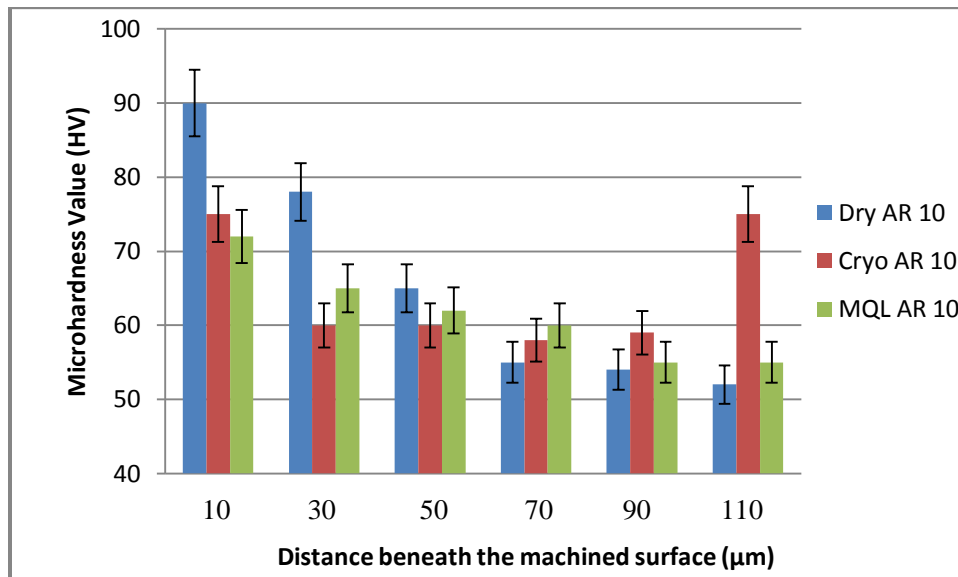

Figure 5.25: Microhardness values vs. distance beneath the machined surface for AR specimens machined at 350 m/min cutting speed and 0.1 mm/rev feed
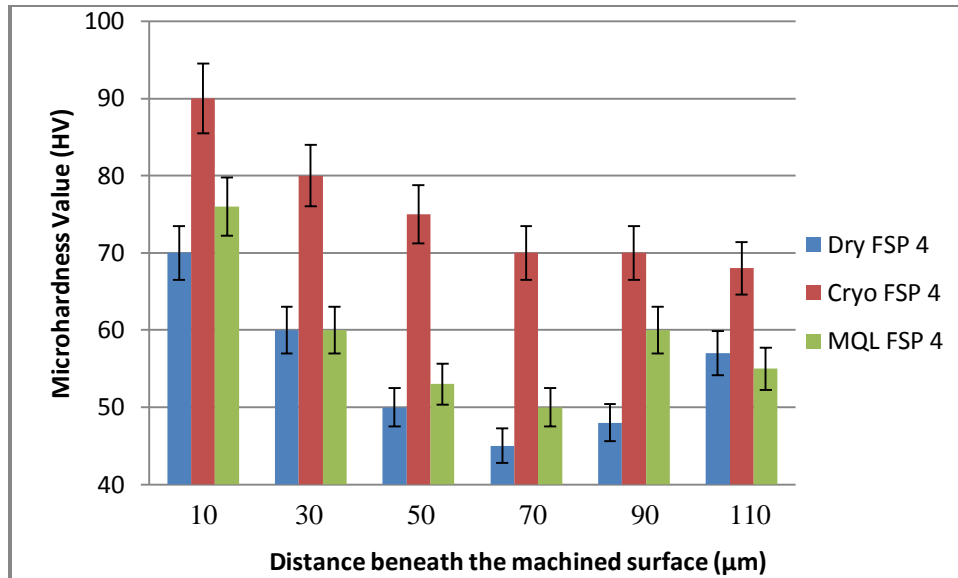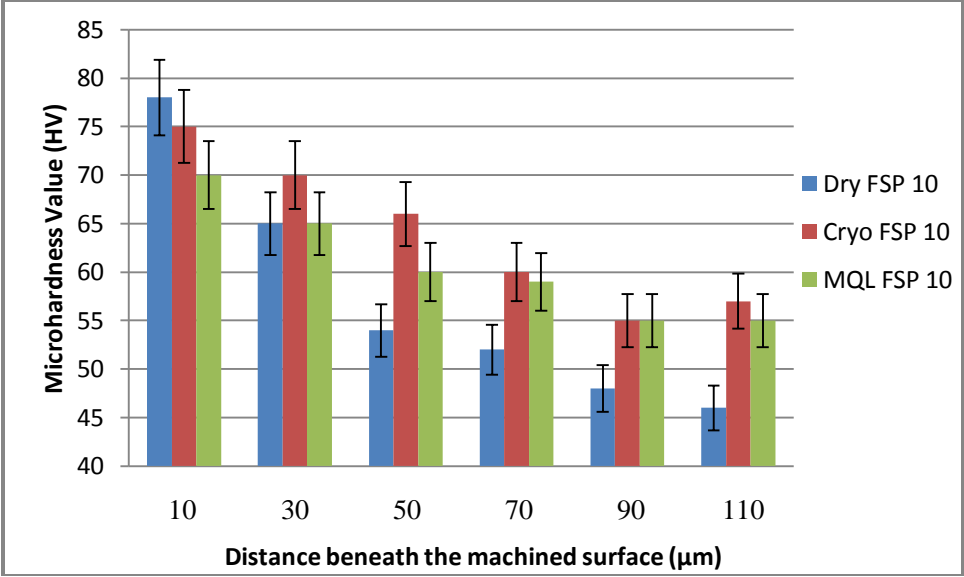
Figure 5.26: Microhardness values vs. distance beneath the machined surface for AR specimens machined at 350 m/min cutting speed and 0.1 mm/rev feed

CHAPTER 6
SUMMARY, CONCLUSIONS AND FUTURE WORK

6.1 Summary

- The focus of this research is on friction stir processing (FSP) of *Mg AZ31B-O* alloy using cryogenics followed by orthogonal machining under different cooling conditions and with various cutting parameters. Light-weight alloys are being extensively used in aerospace and automotive industries because of the reduction in the fuel consumption and toxic emissions. Magnesium alloys are considered as one of the lightest construction metals on earth.

- FSP experiments are performed on *Mg AZ31B-O* alloy sheet of dimensions 115 mm X 115 mm X 3 mm using different coolants such as Swiss Lube coolant, liquid nitrogen coolant, and applied on the top and underneath the fixture. The processing conditions of translational feed 500 mm/min and rotational speed of 1200 rpm and cryogenic as cooling condition are studied in an attempt to achieve an ultrafine grain size and high microhardness values with improved homogeneity across the thickness of the sheet. Thirty six specimens are friction stir processed at these fixed processing conditions.

- The effect of the process parameters on the resultant processed material is investigated. The effect of stirring conditions (rotational and translational speeds), and the effect of the coolant application on the resultant microstructure and microhardness of a multiple overlapping passes are investigated on the processed material. Two locations of coolant application have been studied, underneath the fixture through the backing plate, and the coolant on the top of sheet's surface. Different cooling conditions of Swiss lube, liquid nitrogen are applied on the top surface and underneath the fixture at bottom, and the application of liquid nitrogen on top as well as underneath the fixture was found to be the best combination for achieving smaller grain size.

6.2 Conclusions

- Microstructure of different FSP samples processed at different cooling conditions and processing conditions are observed and the grain size is measured. The MP FSP was started with MP (1-sided) with Swiss Lube coolant underneath the fixture and the grain size was found to be 12 µm at the bottom region. MP (2-sided) with Swiss Lube coolant underneath the fixture has shown no improvement and the resulting grain size was 12 µm in the bottom region. With MP (1-sided) with flood coolant on top and underneath the fixture the grain size was refined to 7 µm. MP (1-sided) with flood coolant and 45 seconds waiting time between successive passes helped in further refining the grain size to 3-5 µm average. For MP technique with cryogenic on top, as well as at bottom, the grain size was refined to ultrafine grains of size 1-2 µm.

- Microhardness measurements are made across various depths from the bottom surface of the FSP sheet. High microhardness values in the range of 100-125 HV, which is 2-2.5 times higher than the original hardness value, 50-55 HV, are found in the cryogenic samples.

- Thirty six disks of 75 mm diameter are produced from the FSP sheets and an additional 36 are made from AR material for the orthogonal machining experiments. The initial grain size (average 10-12 µm), and the microhardness of the virgin material (average 50 HV) are measured.

- Orthogonal machining experiments are performed on all 72 disks using the cooling conditions of dry, MQL and cryogenic and different feed rates and cutting speeds. The cutting edge radius value was kept constant at 45 µm for all these experiments. Cutting forces are measured during the experiments and at different speeds and feed values. They are found to be slightly high in the case of cryogenic machining, which is due to high forces required at low cutting temperatures. The cutting force values for dry machining is in the range of 150-350 N, for MQL machining it is in the range of 140-340 N and for cryogenic machining it is the

range of 140-370 N. Different types of chips are obtained during the varied machining processes.

- Microhardness measurements are made across various depths from the finished layer on the machined surface to give a new insight into the work-hardening process induced during the machining operation. Microstructure is observed for all the samples obtained under these machining conditions and several grain parameters such as surface grain size, surface layer thickness, and microhardness values are measured. Grain size in the order of 0.5-1 µm or < 0.5 µm is found in the case of cryogenic and dry samples. Surface layer thickness of 20-30 µm with ultrafine grains was found in some of the cryogenic and dry samples. All the samples are studied using these parameters and the graphs are plotted. The microstructure analysis gives an interesting new insight, with a comprehensive picture of the microstructure changes induced by the machining process incorporating the effect of change in machining conditions, cutting parameters and FSP.

- In the current research project it is found that the stirring conditions (rotational and translational speeds) significantly affect the process and the resulting grain structure, and have different effect for different materials. In this research, a range of stirring conditions that provide good processed material quality which is void of any visible defects and fine grains for *Mg AZ31B-O* alloy are used. Cryogenic cooling during FSP helps in obtaining a more refined grain size as it reduces the grain growth of the recrystallized grain by lowering the process temperature.

- The effect of cutting conditions is studied to better understand how grain size is refined and microhardness is increased.

6.3 Future work

- Methodologies for producing more uniform materials should be investigated both in the plane of the sheet and through the thickness of the sheet. The fixture can be redesigned for better cooling when using cryogenic cooling.

- It would be very desirable to make microhardness measurements on the bottom surface, or very close to the bottom surface, of the FSP sheet and on the machined surface layer of the disks. Similarly, microstructure could be observed at high magnification using a TEM or atomic force microscope. This will help in better understanding of the effects of FSP and machining on the critical points in the material. The sample preparation for TEM sample would likely require months of work and intensive training.

- FSP tools of different tool geometries such as trimmed, threaded-pin, etc., could be investigated for their ability to generate more uniform grain size across the thickness of the sheet. Effect of tool inserts of different edge radii values can be studied on the machining of FSP and AR disks. The tool diameter can be increased to reduce the number of passes in multiple pass FSP.

- The surface integrity aspects such as surface roughness, residual stress and corrosion values on the material after being FS processed could be investigated.

- Different numerical models could be used to simulate multiple pass FSP using cryogenic cooling and to provide a good estimate for the material behavior during the process. This also helps in designing the process parameters such as the rotational speed, translational feed, and also to find the appropriate geometry of tools that provide the desired fine grain homogeneous structure. It is especially important for strain-rate and stress effects on the process.

- FEM models computational tools such as the CFD must be utilized to design the process parameters, tool geometry, the fixtures, and flow rates of cryogenic cooling for the optimum performance of MP FSP and for different materials.

APPENDIX

(i) Eight-pass multiple friction stir processing CNC machine program for HAAS milling machine

In this CNC program, the first step consists of the drill cycle using a 25 mm diameter drill tool to make eight different holes at specified positions in the thickness direction of *Mg AZ31B-O* alloy sheet, 115 mm length X 115 mm width X 3 mm thick. The second step consists of the friction stir processing cycle and these eight drilled holes are used for guiding the pin of the friction stir tool to make eight overlapping passes on the sheet. Each pass is made along the length of the sheet giving a translational feed to the rotating FSP tool. T1 is the drill tool and T2 is the FSP tool. S1200 is the rotational speed of the FSP tool in rpm and F20 is the translation feed of the FSP tool in inches/min.

```
G17 G40 G49 G64 G80 G98
T1 M06 (T)
G90 G54 G00 X0.562 Y1.4
S1500 M03
G43 H00 Z1. M08
G01 F40. Z0.1
G81 G99 Z-0.125 R0.1 F4. (drill cycle starts)
X0.937
X1.312
X1.687
X2.062
X2.437
X2.812
X3.187
G80 G00 Z3. M09
G17 G40 G49 G64 G80 G98 (drill cycle ends)
T2 M06 (stir tool)
```

G90 G54 G00 X0.562 Y-1.4 (FSP pass 1)

S1200 M04

G43 H02 Z1. M08

G01 Z0.1 F40.

Z-0.1255 F5.

Y-3.2 F20.

Z0.1 F5.

G00 Z1

X0.937 Y-1.4 (FSP pass 2)

Z-0.1255 F5.

Y-3.2 F20.

Z0.1 F5.

G00 Z1

X1.312 Y-1.4 (FSP pass 3)

Z-0.1255 F5.

Y-3.2 F20.

Z0.1 F5.

G00 Z1

X1.687 Y-1.4 (FSP pass 4)

Z-0.1255 F5.

Y-3.2 F20.

Z0.1 F5.

G00 Z1

X2.062 Y-1.4 (FSP pass 5)

Z-0.1255 F5.

Y-3.2 F20.

Z0.1 F5.

G00 Z1

X2.437 Y-1.4 (FSP pass 6)

Z-0.1255 F5.

Y-3.2 F20.

Z0.1 F5.

G00 Z1

X2.812 Y-1.4 (FSP pass 7)

Z-0.1255 F5.

Y-3.2 F20.

Z0.1 F5.

G00 Z1

X3.187 Y-1.4 (FSP pass 8)

Z-0.1255 F5.

Y-3.2 F20.

Z0.1 F5.

G00 Z1

G00 Z4. M09

G53 G49 Y0 Z0 M05

T1 M06

M30

(ii) Cutting temperature measurements during machining

The emissivity value was calculated by using a k-type thermocouple and the infrared camera by calibrating the machining disk for its room temperature emissivity. The disk was heated to different temperatures and temperature values are recorded using both thermocouple and infrared camera (A FLIR Systems ThermaCam PM695). From the known temperature (from the thermocouple) and the apparent temperature reading of the infrared camera, the thermal emissivity of the *Mg AZ31B-O* alloy disk is determined. The temperature at the center of the disk was adjusted to room temperature in the Thermacam (infrared imaging system software) and the emissivity value was found to be 0.5. The emissivity value is used to calculate the workpiece-tool insert interface temperature by processing the thermographic camera images that had been stored in the computer.

Sample infrared images are shown in Figures A1- A3. The different spots shown in the figures are highest temperature values recorded in the cutting zone at workpiece-tool interface. The disk size was small at 75 mm, and hence, the zoom feature on the infrared camera was used, which was later found to have affected the accuracy of the temperature measurements. The cutting temperature measurements on the same *Mg AZ31B-O* alloy were made by Zhengwen [49] in his research work and they are as shown in Figure A4. He observed the maximum temperature on the machined surface under different conditions using an infrared camera. The maximum temperature of 130 ºC was measured under dry machining with a tool insert of edge radius 30 µm and the temperature was reduced to 50 ºC using cryogenic cooling. He also observed the cutting temperature for a tool insert of edge radius 70 µm using cryogenic cooling, and it was found to have increased to 70 ºC.

Figure A1: Dry-machined FSP sample at 0.1 mm/rev feed and 150 m/min cutting speed
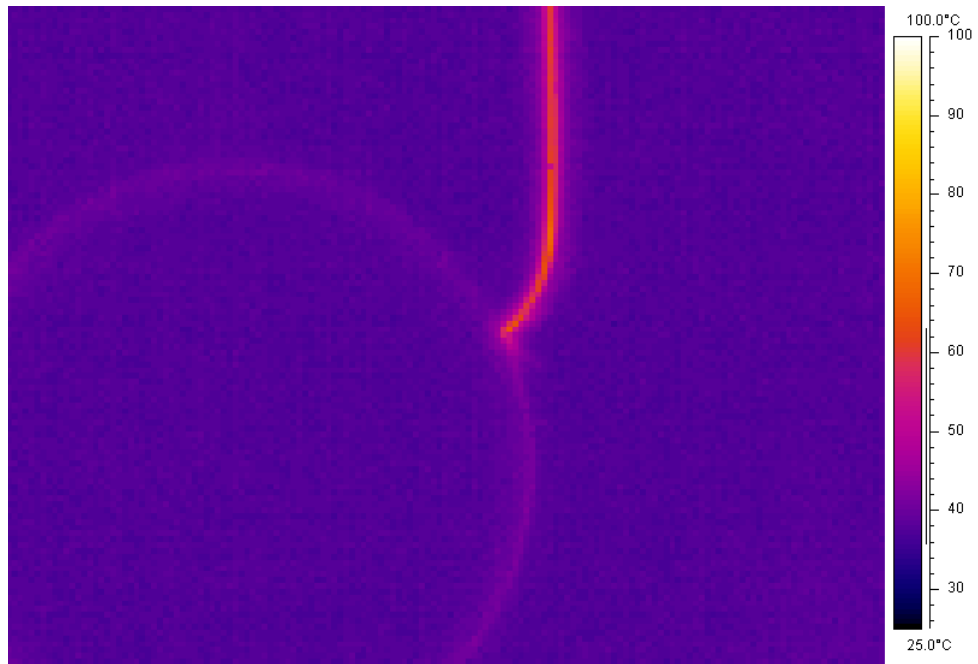
Figure A2: MQL machined FSP sample at 0.1 mm/rev feed and 150 m/min cutting speed
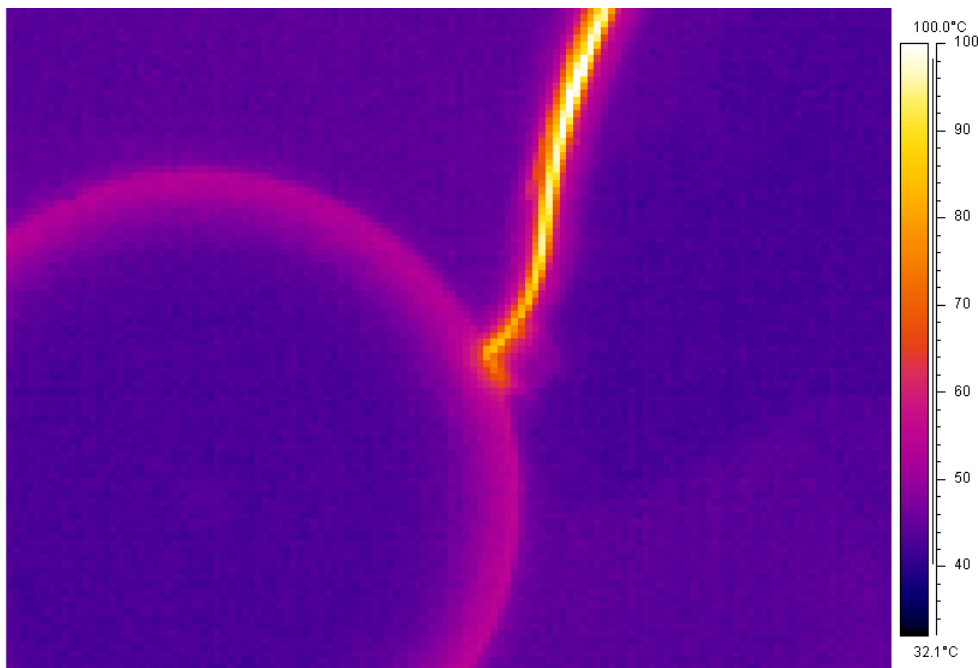
Figure A3: Cryogenically machined FSP sample at 0.1 mm/rev feed and 150 m/min cutting speed
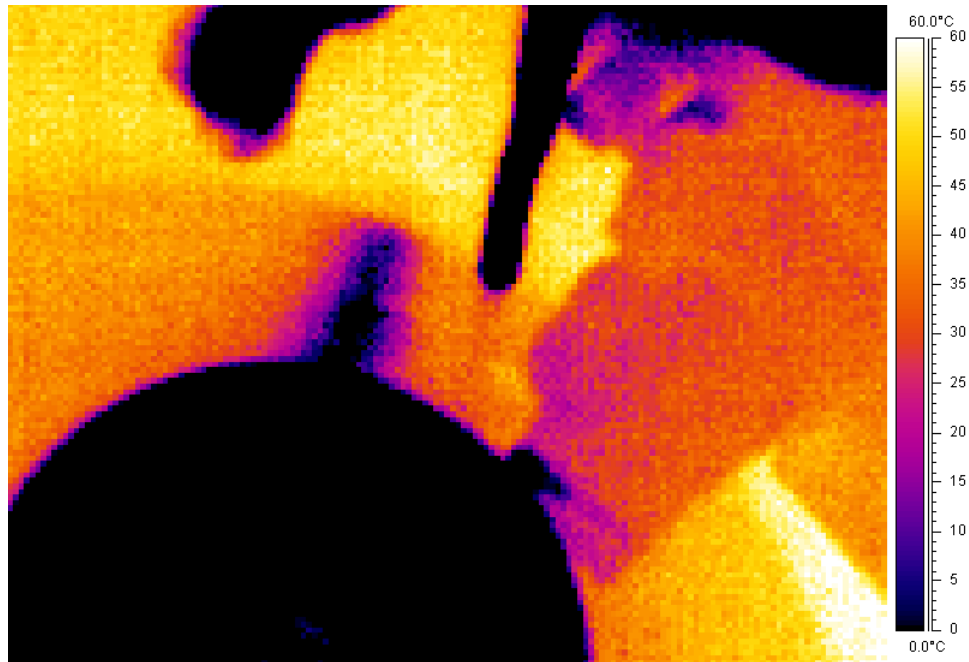
Figure A4: Maximum temperature on the machined surface under different machining conditions at 0.1 mm/rev feed and 100 m/min cutting speed [49]
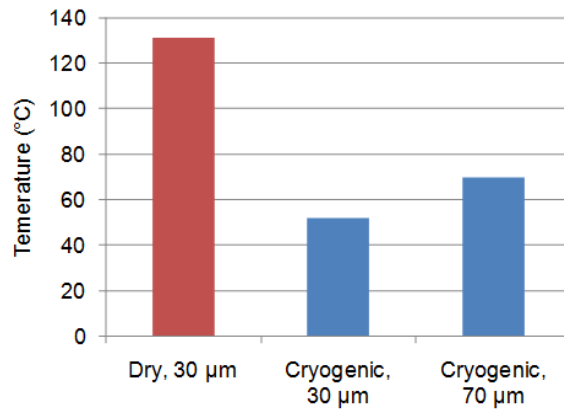
(iii) Cutting force and feed force variation with time

Cutting and feed force data with the cutting time is plotted in figures A5-A7, in order to observe the scattered values of the forces. Figure A5-A7 show how the cutting force and feed force values vary with the cutting time.

Figure A5: Cutting force and feed force variation with time for Dry machined AR sample at 0.1 mm/rev feed and 50 m/min cutting speed
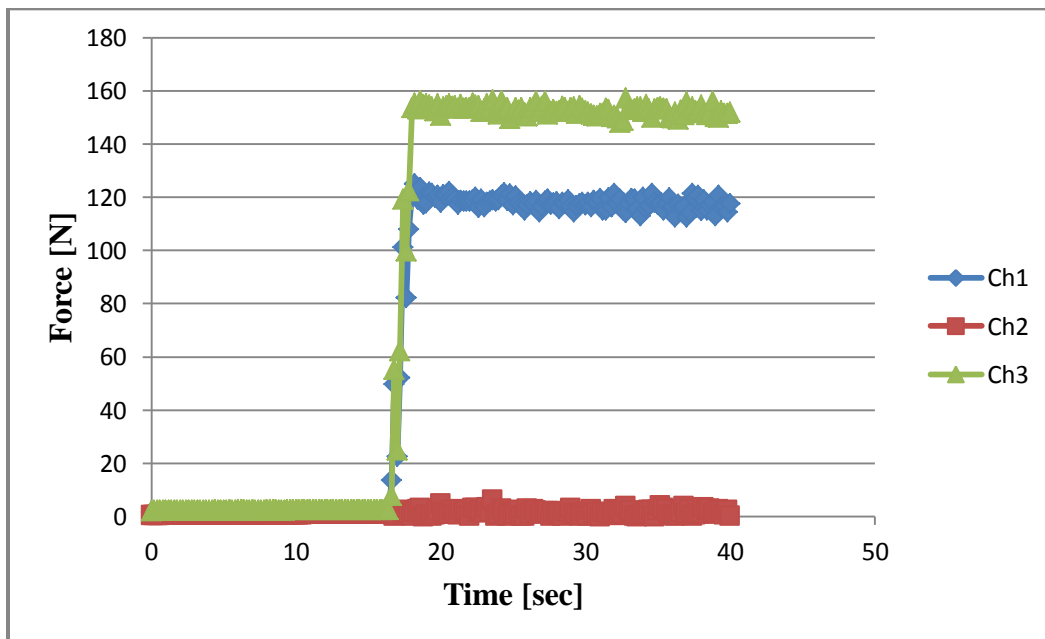
Ch1, Ch 2 and Ch3 stand for Channels 1, 2 and 3, respectively. Ch 1 represents the feed force values and Ch3 represents the cutting force values.

131

Figure A6: Cutting force and feed force variation with time for Dry machined AR sample at 0.2 mm/rev feed and 250 m/min cutting speed
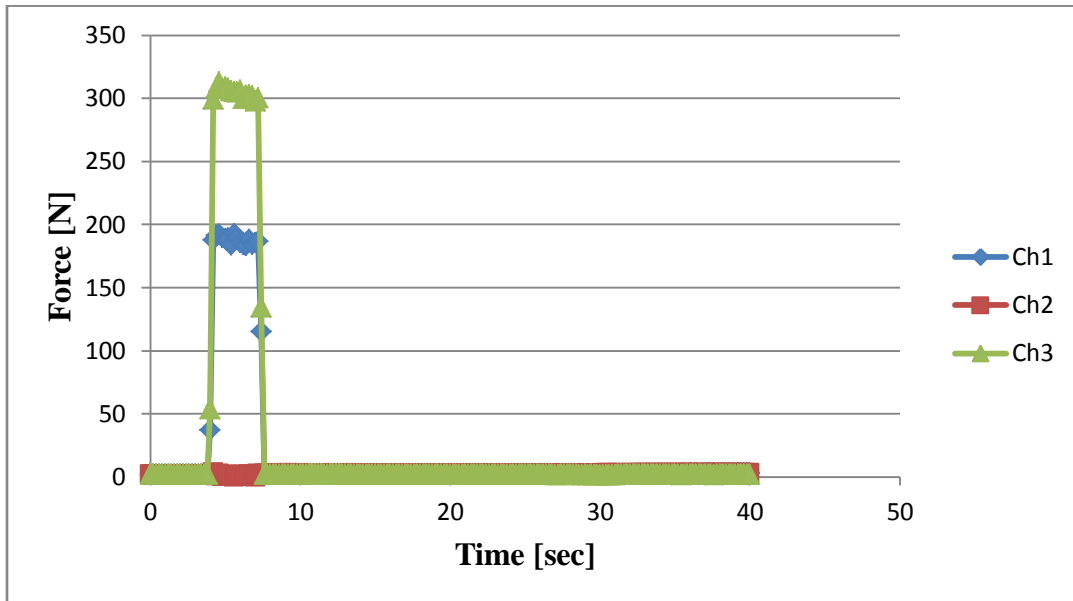
Figure A7: Cutting force and feed force variation with time for Dry machined AR sample at 0.3 mm/rev feed and 350 m/min cutting speed

REFERENCES

1.   B. Darras, "Integrated thermo-mechanical investigations of friction stir processing of light weight alloys", Ph.D Thesis, University of Kentucky, Lexington, KY, US, 2008.

2.   W.M. Thomas, E.D. Nicholas, J.C. Needham, M.G. Murch, P Temlesmith, C.J. Dawes, GB Patent Application No. 9125978.8, December 1991.

3.   R. Itharaju and M. Khraisheh, "On the forces generated during friction stir processing of aluminum 5052 sheets", Ultrafine Grained Material III TMS, 2004.
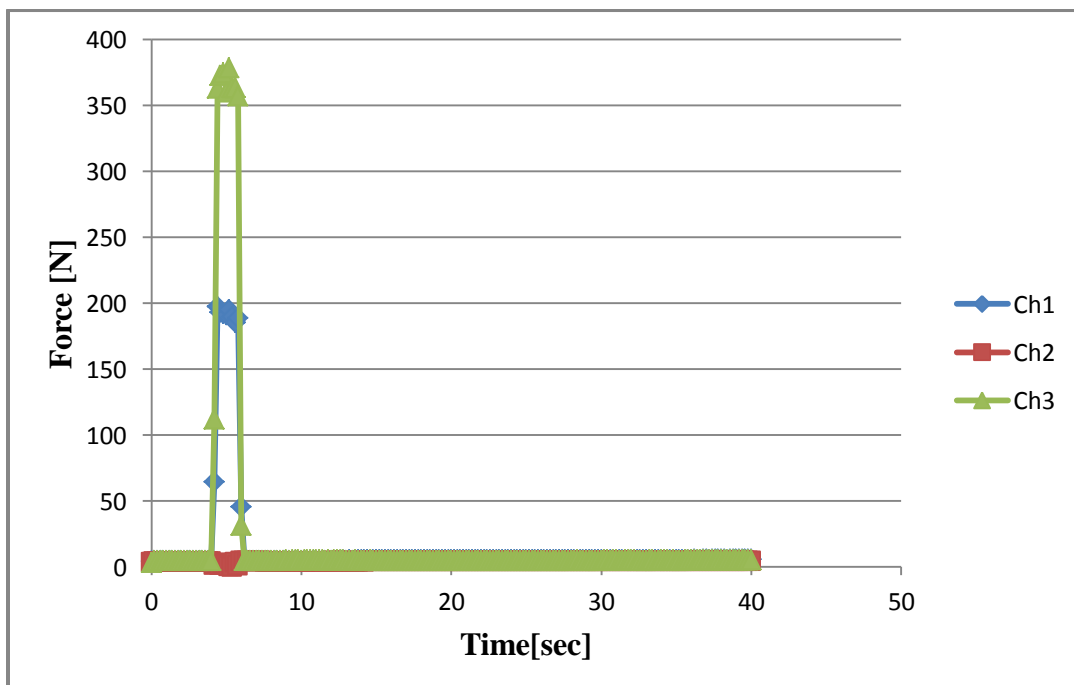
4.   R. Johnson and S. Kallee, "Friction stir welding", Materials World, 1999, Vol. 7, No. 12, pp. 751-753.

5.   R. Mishra and M.W. Mahoney, "Friction stir processing: A new grain refinement technique to achieve high strain superplasticity in commercial alloys", Material Science Forum, 2001, Vols. 357-359, pp. 2869-2877.

6.   J.Su, T. W. Nelson and C. J. Sterling, "Friction stir processing of large-area bulk UFG aluminum alloys", Scripta Materialia, 2005, Vol. 52, pp. 135-140.

7.   Z. Ma, R. Mishra and M. Mahoney, "Superplasticity in cast A356 induced via friction stir processing", Scripta Materialia, 2004, Vol. 50, pp. 931-935.

8.   M. Khraisheh, B. Darras, P. Kalu, M. Adams-Hughes and N. Chandra, "Correlation between the microstructure and forces generated during friction stir processing of AA5052", Materials Science Forum, 2005, Vols. 475-479, pp. 3043-3046.

9.   M. Mahoney, A. Barnes, W. Bingel and C. Fuller, "Superplastic forming of 7475 Al sheet after friction stir processing", Material Science Forum, 2004, Vol. 447-448, pp. 505-512.

10.   L.B. Johannes, and R.S. Mishra, "Multiple passes of friction stir processing for the creation of superplastic 7075 aluminum", Materials Science and Engineering, 2007, Vol. A 464, pp. 255–260.

11.   P. Cavaliere and P. Marco, "Superplastic behaviour of friction stir processed AZ91 magnesium alloy produced by high pressure die casting", Journal of Materials Processing Technology, 2007, Vol. 184, pp. 77-83.

12. Z. Ma, R. Mishra and M. Mahoney, "Superplastic deformation behavior of friction stir processed 7075Al alloy", Acta Materialia, 2002, Vol. 50, Issue 17, pp. 4419-4430.

13. L. Johannes, I. Charit, R. Mishra and R. Verma, "Enhanced superplasticity through friction stir processing in continuous cast AA5083 aluminum", Materials Science and Engineering A, 2007, Vol. 464, pp. 351-357.

14. R. Mishra, L. Johannes, I. Charit and A. Dutta, "Multi-pass friction stir superplasticity in aluminum alloys", Proceedings of NSF DMII Grantee Conference, Scottsdale, Arizona, DMI-0323725, 2005.

15. I. Charit and R. Mishra, "High strain-rate superplasticity in a commercial 2024 Al alloy via friction stir processing", Materials Science and Engineering A, 2003, Vol. 359, Issues 1-2, pp. 290-296.

16. K. Jata and S. Semiatin, "Continuous dynamic recrystallization during friction stirs welding of high strength aluminum alloys", Scripta Materialia, 2000, Vol. 43, Issue 8, pp.743-749.

17. Y. Kwon, N. Saito and I. Shigematsu, "Friction stir process as a new manufacturing technique of ultrafine grained aluminum alloy", Journal of Materials Science Letters, 2001, Vol. 21, pp. 1473-1476.

18. M. Mahoney, W. Bingel, S. Sharma and R. Mishra, "Microstructural modification and resultant properties of friction stir processed Cast NiAl Bronze", Material Science Forum, 2003, Vols. 426-432, pp. 2843-2848.

19. M. Sutton, B. Yang, A. Reynolds and R. Taylor, "Microstructural studies of friction stir welds in 2024-T3 aluminum", Materials Science and Engineering A, 2002, Vol. 323, pp. 160-166.

20. M. Santella, T. Engstrom, D. Storjohann, and T. Pan, "Effects of friction stir processing on mechanical properties of the cast aluminum alloys A319 and A356", Scripta Materailia, 2005, Vol. 53, pp. 201-206.

21. M. Adams-Hughes, P. Kalu, M. Khraisheh and N. Chandra, "Microcharacterization and texture analysis of friction stir processed AA5052 alloy", Friction Stir Welding and Processing III, TMS annual meeting, 2005, pp. 3-10.

22. Y. Sato, H. Park, A. Matsunaga, A. Honda and H. Kokawa, "Novel production for highly deformable Mg alloy plate", Journal of Material Science, 2005, Vol. 40, pp. 637-642.

23. A. Denquin, D. Allehaux, M.-H. Campaganc and G. Lapasset, "Relationship between microstructural variations and properties of friction stir welded 6056 aluminum alloy", Welding in the World, 2002, pp.14-19.

24. H. Park, T. Kimura, T. Murakami and Y. Nagano, "Microstructures and mechanical properties of friction stir welds of 60% Cu-40% Zn copper alloy", Materials Science and Engineering A, 2004, Vol. 371, Issues 1-2, pp. 160-169.

25. R. Mishra, Z.Y. Ma and I. Charit, "Friction stir processing: a novel technique for fabrication of surface composite", Material Science and Engineering A, 2003, Vol. 341, Issues 1-2, pp. 307-310.

26. C. Lee, J. Huang and P. Hsieh, "Mg based nano-composites fabricated by friction stir processing", Scripta Materialia , 2006, Vol. 54, pp. 1415-1420.

27. R. Zettler, A. Blanco, J. Santos and S. Marya, "The effect of process parameters and tool geometry on thermal field development and weld formation in friction stir welding of the alloys AZ31 and AZ61", Magnesium Technology, TMS, 2005, pp. 409-423.

28. Du XingHao, and Wu BaoLin, "Using two-pass friction stir processing to produce nanocrystalline microstructure in AZ61 magnesium alloy", Science in China Series E: Technological Science, 2009, Vol. 52, no. 6, pp. 1751-1755.

29. Z.Y. Ma, S.R. Sharma, and R. Mishra, "Effect of multiple-pass friction stir processing on microstructure and tensile properties of a cast aluminum silicon alloy", Scripta Materialia, 2006, Vol. 54, pp. 1623–1626.

30. C. Chang, X. Du, and J. Huang, "Achieving ultrafine grain size in Mg–Al–Zn alloy by friction stir processing", Scripta Materialia, 2007, Vol. 57, pp. 209-212.

31. S. Benavides, Y. Li, L. E. Murr, D. Brown and J. McClure, "Low-temperature friction-stir welding of 2024 aluminum", Scripta Materialia, 1999, Vol. 41, Issue 8, pp. 809-815.

32. L. Fratini and G. Buffa, "CDRX modeling in friction stir welding of aluminum alloys", International Journal of Machine Tools & Manufacture, 2005, Vol. 45, pp. 1188-1194.

33. S. Aljoaba, I.S. Jawahir, O. Dillon, M. Ali, M. Khraisheh, "Modeling of friction stir processing using 3d CFD analysis", Material Forming 12th ESAFORM Conference, Holland, April 2009.

34. G. Buffa, L. Fratini, S. Pasta and R. Shivpuri, "On the thermo-mechanical loads and the resultant residual stresses in friction stir processing operations", CIRP Annals - Manufacturing Technology , 2008, Vol. 57, pp. 287–290.

35. C. Chang, C. Lee and J. Huang, "Relationship between grain size and Zener-Holloman parameter during friction stir processing in AZ31 Mg alloys", Scripta Materialia, 2004, Vol. 51, pp. 509-514.

36. S. Aljoaba, "Modeling of friction stir processing using 3D CFD analysis", Master's Thesis, University of Kentucky, Lexington, KY, US, 2009.

37. International Magnesium Association Technical Committee, "Machining of Magnesium and Magnesium Alloys", Metals Handbook, 1989, Vol. 16, pp. 820–830.

38. H.K. Tönshoff and J. Winkler, "The Influence of Tool Coatings in Machining of Magnesium", Surface Coating Technology, 1997, Vol. 94, pp. 610–616.

39. F.Z. Fang, L.C. Lee, X.D. Liu, "Mean flank temperature measurement in high speed dry cutting of magnesium alloy", Journal of Materials Processing Technology, 2005, Vol. 167, Issue 1, pp. 119-123.

40. Machining of magnesium and magnesium alloys, ASM handbook, 1989, Vol. 16, pp. 826.

41. M. Arai, S. Sato, M. Ogawa, H. Shikata, "Chip control in finish cutting of magnesium alloy", Journal of Materials Processing Technology, 2nd International Conference on Production Engineering, 1996, Vol. 62, Issue 4, pp. 341-344.

42. A. Spicer, J. Kasi, C. Billups, and J. Pajec, "Machining magnesium with water based coolants", SAE Technical paper 910415, 1991.

43. M. Videm, R.S. Hansen, N.Tomac, and K. Tonnesen, "Metallurgical Considerations for Machining Magnesium Alloys", SAE Technical Paper 940409, 1994.

44. N. Tomac, K. Tonnessen, "Formation of flank build-up in cutting magnesium alloys", Ann. CIRP 40, 1991, Vol. 1, pp. 79–82.

45. E.M. Trent, P.K. Wright, Metal Cutting, Butterworth–Heinemann, USA, 2000.

46. www.matweb.com

47. R.L. Smith and G.E. Sandland, "An Accurate Method of Determining the Hardness of Metals, with Particular Reference to Those of a High Degree of Hardness," *Proceedings of the Institution of Mechanical Engineers*, 1922, Vol. I, pp. 623–641.

48. ASM handbook on Machining, 1989, Volume 16, pp. 25.

49. P. Zhengwen, "Cryogenic Machining and Burnishing of AZ31B Magnesium Alloy for Enhanced Surface Integrity and Functional Performance", Ph.D Thesis, University of Kentucky, Lexington, KY, US, Anticipated 2012.

VITA

The author was born in Hyderabad, Andhra Pradesh, India on November 4, 1984. He finished his Bachelors in Mechanical Engineering from Osmania University, College of Engineering, India in 2006. Then, he pursued a Master's degree in Manufacturing Systems Engineering at the University of Kentucky, Lexington, USA. During his graduate study, he worked as a Research Assistant and a Teaching Assistant for the Machining Research Laboratory at the Institute for Sustainable Manufacturing in the University.

Anwaruddin Mohammed

Date: 12/07/2011